ISSN No. 2231-3273

INTERNATIONAL JOURNAL OF ENGINEERING SCIENCES AND MANAGEMENT

A Bi-annual Research Journal of

DRONACHARYA GROUP OF INSTITUTIONS

GREATER NOIDA, U.P., INDIA

Vol. III | Issue I | Jan-Jun 2013

ISSN No. 2231-3273

INTERNATIONAL JOURNAL OF ENGINEERING SCIENCES AND MANAGEMENT

Vol. III | Issue I | Jan-Jun 2013

ISSN No. 2231-3273

INTERNATIONAL JOURNAL OF ENGINEERING SCIENCES AND MANAGEMENT

A Bi-annual Research Journal of
DRONACHARYA
GROUP OF INSTITUTIONS
GREATER NOIDA, U.P., INDIA

Volume III | Issue I | Jan-Jun 2013

INTERNATIONAL JOURNAL OF ENGINEERING, SCIENCES AND MANAGEMENT

Editorial Information:
For details please write to the Executive Editor, International Journal of Engineering, Sciences and Management, Dronacharya Group of Institutions, # 27, Knowledge Park-III, Greater Noida – 201308 (U.P.), India.

Telephones:
Landline: +91-120-2323854,2323855,2323856, 2323857
Mobile: +91-8826006878

Telefax:
+91-120-2323853

E-mail:
advisor.r&d@gnindia.dronacharya.info
director@gnindia.dronacharya.info
info@dronacharya.info

Website:
www.dronacharya.info
www.ijesm.in

ADVISORY BOARD

MEMBERS

FROM THE DESK OF
EXECUTIVE EDITOR...

Dear Readers,

It gives us immense pleasure to present Volume III / Issue I of our esteemed International journal of Engineering, Sciences and Management (ISSN: 2231-3273). A new look has been given to the illustrious Editorial board wherein members from far and wide have accepted our invitation to be a part of the journal. Their willing acceptance to our request was a matter of great pride and honor. It is certain that their rich experience and varied expertize will navigate the journal to attain an envious position in the area of research and development. We are extremely happy to inform that the Journal has been indexed by Jour Informatics and by others namely Copernicus, J-Stage, Pro-Quest, Google Scholar etc is under process.

Large number of research papers were received from all over the globe for publication and we thank each one of the authors personally for soliciting the journal. We also extend our heartfelt thanks to the reviewers and members of the editorial board who so carefully perused the papers and carried out justified evaluation. Based on their evaluation, we could accept fifteen research papers for this issue across the disciplines. We are certain that these papers will provide qualitative information and thoughtful ideas to our accomplished readers. We thank all the readers profusely who conveyed their appreciation on the quality and content of the journal and expressed their best wishes for future issues.

The publication of this journal would not have been possible without the guidance and support of our honorable Chairman and the Management Board. We convey our profound regards to the Director of the Institute, the Editorial Board, the Advisory board and all office bearers who have made possible the publication of this journal in the planned time frame.

We humbly invite all the authors and their professional colleagues to submit their research papers for consideration for publication in our forthcoming issue i.e. Vol III / Issue II / Jul to Dec 2013 as per the "Scope and Guidelines to Authors" given at the end of this issue. Any comments and observations for the improvement of the journal will be most welcome.

We wish all of you joyous reading of these research papers and a very Happy New Year 2013.

Sincerely,

Wg Cdr (Prof.) TPN Singh
Executive Editor
International journal of Engineering, Sciences and Management (IJESM)
A bi-annual Research journal of Dronacharya Group of Institutions, Greater Noida, UP, India.

January 2013

ISSN No. 2231-3273

CONTENTS

PERFORMANCE OF OPEN-SOURCE DESKTOP APPLICATIONS ON A MULTICORE PROCESSOR-BASED MACHINE

(Invited Paper)

Pradeep Nair*
E-mail: pnair@fullerton.edu;
Computer Engineering Program
California State University, Fullerton CA 92831, USA
Phone no. +1-657-278-3375
corresponding author

Aparna Harikumar Asha
E-mail: aparna@csu.fullerton.edu;
Department of Computer Science
California State University, Fullerton CA 92831, USA

Susamma Barua
E-mail: sbarua@fullerton.edu
Computer Engineering Program
California State University, Fullerton CA 92831, USA

ABSTRACT

The use of open-source desktop applications has been on the rise in recent times. The use of multi-core processors in personal computers is also fairly commonplace now. In this paper, the performance of some of the open-source desktop applications was analyzed on a dual-core processor-based personal computer with the goal of identifying performance bottlenecks. Out of the seven applications whose performance was analyzed, five applications yielded CPI values greater than 1. Interactive applications generally resulted in lower CPI values. The performance of some of the applications was significantly affected by factors such as branch prediction inaccuracy and main memory accesses.

Keywords: *Performance analysis; open-source; multicore; desktop applications*

1.INTRODUCTION

The improvement in personal computing capabilities in recent decades can be attributed largely to Moore's law[1], an observation by Intel Corporation co-founder Gordon Moore, which predicted that the number of components (transistors) that can be integrated on to a given area of silicon real estate of an Integrated Circuit (IC) chip increases at a rapid rate. Since 1975, integration density of the components was predicted to double every two years. Moore's law later led to the prediction by Intel Corporation executive David House that, if improvements in transistor speeds are also taken into consideration, the performance capabilities of processor ICs doubles approximately every 18 months[2]. Subsequently, the performance capabilities of computers, including those of personal computers, have continued to increase steadily. It is now common for state-of-the art personal computers (desktop and laptop computers) to contain processor chips composed of millions of transistors. Such processor chips, known as multicore processors, can support 64-bit computing and often employ multiple logical processing cores on one IC platform. Several of the leading processor companies now design and/or build multicore microprocessors[3].

Desktop applications such as word processing, spreadsheet, presentation software, media player etc. have been popular since the advent of personal computers. These applications have evolved along with personal computers and are used not only by the scientific and engineering communities, but also by other users from the fields of arts, business, humanities, social sciences, law, sports, entertainment etc. The speed performance of these desktop applications plays a significant role in the overall 'computer experience' of many users. In this paper, we analyze the performance of common desktop applications on a personal laptop computer based on the Intel® Core™ 2 Duo multicore processor, which consists of two processor cores (dual-core) [4, 5, 6]. The objective of this work is to identify the possible performance bottlenecks when such applications are run on machines based on the CoreTM 2 Duo or similar dual-core processors. Identification of bottlenecks can indicate how well-suited current multicore processors are for common desktop applications and whether further performance improvement is plausible. The knowledge

obtained through bottleneck identification could then be applied for achieving potential future hardware improvements, or application software improvements, or both.

The remainder of this paper is organized in the following manner: Section 2 discusses related work. Section 3 describes the methodology and tools adopted in this work. Section 4 analyzes the results and section 5 concludes the paper.

2. RELATED WORK

Numerous papers in the literature have been devoted to the study of the performance of desktop applications. Some of these are from the previous decades and some have been published recently. A common factor underlying these papers is that whenever newer hardware microarchitectures or software paradigms have been introduced, the topic of performance of desktop applications has been revisited. This could be attributed to the high impact of desktop applications on general purpose computing.

A comparison of the performance of three personal computer operating systems namely Windows for Workgroups, Windows NT and BSD UNIX when running the Wish, Ghostscript and World-Wide Web Server applications was performed by Chen et al[7].

Casmira et al. describe a toolset for dynamic execution tracing called PatchWrx, with a goal to capture operating system activity when workloads are run on the Windows NT 4.0 operating system[8]. The workloads considered in this work included desktop applications such as Microsoft Word 97, Visual C++ V5.0, Microsoft CD Player, Internet Explorer V2.0 etc.

Zhou et al. analyzed the performance of personal computer workloads running on Intel Pentium processor-based machines and the Windows 95 operating system[9]. The applications analyzed included WinWord, Microsoft PowerPoint, Access, Excel, Notepad, Internet Explorer etc.

Flautner et al. investigated the effects of multiprocessing on interactive desktop workloads[10]. They studied the amount of thread-level parallelism in interactive desktop workloads and the ability of the available thread-level parallelism in these workloads to contribute to higher performance. The workloads considered in this work included Acrobat viewer, Ghostview, Netscape, etc. The authors concluded that using two processors resulted in improved performance for the applications considered in this study. More recently, Blake et al. investigated whether current desktop applications exhibit enough thread-level parallelism to exploit the enhanced hardware capabilities offered by multicore processors[11]. They studied the execution characteristics workloads such as Microsoft PowerPoint, Word, Acrobat Reader, Quick Time Player, Firefox, Safari ITunes etc. The performance of the desktop applications was studied using the Windows 7 operating system from Microsoft and the OS X Snow Leopard system from Apple. The authors observed that even though the code of many modern desktop workloads contain multiple threads, these threads are often interdependent and are, therefore, not amenable to parallel execution. They conclude that unless software changes to achieve more parallelism occur, increasing the number of cores may not yield significant benefits for personal computing applications.

In this work, our aim is to identify the execution bottlenecks encountered by open-source desktop applications on a machine based on the Core™ 2 Duo dual-core processor from a microarchitectural standpoint. We chose to focus on open-source desktop applications due to the fact that many of these applications are now being used increasingly around the world[12]. This is mainly because these applications provide more language options, are available free of cost, and are relatively more accessible in places with slow Internet speeds, which include large parts of the developing world. To the best of our knowledge, there are not many papers that analyze the performance of open-source desktop applications on multicore processors.

3. METHODOLOGY AND TOOLS

Performance data was collected on a mobile personal computer (laptop PC) based on the Windows XP operating system and the Intel® Core™ 2 Duo microprocessor[13], [14] using the Intel® VTune ™ Amplifier XE 2013 performance analyzer[15]. The PC was powered from the AC wall outlet during the data collection process. Prior to data collection, the hard disk was analyzed for fragmentation using the Windows Disk Defragmenter utility. Data collection was performed after confirming that no defragmentation was required. The hardware and software configuration details of the PC pertaining to this work are shown in Table 1.

Table 1. Hardware and Software Configuration of the PC used for performance analysis

Attribute	**Details**
Operating system	Windows XP Professional SP3
Processor	45 nm Intel® CoreTM 2 Duo T6400
Processor clock speed	2 GHz.
Number of processor cores	2
Front Side Bus (FSB) speed	800 MHZ.
L1 cache	Two L1 I-caches, each of size 32KB; two L1 write-back D-caches,each of size 32 KB
L2 cache	2 MB shared cache
Chipset	Mobile Intel 965 Express chipset family
Main Memory Size	3 GB
Total hard drive capacity	298 GB
Hard disk free space	257 GB

During the data collection process, applications were invoked and analyzed, one at a time, through the VTune Amplifiler performance analyzer, which was configured in the event-based sampling mode for performance data collection. Events that reflect microarchitectural behavior such as dynamic instruction mix, cache behavior, branch-prediction events etc. were monitored through event-based sampling, which is a non-intrusive method of performance data collection; it collects event-based samples and extrapolates the sampling information to provide overall execution-related information.

Applications: In this work, we analyzed the following applications: LibreOffice 3.6 swriter (text editor application), LibreOffice 3.6 scalc (spreadsheet application), simpress (presentation application), sdraw (drawing and painting application) [16]; VideoLan VLC 2.0.4 (audio and video player) [17]; and JPEGView (image viewer and editor application) [18]. The applications were run for similar durations. The total elapsed times for various execution cases, as reported by VTune, are shown in Table 2. This includes the overhead for starting and stopping the performance analyzer. The usage patterns relating to the analyzed applications are shown in Table 3.

Table 2. Elapsed times for various execution cases

Application	swriter	scalc	simpress	sdraw	VLC (audio)	VLC (video)	JPEGView
Elapsed time	205.553s	206.038s	210.663s	208.52s	211.713s	205.359s	212.391s

Table 3. Usage patterns for various applications

Application	**Usage pattern**
swriter	typing words of varying widths; typing speed variations; saving typed data using menu features
scalc	entry of character strings and numbers into spreadsheet columns; use of formulas; graphing; data saving using menu features
simpress	slide preparation; alteration of content font size and types; slide show; saving of typed data using menu features
sdraw	use of regular and irregular shapes; use of curved and straight line; create shapes; use of text box; data saving using menu features
VLC (audio)	audio playback of a single mp3 file; volume adjustment; screen maximization
VLC (video)	continuous, automated video playback of four AVI files; volume adjustment; screen maximization
JPEGView	manual picture slideshow; use of zoom features; use of rotate and resize features

4. RESULTS

One of the important metrics of overall performance is the average number of clock cycles taken to process one instruction. This metric is abbreviated as CPI ("Clocks per Instruction"). For an out-of-order processor, the ideal CPI value should be less than 1, or an "Instructions per Cycle" (IPC) value greater than 1, due to the fact that there are multiple execution units within such processors that can simultaneously execute more than one instruction. For a multicore processor, the ideal CPI value for an application should be much lower than 1due to the presence of more than one logical processor within the same physical processor chip.

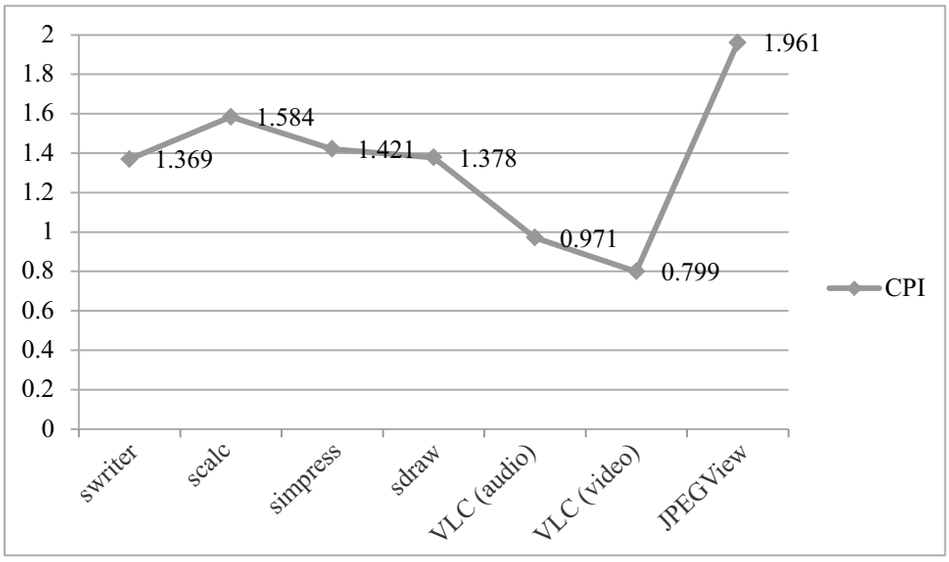

Fig. 1. CPI values recorded for different desktop applications

The CPI values recorded for the various applications considered in this work are shown in Figure 1. For the majority of the applications that we considered, the CPI value was greater than 1 even though we used a dual-core processor-based machine. The exception to this observation was the VLC player, both for audio as well as video playback. The highest CPI value of 1.961 was recorded for JPEGView. In general, applications which heavily rely on user interaction (all applications in Fig. 1 except VLC (audio) and VLC (video) resulted in high CPI values, which points to the fact that the use of a dual-core processor-based machine does not necessarily guarantee high speed performance for all applications.

The total number of processor instructions that make up an application is another factor that determines overall application execution time. The total number of retired instructions, or instruction count (IC) was measured for each application. The corresponding results are shown in Figure 2. The measured IC values were in the order of billions. The highest number of retired instructions, in excess of 65 billion instructions, was recorded for the VLC (video) application. The low CPI value encountered by this application allows for the retirement of such a large number of instructions within the duration of data collection, which is similar for all the applications considered in this work. On the other hand, the high CPI value associated with JPEGView only allows for the processing of a much smaller number of instructions within the duration of data collection.

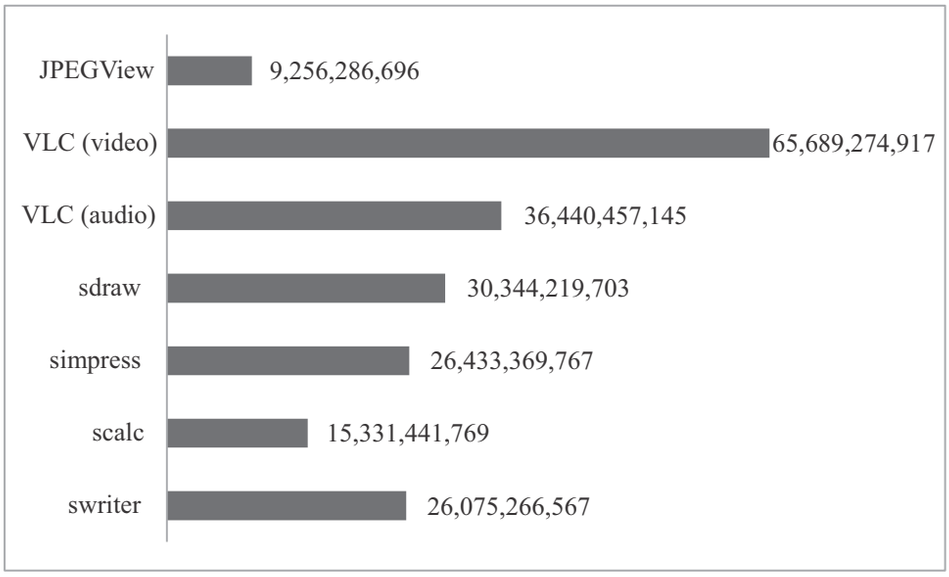

Fig. 2. IC values measured for different desktop applications

The proportion of various instruction types within an application can have an effect on performance. It also helps determine the relative importance of various microarchitectural features for that application: The presence of a large number of load and store-type instructions could result in a high amount of memory access, which could slow down the overall processing time.Similarly, the presence of a large number of conditional instructions will result in a relatively higher dependency on branch predictor accuracy to achieve high performance. The instructions of the various desktop applications were profiled and the proportion of the branch instructions was calculated in addition to determining the proportions of instructions that include memory accesses within them. These results are depicted in Figure 3. The low CPI values recorded in figure 1 for VLC (audio) and VLC (video) can be attributed partly to the relatively lower percentage of load, store and branch operations associated with these cases. The high percentage of load, store and branch operations in the case of sdraw and JPEGView is likely to be a cause of low CPI values associated with these applications. Interestingly, JPEGView has a higher CPI than sdraw in spite of the fact that the former contains a relatively lower percentage of branch and memory operations.

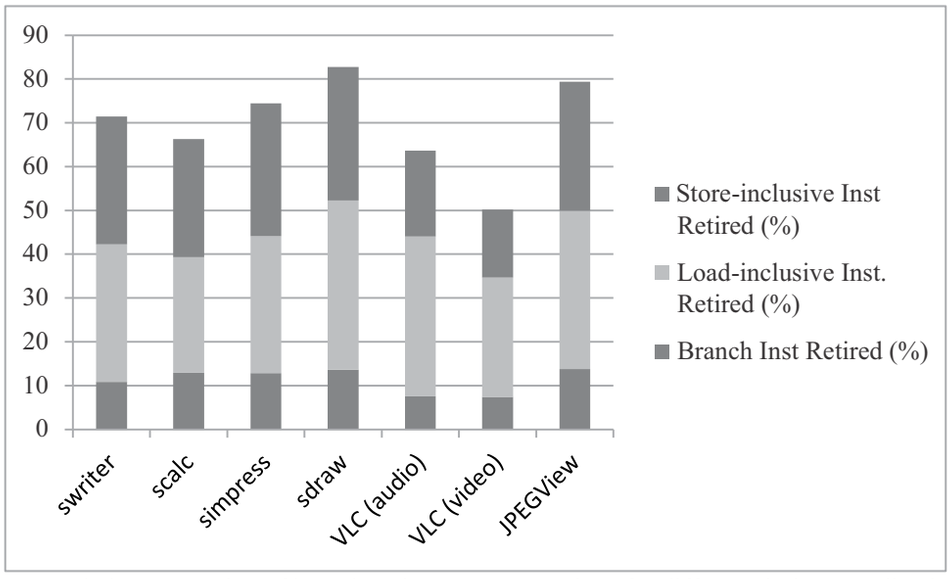

Fig. 3. Relative proportion of branch and memory operations for different desktop applications

The accuracy of branch prediction can have a significant effect on the overall performance. Branch misprediction often requires the stalling and flushing of processor pipelines, which results in significant adverse effects on performance. The effect of branch misprediction on the performance of different applications was determined by recording the 'Branch Mispredict' ratio. This is a VTune-performance metric and is defined in VTune as the ratio of cycles of wasted work due to branch misprediction to the total number of cycles. The 'Branch Mispredict' values for various applications are shown in Table 4. Based on the results obtained, it can be speculated that the performance of simpress and sdraw is adversely affected due to branch misprediction while the performance of the other applications are not affected significantly due to the accuracy of the branch predictor structures in the processor.

Table 4. 'Branch Mispredict' ratio for various desktop applications

Application	swriter	scalc	simpress	sdraw	VLC (audio)	VLC (video)	JPEGView
Branch Midpredict ratio	0.047 (low)	0.047 (low)	0.053 (high)	0.067 (high)	0.017 (low)	0.030 (low)	0.029 (low)

The Level-1 Data (L1 D) cache performance was estimated by recording the number of outstanding L1 D cache misses at any cycle and expressing it as a percentage of total number of instructions retired. The corresponding results are shown in Figure 4. The “low-CPI” applications, VLC (audio) and VLC (video) have a smaller percentage of outstanding L1 D cache misses when compared to others whereas JPEGView, which has the highest CPI among the chosen applications, has the highest percentage of outstanding L1 D cache misses.

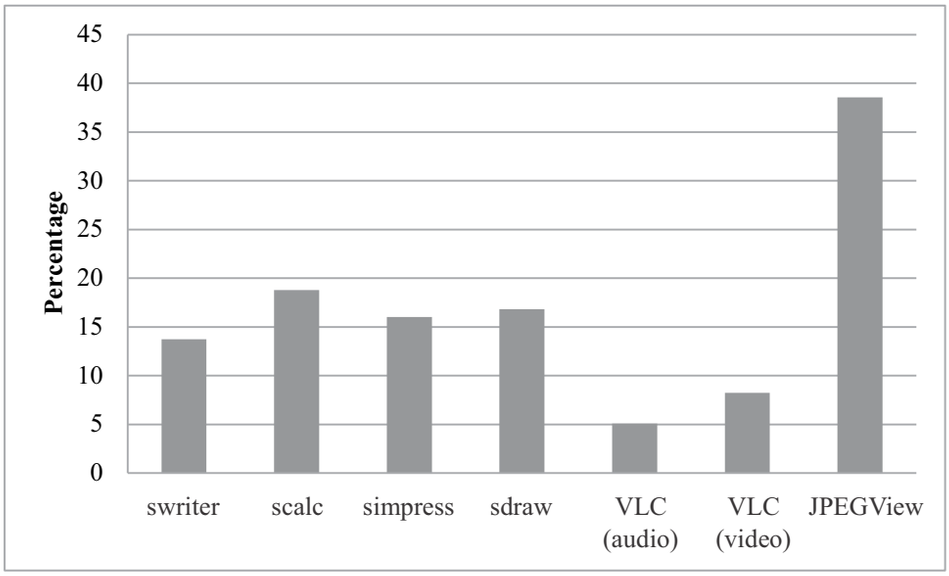

Fig. 4. Outstanding L1 D cache misses as a percentage of IC

The Instruction Fetch Unit (IFU) miss rate, expressed as a percentage of total IFU reads, is shown in Figure 5 below. All the four chosen LibreOffice applications (swriter, scalc, simpress, and sdraw) encountered a relatively high IFU miss rate.

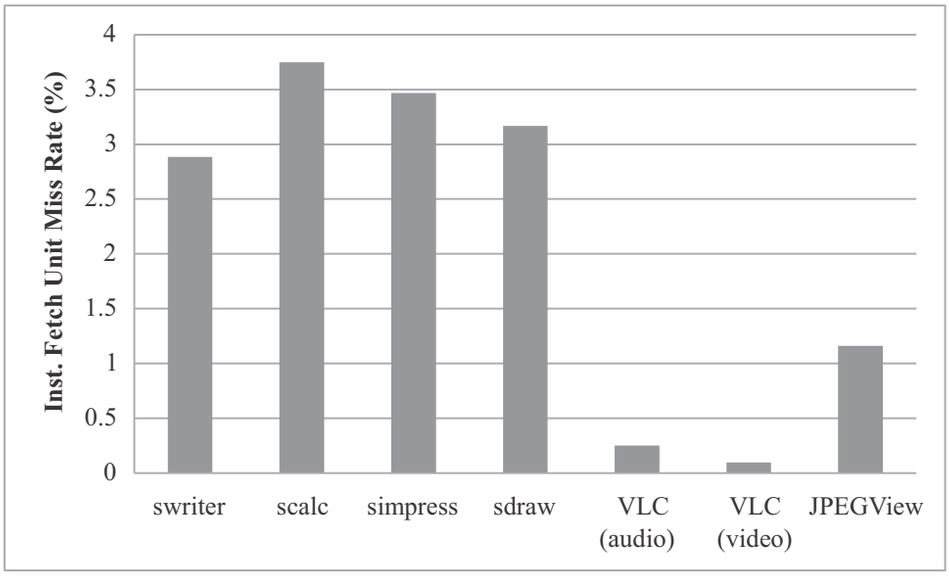

Fig. 5. IFU Miss Rate (%)

The effect of missing the last-level cache (LLC) was determined by recording the 'LLC Miss' ratio of VTune. This is the ratio of cycles that contain outstanding LLC misses to the total number of cycles. It provides a measure of the amount of the number of memory accesses that need to be served by the slower and remotely-located DRAM, which degrades performance. The LLC Miss ratios for the various applications are shown in Table 5. Except swriter, VLC (audio) and VLC (video), all the other applications encountered a high LLC miss ratio.

Table 5.'LLC Miss' ratio for various desktop applications

Application	swriter	scalc	simpress	sdraw	VLC (audio)	VLC (video)	JPEGView
Branch LLC Miss ratio	0.025 (low)	0.073 (high)	0.099 (high)	0.136 (high)	0.0000 (low)	0.034 (low)	0.129 (high)

5. CONCLUSION

In this paper, we analyzed the performance of some of the open-source desktop applications, from a microarchitectural standpoint, on a personal computer based on the Intel® CoreTM 2 Duo dual-core processor and the Windows XP Professional Operating System. Five out of the seven applications analyzed resulted in CPI values greater than 1, which is far higher than the ideal CPI. Interactive applications generally resulted in lower CPI values, which point to the fact that the use of multicore processors alone cannot guarantee high performance for such applications. The performance of some of the applications was significantly affected by factors such as branch prediction inaccuracy and main memory accesses.

REFERENCES

1. Moore, G.E. Cramming More Components onto Integrated Circuits, Electronics, 38, 1965, p.114-117.
2. Edwards, C. The Many Lives of Moore's Law, Engineering and Technology Magazine, 3, 2008.Available online at http://eandt.theiet.org/magazine/2008/01/moores-law.cfm
3. Blake, G; Dreslinski, R.G. & Mudge, T. A Survey of Multicore Processors, IEEE Signal Processing Magazine, 26, 2009, p. 26-37.
4. Wechsler, Ofri. Inside Intel® Core™ Microarchitecture: Setting New Standards for Energy Efficient Performance, Intel® White Paper, 2006. Available online at http://www.intel.com/pressroom/kits/core2duo/pdf/icm_whitepaper.pdf
5. Doweck, J. Inside Intel® Core™ Microarchitecture and Smart Memory Access: An In-Depth Look at Intel Innovations for Accelerating Execution of Memory-Related Instructions, Intel® White Paper, 2006. Available online at http://software.intel.com/sites/default/files/m/3/4/d/6/3/18374-sma.pdf
6. Nisar, A; Ekpanyapong, M; Valles, A.C & Sivakumar, K. Original 45nm Inside Intel® Core™ 2 Processor Performance, Intel® Technology Journal, 12, p. 157-168.
7. Chen, P.B; Endo, Y; Chan, K, Mazieres, Dias, A; Seltzer, M & Smith, M.D. The Measured Performance of Personal Computer Operating Systems. ACM Transactions on Computer Systems, 14, 1996, p. 3-40.
8. Casmira, J.P; Hunter, D.P & Kaeli D.R. Tracing and Characterization of Windows NT-based System Workloads, Digital Technical Journal, 10, 1998, p. 12-21.
9. Zhou, M & Smith, A.J. Analysis of Personal Computer Workloads. University of California, Berkeley, USA, 1999, Report No.UCB/CSD-99-1038.
10. Flautner, K; Uhlig, R; Reinhardt, S & Mudge, T. Thread-level Parallelism and Interactive Performance of Desktop Applications. Presented at the 9th International Conference on Architectural Support for Programming Languages and Operating Systems, Cambridge, MA, USA, November 12-15, 2000, p. 129-138.
11. Blake, G; Dreslinski, R.G; Mudge, T. & Flautner, K. Evolution of Thread-Level Parallelism in Desktop Applications. Presented at the 37th International Symposium on Computer Architecture, Saint-Malo, France, June 19-23, 2010. P. 302-313.
12. Apache Software Foundation blog: 5 Million Downloads of Apache OpenOffice (incubating), June 20, 2012; Available online at https://blogs.apache.org/OOo/entry/5_million_downloads_of_apache
13. Intel® Core™ 2 Duo T6400 specifications. Available online at http://ark.intel.com/products/40479/Intel-Core2-Duo-Processor-T6400-2M-Cache-2_00-GHz-800-MHz-FSB
14. CPU World: Intel Core 2 Duo Mobile T6400 AW80577GG0412MA specifications. Available online at http://www.cpu-world.com/CPUs/Core_2/Intel-Core%202%20Duo%20Mobile%20T6400%20AW80577GG0412MA.html
15. Intel® VTune™ Amplifier XE 2013 Product Brief. Available online at http://software.intel.com/en-us/sites/default/files/Intel_VTune_Amplifier_XE_2013_PB.pdf
16. LibreOffice: The Document Foundation. Available online at http://www.libreoffice.org/
17. VideoLan Organization. Available online at http://www.videolan.org/vlc/index.html
18. JPEGView. Available online at http://sourceforge.net/projects/jpegview/

DESIGN OF EFFICIENT MULTIMODAL SYSTEMS

Ms. S.A.Chhabria*
Department of Information Technology
G.H.Raisoni College of Engg.
Digdoh Hills, CRPF Gate No. 3, Nagpur
E-mail: sharda_chhabria@yahoo.co.in,
Corresponding author

Dr. R.V.Dharaskar
Director, MPGI Integrated campus, Nanded

Dr. V.M.Thakre
Department of CSE
Amravati University, Amravati

ABSTRACT

Human computer interaction is a discipline concerned with design, evaluation, and implementation of interactive computing systems for human use. In this paper multimodal system is designed using different methods like scan line, connected component, self organized markov model, dynamic time wrapping algorithm for speech, hand ,and eye are discussed. These methods are compared based on parameters like accuracy, complexity, background and number of gestures.

Keyword: *Multimodal system, Gesture recognition, speech recognition, Hand Gestures.*

1.INTRODUCTION

The technology in developing human-machine interfaces for disabled people has been increasing in last years. The technology is becoming mature enough to be widely available to the public and real-world computer vision applications start to emerge. Human computer interaction interfaces need to be as intuitive and natural as possible. One key challenge for gesture recognition systems is that they must perform in uncontrolled real-world environments. This means heavily non-uniform backgrounds with large number of moving objects and possibly harsh illumination conditions. To have the human computer interaction be as natural as possible, it is desirable that computers be able to interpret all natural human actions. Hence, computers should be able to interpret human hand, body, and facial gestures, human speech, eye gaze, etc. In situations where background noise is relevant and the human cannot interact by voice, an alternative interface must be available; therefore a multimodal system is required. Gesture interpretation can be seen as a way for computers to begin to understand human body language, thus building a richer bridge between machines and humans than primitive text user interfaces or even GUIs, which still limit the majority of input to keyboard and mouse. Thus the system is needed for interpreting multiple sensing modalities in the context of human computer interface. There are various applications of HCI. A dynamic environment makes the user free to interact with the computing devices without any physical contact with it. This characteristic of HCI makes it particularly very much suitable for the teaching methodology that is quite dependent on hand gestures. Also learning for students could be made easier if the complex commands of the dynamic applications of computers are controlled through easier hand gestures, for example browsing images in an image browsers with the help of hand gestures or controlling the power point presentations with the usage of hand gestures without the need of learning various commands involved, from a distance without the need of any physical contact with the devices. This paper discusses multimodal systems built using different gesture recognition methods like scan like ,connected component, self organized markov model, dynamic time wrapping algorithm for speech,hand,and eye are discussed. The applications developed are for moving a toy wheelchair and medical images.

These methods are compared based on parameters like accuracy, complexity, background and number of gestures. The rest of the paper is organized as follows. Section II describes the various algorithms implemented to develop multimodal systems. The experimental results of different methods are shown in Section III. Finally, the main conclusions are summarized in Section IV.

2. GESTURE RECOGNITION METHODS

2.1 Scan Line Method For Eye: [1] The coherence algorithm works for detecting the motion of eye. This algorithm operates on the frames extracted from the video of the eye. From the frame, the algorithm extracts the pixels which lie on the vertical edges of the rectangular area selected by the user. These pixels are then processed to determine the RGB values. When the user is looking straight in front, the pixels on both the vertical lines are black. This is interpreted as the "center" direction of the user's eye. When user looks towards left, the pixels on the left vertical line are black, but the pixels on the right vertical line are white. The closed eye condition is also recognized by the software.[1]

2.2 Scan Line Method For Hand: [1] Image is captured through camera and stored in memory .Next RGB values are determined.3D array is used to hold pixel detail. Pixel Color is compared. Depending upon the color value of pixel we extract the value of pixel under specific scan lines by using get nearby value () function. The area near each scan line is examined for specific commands. For example, when left hand is moved, area under left scan line is cut and hence it is detected that left hand is moved and same for other movements also. This command is for robot to perform action according to command. [1]

2.3 Connected Component Algorithm: A connected component algorithm finds regions of connected pixels which have the same value. Connected component algorithm works by scanning an image ,pixel-by-pixel(from top to bottom and left to right) in order to identify connected pixel regions, i.e. regions of adjacent pixels which share the same set of intensity values.

The algorithm makes two passes over the image: one pass to record equivalences and assign temporary labels and the second to replace each temporary label by the label of its equivalence class.

As compared to many existing algorithm the advantages of connected component between the technology and conventional labeling algorithms are: (1) all conventional label-equivalence-based algorithms scan an image at least twice, whereas this algorithm scans an image only once;

(2) all conventional label-equivalence-based algorithms assign a provisional label to each object pixel in the first scan and re-label the pixel in the later scan, whereas this algorithm assigns a provisional label to each run in the only scan, and after resolving label equivalences between runs, by using the recorded run data, it assigns each object pixel a final label directly. Therefore, relabeling of object pixels is no longer necessary.

2.4 Hybrid Approach For Speech And Gesture Recognition: The main approaches for analyzing and classifying hand gestures for HCI include combination of SOMM that is Self Organizing Maps and Hidden Markov Models. Gesture taxonomy can be formalized in a scaling continuum: gesticulation, speech-linked pantomime and sign language. Gesture recognition consists of various phases. i. image capturing, ii. Feature extraction of gesture iii. Gesture modeling (Direction, Position, generalized), 2.Speech recognition consists of various phases i. taking voice signals ii. Spectral coding iii. Unit matching (BMU) iv. Lexical decoding v. syntactic, semantic analysis. Compared with many existing algorithms for gesture and speech recognition, SOM provides flexibility, robustness against noisy environment. This project involves one hardware like wheelchair robot which takes movement according to the commands. Command like move to left, move to right, move up and the gesture symbols like fingers one, two, three also head movement left or right. Hardware takes delay between commands. In speech recognition training of large number of speech utterances along with their transcriptions into phonemes is done.Kohonen Algorithm for training the database is done.

Viterbi Algorithm is used for finding sequence of hidden states that result in sequence of observed images. Baum-Welch algorithm is used for finding set of state transition and output probabilities of sequence. [3]Time complexity for this method is O (n2).

2.5 Dynamic Time Wrapping Algorithm: This algorithm sp is used for both speech and hand gesture.DTW is a time series alignment algorithm that aims at aligning two sequences of feature vectors by warping the time axis iteratively until an optimal match(according to a suitable metrics) between the two sequences is found. Consider two sequences of feature vectors:

A = a1,a2,…….ai……, an

B= b1, b2 …bj……., bm

[I] Design of Speech Recognition Module: Vocalizations in human can vary widely in terms of their accent, pronunciations, articulation, roughness, nasality, pitch, volume, and speed; moreover, during transmission irregular speech patterns can be further distorted by background noise and echoes, as well as electrical characteristics. All these sources of variability make speech recognition, even more complex problem.

- Raw speech is typically sampled at a high frequency, e.g. 16 KHz over a microphone or 8 KHz over a telephone. This yields a sequence of amplitude values over time.

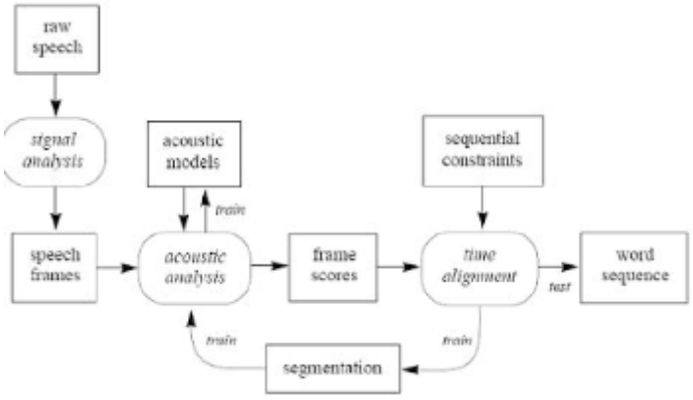

Figure 1:Speech Recognition Module

- Signal analysis: Raw speech should be initially transformed and compressed, in order to simplify subsequent processing. Some popular methods are Fourier analysis(FFT),Perceptual Linear Prediction(PLP), Linear Predictive Coding (LPC).
- For removing noise kalman filter is used. Kalman filter is a tool that can estimate the variables of a wide range of processes. It estimates the states of a linear system.
- Speech frames: The result of signal analysis is a sequence of speech frames, typically at 10 msec intervals, with about 16 coefficients per frame.
- Speech Recognition: In this approach every word is modeled by a sequence of trainable states, and each state indicates the sounds that are likely to be heard in that segment of the word, using a probability distribution over the acoustic space. Probability distributions can be modeled parametrically, by assuming that they have a simple shape and then trying to find the parameters that describe it or non-parametrically, by representing the distribution directly.

[ii] Design of Hand Gesture Recognition:

Frames from video sequences captured through webcam are processed and analyzed in order to remove noise, find skin tones and label every object pixel. Once the hand has been segmented it is identified as a certain posture or discarded. Pattern recognition is done by means of dynamic time wrapping algorithm. Finally depending upon the gesture, action is performed on the medical image.

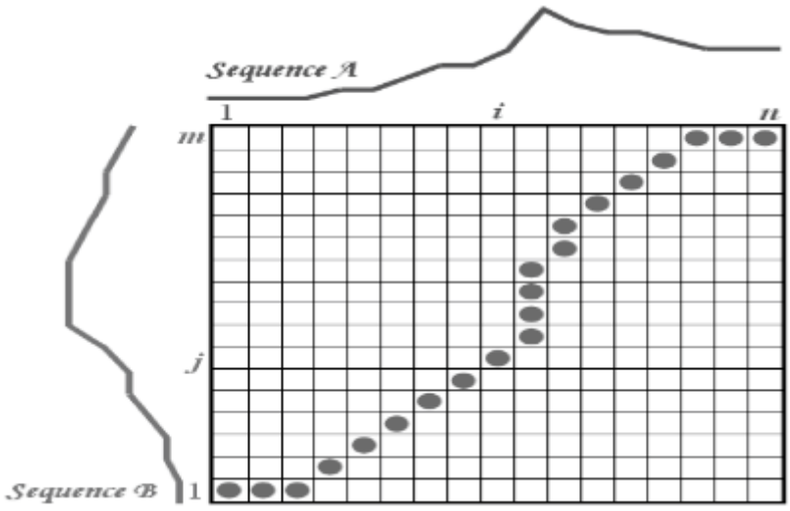

Figure 2. Graph showing working of Dynamic Time algorithm

3. EXPERIMENTAL RESULTS

Summary of Accuracy. Time complexity, no of gestures used in various algorithms is shown in table. It is concluded that Fast DTW gives the best results.

GESTURE RECOGNITION USING DTW FOR MEDICA

Right Arm Raised

Figure 3

Hand in Horizontal

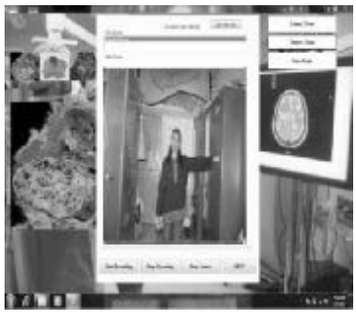

Figure 4

Commands implemented are Move Up, Move Down, Move To Right, Move To Left, Zoom, Crop. Select 1, Select 2, Select 3 [Input Speech] .System is trained for different users and response time is noted. Result is shown as below:

METHOD	Accuracy	Complexity	No. of Gestures	Background
Scan Line for Hand	80	O(n2)	5	Static
Connected Component Algorithm for Hand & Head	85	O(n3)	4	Dynamic
Self Organizing Markov Model for speech	93	O(n2)	5	Dynamic
Self Organizing Markov Model for hand	94	O(n2)	05	Dynamic
Fast Dynamic Time wrapping for speech	98	0(n/2)	10	Dynamic
Fast Dynamic Time wrapping for hand	91	O(n)	09	Dynamic

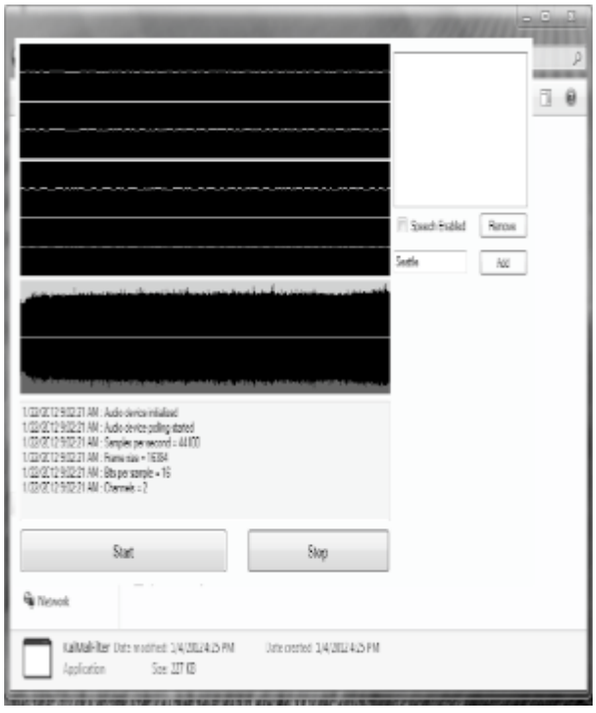

Figure 5

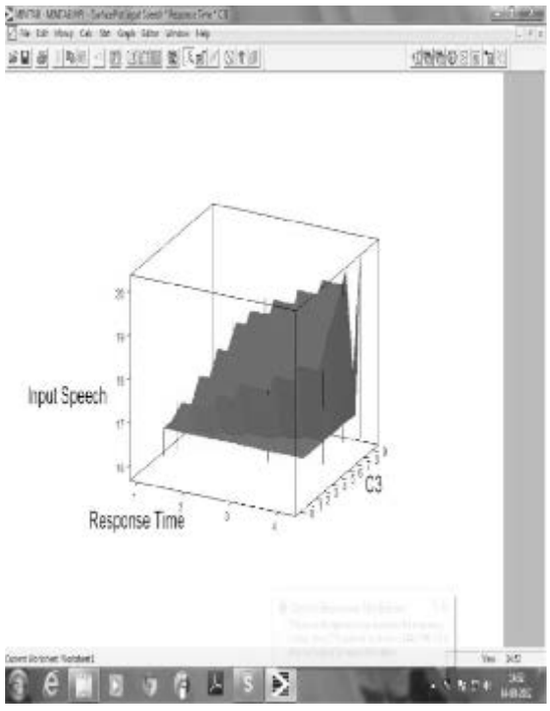

Figure 6

X –Axis : Response Time

Y-Axis : Input Speech

Z-Axis : Accuracy

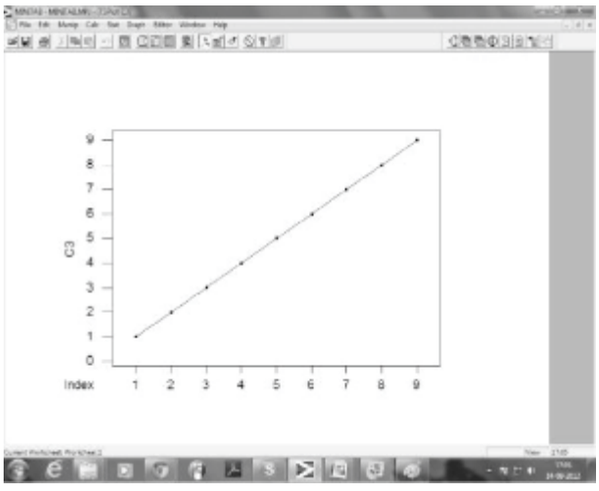

Figure 7: input speech vs. accuracy increases drastically

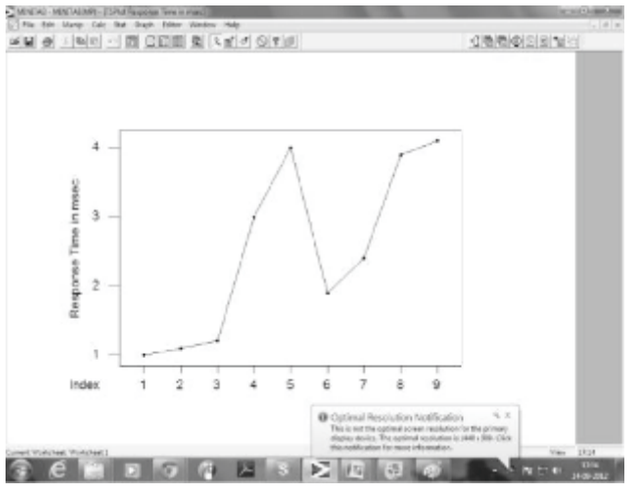

Figure 8: input speech vs. response time

A filter that is inserted in an alternating-current power line to block noise interference that would otherwise travel through the line

in either direction or affect the operation of receivers. A filter used in a radio receiver to reduce noise, usually an auxiliary low-pass filter which can be switched in or out of the audio system.

4.CONCLUSION

Different algorithms are compared and Fast DTW is concluded to be the efficient method. This algorithm is simple and independent of user characteristics. In the project limited number of gestures and speech commands are used. Nine Gestures used are [Left Hand in horizontal, Left hand diagonal down, Left diagonally up, Left hand up, Right Hand in horizontal, Right hand diagonal down, Right diagonally up, Right hand up and Both hands in horizontal position].

Ten speech commands used are Move Up, Move Down, Move To Right, Move To Left, Zoom, Crop. Select 1, Select 2, Select 3.This multimodal system allows user to select any one mode at a time either speech or hand gesture. Depending upon the requirement the mode can be selected.

This project works with 98% accuracy for speech and 91% accuracy for gestures. It works in non uniform background.

Increasing gestures and speech commands will allow a greater degree of control for the end user.

REFERENCES

1. S.A.Chhabria,Dr. R.V.Dharaskar," Multimodal Interface for disabled Persons", International Journal of Computer Science & Communication.vol. 2, Issue-I, March 2011.pp. 223-228.(ISSN:0973-7391)
3. S.A.Chhabria,Dr. R.V.Dharaskar,and Dr. V.M.Thakre "Multimodal Interpretation Gesture Recognition System: A Review" , Published in A International Journal of Computer Applications, NCRTC, NUMBER-7, ARTICLE 8,PP-NO. 397-401.
3. S.A.Chhabria, Dr. R.V.Dharaskar, Nutan Son wane,"Speech and gesture recognition using SOM with markov model", vol. 1. International Journal of research in image, video and signal processing, pp.61–64.
4. S.A.Chhabria, Dr. V.M.Thakre,Annuradha Bhutt,"HCI using speech and Hand Gesture", International Conference on Information computing and Telecommunication-IRNet ,Delhi, 1st-2nd April 2012
5. Yan Meng and Yuyang Zhang and Yaochu Jin "Autonomous Self Reconfiguration of Modular Robots by evolving a Hierarchical Model",2011.
6. Boucher.R.Canal, T.Q.Chu, A.Drogoul, B.Gaudou, V.T.Le, V.Moraru, N.Van Nguyen, Q.A.N.Vu.P.Tailandier,F.Sempe and S.Stincjwich."A Real-Time Hand Gesture system based on Evolutionary Search" in safety, security rescue robotics (SSRR),2011 IEEE International Workshop on page 16.
7. Boukje Habets, Sotaro Kita,Zeshu shao,Asli Ozyurek, and Peter Hagoort, "The Role of Synchrony and Ambiguity in Speech-Gesture Integration during comprehension"2011.
8. Rami AbielmonaEmilm Petriu, Moufid Harb and Slawo e solkowki, "Mission diven robotics for territorial security "IEEE transaction on Computational Intelligence Magzine,2011.
9. M.segers,James Connan, , "Real-time gesture recognition using Eigenvectors" Vaughn Private Bag X17 Bellville,7535,volume III,2009 .
10. Marcelo Worsley and Michael Johnston "Multimodal interactive spaces: magictv and magic map "IEEE vol 978-1-4244- 7903-2010

AN ELEMENTAL TESTING METHODOLOGY OF SECURED KEY-EXCHANGE RECOGNITION BY USING BIDIRECTIONAL ASSOCIATIVE MEMORY

Mahamaya Mohanty*
Dronacharya College of Engineerng,
Knowledge Park-III,Greater Noida,Uttar Pradesh,201308,India
E-mail: mahamayamohanty@yahoo.co.in
Corresponding author

Abinash Panda
CSC India Pvt. Ltd,Banglore560071,India
E-mail: abinashpanda84@gmail.com

ABSTRACT

The main objective of the topic is to test the keys exchanged among two parties are recalled or not to maintain a secured process. For adapting this new technique we have used the bidirectional associative memory which stores the patterns in pairs, so that when one pattern is given as an input ,its respective pattern in the pair is the output. Similarly when one person is sending the encrypted message to another person ,the other person should have the key in the respective pair to decrypt the message from which he can ensure that he has received the correct message thus securing the process of encryption and decryption. It is planned to implement this technique to test the expert systems with the use of Context Sensitive Asynchronous Memory Models (CSYM) and also to implement in mining based applications including time series analysis.

Keywords: *Associative memory, Bidirectional Associative Memory, Diffie-Hellman, Key-Exchange Methodology, Recall Pattern,Recognition, Neural Associative Memory.*

1. INTRODUCTION

The memory of human being is essentially associative. When we attempt to establish a chain of associations, we can restore a lost memory. When we associate memories with each other, we need a recurrent neural network capable of accepting an input pattern on one set of neurons and producing a related, but different, output pattern on another set of neurons. The Neural Associative Memories (NAM)[1][2] are the models of neural network consisting of neuron like and synapse-like elements. At any given point in time the state of the neural network is given by the vector of neural activities, it is called the activity pattern. Neurons always update their activity values based on the inputs they receive (over the synapses). In the simplest neural network models the input-output function of a neuron is the identity function or a binary in the form of active or inactive. The information to be processed by the neural network [3] is represented by an activity patterns. Thus, activity patterns are the representations of the elements processed in the network. The synapses in a neural network are the links between neurons or between neurons and fibers carrying external input. A synapse transmits pre synaptic activity to the postsynaptic site. In the neural network models each synapses has an associated weight value and the postsynaptic signal is simply the product of pre synaptic activity and weight. The input of a neuron is then the sum of the postsynaptic signals of all synapses connecting the neuron. Hence , information is processed in a neural network by activity spread.. In neural associative memories the learning provides the storage of a (large) set of activity patterns during learning, the memory patterns.

2. BASIC CONCEPTS

2.1 Bidirectional Associative Memory (Bam) : The Bidirectional Associative Memory is considered to be a type of recurrent neural network. There are two types of associative memories known as auto-associative and hetero-associative. BAM is hetero-associative, meaning given a pattern it can return another pattern which is potentially of a different size. It is similar to the Hopfield network in that they are both forms of associative memory. However, Hopfield nets return patterns of the same size.The Bidirectional associative memory[4] is heteroassociative, content-addressable memory. A BAM consists of neurons arranged in two layers say A and B. The neurons are bipolar binary. The neurons in one layer are fully interconnected to the neurons in the second layer. There is no interconnection among the neurons in the same layer. The weight from layer A to layer B is same as the weights from layer B to layer A. dynamics involves two layers of interaction. As the memory process information in time and involves the bidirectional data flow, it differs in principle from a linear association, although both networks are used to store

association pairs. It differs from the recurrent auto associative memory in its updated mode.It contains two layers of neurons named as X and Y. In layer X and Y are fully connected with each other. Once the weights are established, input into layer X presents the pattern in layer Y, and vice versa.

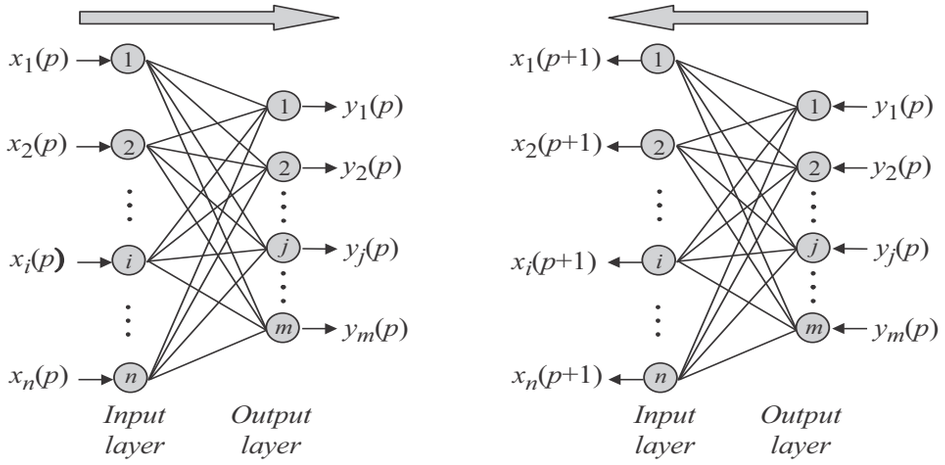

(*a*) Forward direction. (*b*) Backward direction.

Fig 1. BAM Operation

2.2 Diffie-Hellman Key Exchange

The protocol [5] allows two users to exchange a secret key over an insecure medium without any prior secrets.

2.2.1 Some Preliminaries of Key Exchange Method

- An element g is called a generator of a group G if every element in G can be expressed as the product of finitely many powers of g.
- If p - 1 is an integer, then the numbers coprime to p, taken modulo p, form a group with multiplication as its operation. It is written as (Z/pZ)× or Z p*.
- This group is cyclic and any generator, g, of the group is called a primitive root mod p.
- The number of invertible elements modulo n is denoted by f(n).
- The function f is called Euler's Totient function or Euler's f-function.
- In particular, f(p) = p – 1.
- Suppose g is a primitive root mod p. If gx ^{a} y (mod p), then the discrete logarithm or index of y (to the base g) is indg(y) = x mod (f(p)).

2.2.2 The Setup

- Suppose we have two people [12][19]wishing to communicate: Alpha and Beta.
- They do not want Eve (eavesdropper) to know their message.
- Alpha and Beta agree upon and make public two numbers g and p, where p is a prime and g is a primitive root mod p.

Note: Anyone has access to these numbers.

2.2.3 The Exchange Method:

- Alpha chooses a random number a and computes u ^{a} ga (mod p), and sends u to Beta.
- Beta chooses a random number b and computes v ^{a} gb (mod p), and sends v to Alpha.
- Beta computes the key k ^{a} ub ^{a} (ga)b (mod p).
- Alpha computes the key k ^{a} va ^{a} (gb)a (mod p).
- Now, both Alpha and Beta have the same key, namely k = gab (mod p).

3. WORKING OF BIDIRECTIONAL ASSOCIATE MEMORY AND DIFFIE- HELLMAN KEY EXHANGE

Let us assume the some examples to demonstrate the working of Bidirectional Associative Memory and Diffie-Hellman key Exchange before proposing the methodology.

3.1 Working of Bidirectional Associative Memory: The basic idea behind the BAM is to store the pattern pairs so that when there are n-dimensional vector X from set A is presented as input, the BAM recalls m-dimensional vector Y from set B, but when Y is presented as input, the BAM recalls X. To develop such type of BAM, we need to create a correlation matrix for each pattern pair that we want to store. The matrix product of the input vector X, and the transpose of the output vector YT is the correlation matrix . The BAM is the weight matrix which has the sum of all correlation matrices, that is, $\mathbf{W}=\sum_{m=1}^{M}\mathbf{X}_m\mathbf{Y}_m^T$ where M is the number of pattern pairs to be stored in the BAM.

3.1.1 Procedure of Learning : Imagine we wish to store two associations, A1:B1 and A2:B2.

- A1 = (1, 0, 1, 0, 1, 0), B1 = (1, 1, 0, 0)
- A2 = (1, 1, 1, 0, 0, 0), B2 = (1, 0, 1, 0)

These are then transformed into the bipolar forms:

- X1 = (1, -1, 1, -1, 1, -1), Y1 = (1, 1, -1, -1)
- X2 = (1, 1, 1, -1, -1, -1), Y2 = (1, -1, 1, -1)

From there, we calculate $M = \sum {}^tX_iY_i$ where ${}^tX_i$ denotes the transpose. So,

$$M = \begin{bmatrix} 2 & 0 & 0 & -2 \\ 0 & -2 & 2 & 0 \\ 2 & 0 & 0 & -2 \\ -2 & 0 & 0 & 2 \\ 0 & 2 & -2 & 0 \\ -2 & 0 & 0 & 2 \end{bmatrix}$$

3.1.2 Recall : To retrieve the association A1, we multiply it by M to get (4, 2, -2, -4), which, when run through a threshold, yields (1, 1, 0, 0), which is B1. To find the reverse association,we multiply this by the transpose of M.

3.2 Working Of Diffie-Hellman Key Exchange Method

3.2.1 Procedure of Key Exchange

1. User Authentication: Alpha encrypts the message, m, with her private key a, call it ma.
2. Alpha encrypts ma with Beta's public key, v, and sends the message to Beta.
3. Beta recovers ma using his private key b and recovers m by using Alpha's public key u.
4. Thus, Beta is sure that only Alpha could have sent the message.

3.2.2 Demonstration With An Example

1. Suppose Alpha and Beta agree to use p = 47 and g = 5.
2. Alpha chooses a number between 0 and 46, say a = 18.
3. Beta chooses a number between 0 and 46, say b = 22.
4. Alpha publishes ga (mod p), i.e. u = 518 (mod 47) = 2.
5. Beta publishes gb (mod p), i.e. v = 522 (mod 47) = 28.
6. If Alpha wants to know the secret key k, she takes Beta's public number, v = 28, and raises it to her private number, a = 18 (taking the result mod 47).
7. This gives her: 28^18 (mod 47) = 24.
8. If Beta wants to know the secret key, he takes Alpha's public number, u = 2, and raises it to his private number, b = 22 (taking the result mod 47).
9. This gives him: 2^22 (mod 47) = 24.
10. Thus, Alpha and Beta have agreed upon a secret key, k = 24.

4. PROPOSED METHODOLOGY FOR RECOGNITION AND RECALL OF DIFFIE-HELLMAN KEY EXCHANGE USING BAM OF NEURAL NETWORK

The proposed methodology of an information processing perspective is based on three main stages in the formation and retrieval of memory:

- In the first stage encoding or registration (receiving, processing and combining of received information).
- Secondly storage (creation of a permanent record of the encoded information) .
- Finally retrieval, recall or recollection (calling back the stored information in response to some cue for use in a process or activity).

Step 1: When two keys are exchanged between two trusted parties for ensuring the security of the message it forms a pair. As seen in BAM for A1 we have B1, for A2 we have B2 are different recall patterns, thus we form different pairs of keys for different messages to be transmitted among different users .

Step 2: Like recall patterns we can form many number of pairs of keys.

Step 3: When one key is given the other one can be recalled by using BAM of Neural Network.

Step 4: When two keys between two persons gets matched they are restored for secured message exchanging purpose.

Step 5: If there is an arbitration/distortion/mismatch in the recall pattern of BAM then it can be deduced hat wrong key has been shared for the message or the third party has changed the content of the message.

Step 6: This proposed technology helps in testing of the security for the message hat is transmitted between different pairs of parties.

5. CONCLUSION

Here it is shown how various associative memories which are being used in various applications in recent trends. Here it is illustrated by using it in Diffie-Hellman Key Exchange for retrieving the correct pair of keys used during the exchange method of encryption and decryption. Memory is not just a passive store for holding ideas without changing them; it may transform those ideas when they are being retrieved. There are examples that shows what is retrieved is different from what was initially stored. It has been always seen simple associative memories are static and very low memory so that they cannot be applied in the applications where high memory is required. Dynamic Associative memories such as Hopfield, BSB, and BAM are Dynamical memories but they are also capable of supporting very low memory, so they cannot be applied in the applications where high memory requirements are there. A simple model describing context-dependent associative memories generates a good vectorial representation of basic logical calculus. The most powers of the vectorial representation is the very natural way in which binary matrix operators are capable to compute ambiguous situations. This fact represents the very natural way in which the human mind is able to take decisions in the presence of uncertainties. These memories could also be used to develop expert agents to the recent problem domain.

REFERENCES

1. Dr. B D C N Prasad, P E S N Krishna Prasad and Y Sagar, "A Comparative Study of Machine Learning Algorithms as Expert Systems in Medical Diagnosis (Asthma)" CCSIT 2011, Part I, CCIS 131, pp. 570–576, 2010.
2. Andres Pomi and Fernando Olivera, BioMed Central. "Context-Sensitive Auto-Associative Memories as Expert Systems in Medical Diagnosis"
3. Bart Kosko "Neural Networks and Fuzzy Systems - A dynamical Systems Approach to Machine Intelligence" –
4. Z.B. Xu, Y.Leung and X.W.He "Asymmetrical Bidirectional Associative Memories", IEEE Transactions on systems, Man and cybernetics, Vol.24, PP.1558-1564, Oct.1994
5. Ueli M. Maurer and Stefan Wolf (March 2000). "The Diffie–Hellman Protocol". Designs, Codes, and Cryptography (Springer-Verlag) 19 (2–3): 141–171. http://www.springerlink.com/content/r74n758123752440/. Retrieved 2008-09-28.
6. D. Boneh and R. J. Lipton, Algorithms for black-box fields and their application to cryptotography in Advances in Cryptology – CRYPTO 96, (N. Koblitz, ed.), Lecture Notes in Computer Science 1070, Springer, pp. 283–297, 1996.
7. Muzereau, N. P. Smart and F. Vercauteran, The equivalence between the DHP and DLP for ellipti curves used in practical applications, LMS J. Comput. Math., 7, pp. 50–72, 2004. See [www.lms.ac.uk].
8. D. R. L. Brown and R. P. Gallant, , The Static Diffie–Hellman Problem, IACR ePrint 2004/306.
9. V. I. Nechaev, Complexity of a determinate algorithm for the discrete logarithm, Mathematical Notes, 55 (2), pp. 165–172, 1994.
10. V. Shoup, Lower bounds for discrete logarithms and related problems in Advances in Cryptology – EUROCRYPT 97, (W. Fumy, ed.), Lecture Notes in Computer Science 1233, Springer, pp. 256–266, 1997.
11. Feng Bao. Robert Deng, Huafei Zhu (2002). "Variations of Diffie–Hellman problem". ICICS (Springer-Verlag). http://www.i2r.a

star.edu.sg/icsd/publications/Baofeng_2003_Variations%20of%20Diffie%20Hellman%20problems.pdf. Retrieved 2005-11-23.
12. Dan Boneh (1998). "The Decision Diffie–Hellman Problem". ANTS-III: Proceedings of the Third International Symposium on Algorithmic Number Theory (Springer-Verlag): 48–63. http://theory.stanford.edu/~dabo/papers/DDH.ps.gz. Retrieved 2005-11-23.
13. Emmanuel Bresson and Olivier Chevassut and David Pointcheval (2003). "The Group Diffie–Hellman Problems". SAC '02: Revised Papers from the 9th Annual International Workshop on Selected Areas in Cryptography (Springer-Verlag): 325–338. http://www.di.ens.fr/~bresson/papers/BreChePoi02b.pdf. Retrieved 2005-11-23.
14. Eli Biham and Dan Boneh and Omer Reingold (1999). "Breaking generalized Diffie–Hellman modulo a composite is no easier than factoring". Information Processing Letters (Elsevier North-Holland) 70 (2): 83–87. doi:10.1016/S0020-0190(99)00047-2. http://www.wisdom.weizmann.ac.il/~reingold/publications/CGDH.PS. Retrieved 2005-11-23.
15. Michael Steiner and Gene Tsudik and Michael Waidner (1996). "Diffie–Hellman Key Distribution Extended to Group Communication". ACM Conference on Computer and Communications Security: 31–37. http://citeseer.ist.psu.edu/steiner96diffiehellman.html. Retrieved 2005-11-23.
16. Whitfield Diffie and Martin E. Hellman (November 1976). "New Directions in Cryptography". IEEE Transactions on Information Theory IT-22 (6): 644–654. http://citeseer.ist.psu.edu/diffie76new.html. Retrieved 2005-11-23.
17. Diffie, W. and Hellman, M. "New Directions in Cryptography." IEEE Trans. Info. Th. 22, 644-654, 1976.
18. Hershey, J. E. Cryptography Demystified. New York: McGraw-Hill, pp. 162-166, 2003.
19. Schneier, B Applied Cryptography: Protocols, Algorithms, and Source Code in C, 2nd ed. New York: Wiley, pp. 513-516, 1996.
20. Satish Kumar. "Neural Networks, A Classroom Approach”
21. Jeffrey Blustein. "The Moral Demands of Memory"
22. Martin T. Hagan, Howard B. Demuth, Mark Beale. "Neural Network Design"

INCREASING PRODUCTION CAPACITY OF HEAT SHRINK TUBING OPERATION THROUGH DEVICE RECONFIGURATION

Sang June Oh*
Assistant Professor, Department of Mechanical Engineering
California State University Fullerton, Fullerton, CA 92831, USA
Email: sjoh@fullerton.edu, TEL: +1 657-278-2458
Corresponding author

Hieu Luong
Graduate Student, Department of Mechanical Engineering
California State University Fullerton, Fullerton, CA 92831, USA

ABSTRACT

The objective of this paper is to present a device reconfiguration of heat shrink tubing operation to increase production capacity of bonding PTFE shrink tubing over stainless steel hypodermic tube and stainless steel wire. The existing laminator unit uses a sealed linear actuator to traverse a single port thermal nozzle along specified linear path while holding the unassembled PTFE tube, hypodermic tube and stainless wire with a clamp mechanism. An upgrade of the existing heat shrinking operation was necessary since the existing production capacity of these hypotube assembly was unable to meet the increased in market demand. Increasing the number of laminators was not an option due to limited resources, and facilitating the speed control parameters of the laminator could not improve the production rate as desired. The only viable option was to redesign the laminator itself. Through revamped design of the clamp mechanism and the heating nozzle in the laminator, the production capacity of the hypotube assembly increased by a factor of four times. The reconfiguration method presented in this paper can easily be applied to any heat shrink tubing operation because of its simplicity and minimal reconfiguration cost.

Keywords: *heat shrinking operation, hypodermic tube, heat shrink tubing, PTFE shrink tubing.*

1.INTRODUCTION

Many of the devices used in the medical industry require a process that bonds a plastic tube to a stainless steel hypodermic tube. For simplicity, this process will be referred as the outer jacket (OJ) heat shrinking process throughout the paper. Some history of the heat-shrinking process can be viewed in [1], although the current heat shrinking technology is quite different compared to twenty years ago [2][3]. The components that are processed during the OJ heat shrinking operation are a stainless steel core wire, a PTFE shrink tube, and a stainless steel hypodermic tube. The core wire runs along the inner diameter of the assembly. The hypodermic tube goes over the core wire while the PTFE tube covers both the core wire and the hypodermic tube, and extends past the distal end of the hypodermic tube. The SolidWorks image of the assembly components is shown in Figure 1. In any medical device, the distal end refers to the furthest point on the device from the user. On the other hand, the proximal end refers to the point closest to the user during actual use. The actual existing laminator used in this research study is a BEAHM laminator, readily available in the industry. A SolidWorks model is illustrated in Figure 2. Once the components are aligned, they are clamped into a horizontal BEAHM laminator where heat is used to bond the Polytetrafluoroethylene (PTFE) tube to the hypodermic tube. This layout of components in the BEAHM laminator is shown in Figure 3.

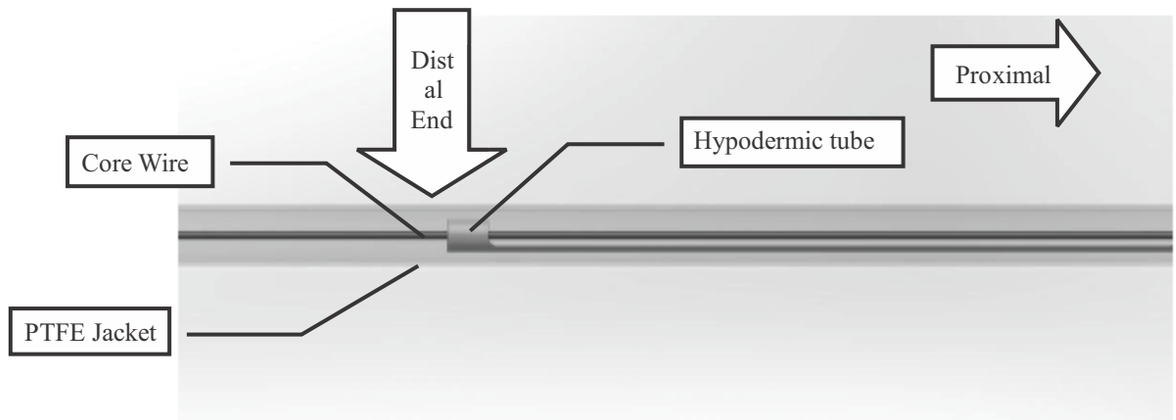

Figure 1. Image of the assembly components

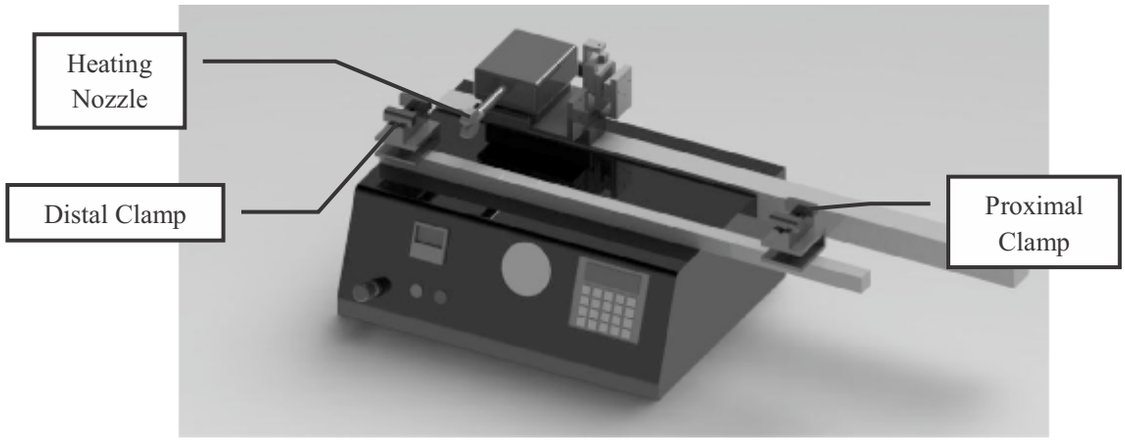

Figure 2. Image of existing BEAHM laminator

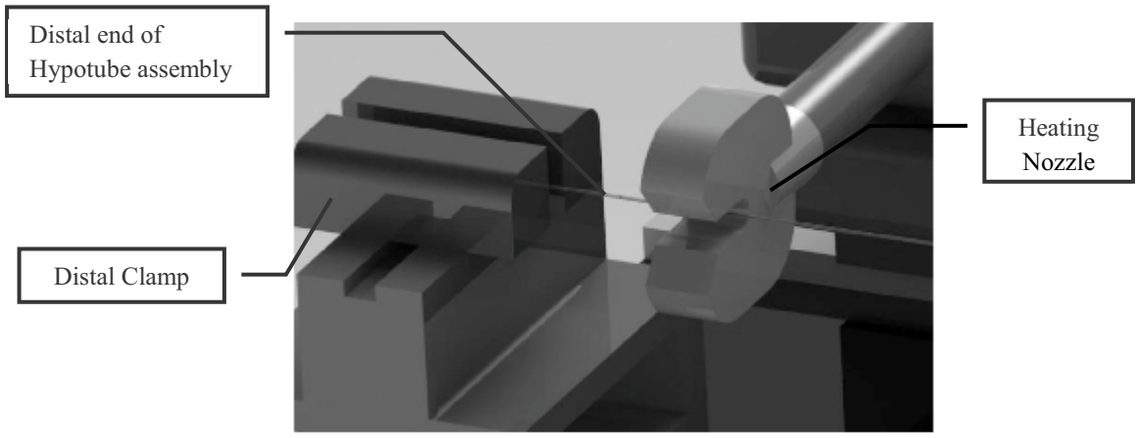

Figure 3. Placement of Hypotube assembly in BEAHM laminator

The process starts with the distal end of the core wire and PTFE shrink tube being clamped into the left side of the laminator. At this point of the process, the hypodermic tube is still able to slide freely in the assembly. Care must be taken when handling the assembly as the hypodermic tube may slide proximally which would cause an incorrect bond. After the distal end is clamped, the heat shrinking cycle is started. When the nozzle passes over the distal end of the hypodermic tube, the PTFE tube would shrink over the hypodermic tube, bonding the two together. Once bonded, tension is applied to the proximal end of the unit before it is secured with the proximal clamps. The assembly is clamped in tension so that it will align with the heater nozzle. Each laminator is capable of one unit per program cycle. Unfortunately, this capacity is unable to meet the production demands. A need to address this shortage was the motivation of this research study. Remember, the objective of this research was to increase the capacity of the OJ heat shrinking operation. The major constraint of this was that it could not increase the footprint of the production line. This process was performed inside a clean room and since space is limited, additional floor space for this project was not allowed. In addition, one 1.8 meter by 1.8 meter table could accommodate only one heat laminator. No additional BEAHM heat laminator was allowed due to limited resources.

2. DESIGN METHODOLOGY AND ANALYSIS

The simplest possible solution to increase the capacity of the heat laminator is to raise the speed of the operating machine. However, limitation in speed of the linear actuator to traverse the thermal nozzle along a specified path will not significantly increase the productivity. A wide range of laminar processing parameters was available; however, this again did not increase the output rate. In essence, modifying processing parameters only marginally increased the throughput, which was still insufficient to meet demand. The next viable option was to redesign parts of the laminator in order to process multiple hypotube assembly per machine operating cycle. In order to achieve this, it required redesigning of the clamping mechanism, heating nozzle, and a separate control box. However, this paper will focus only on the clamping mechanism. Based on the forecasted volumes it was determined that four units per heat shrinking cycle would satisfy the demand.

2.1 Distal Clamp Synthesis: In order to ensure that all units receive the proper amount of heat, each unit must be held flat and straight during the heat shrinking process [4]. This could not be achieved with the original pneumatic gripper. Therefore, a new clamping mechanism was required. Please observe Fig. 3 for the placement of the hypotube assembly in the laminator before the operation. The design requirement for the distal (left) clamp was: it must hold the assembly part for the entire shrinking process; all clamps must be accessible to the operator; each unit must be clamped individually; each clamp must open and close

individually; and finally the clamp must be adjustable in order to align with the heating nozzle. Given these requirements, the use of miniature pneumatic cylinders to clamp the parts was sought. The pneumatic clamps would hold the part for the entire process unless there is a loss of pneumatic pressure, in which case the entire equipment and the heat source would also be compromised. With the small profile of the miniature pneumatic cylinders, the clamps can be designed such that they are close together, which would minimize the overall size of the nozzle. The stroke of the pneumatic cylinders helps make each clamp accessible to the operator. With a programmable logic controller (PLC), the pneumatic cylinders could be activated individually as necessary. The original T-slot aluminum frame was utilized for the adjustability of the clamp. This frame allowed the clamps to be adjustable in the X coordinate direction. For additional adjustability in the coordinates Y and Z direction, the brackets were slotted perpendicular to the axis of the T-slot frame and mounted to a micrometer stage. This allowed the user to be able to adjust the location of the clamp to match the heating nozzle. An image of the clamp redesign can be found in the Figures 4 and 5.

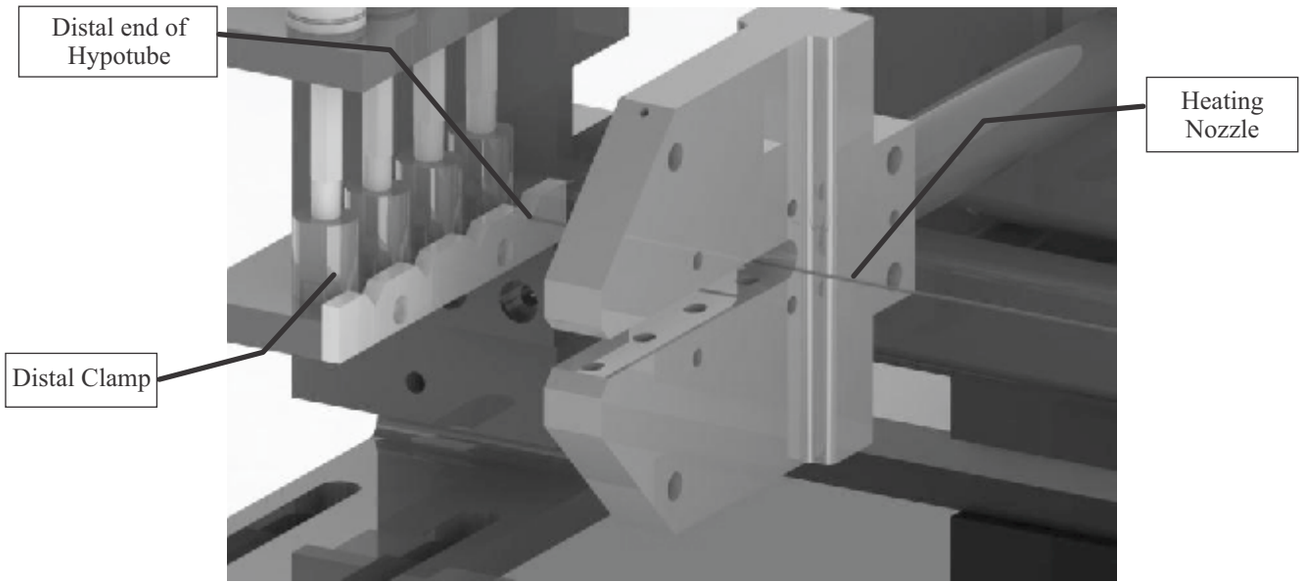

Figure 4. Close up view of clamp redesign

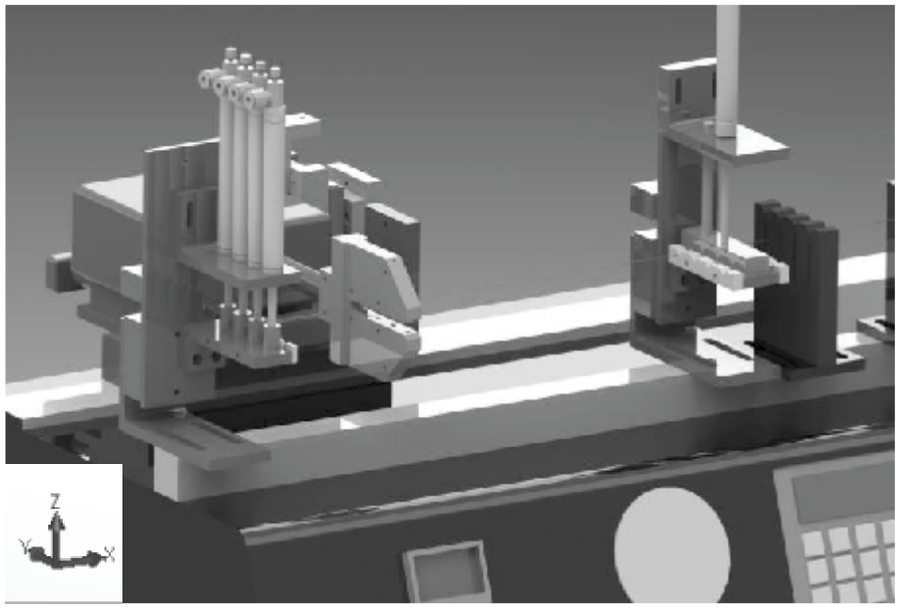

Figure 5. Overall view of the clamp redesign (both the distal and proximal clamp is shown)

The distal side of clamp mechanism was designed such that the operator would be able to access to all four clamping locations from one side of the equipment. With this, the clamping bracket and pneumatic cylinder can be modeled as a cantilever beam with an evenly distributed load. The cantilever beam stress equation and deflection equation were used to determine the proper material for the clamp brackets. Equation (1) was used to calculate the stress while Equation (2) was used to calculate the deflection [5].

$$\sigma = \frac{Mc}{I} \tag{1}$$

where σ stress, M = bending moment, and I = distance from the neural axis to the top of the beam.

$$y = -\frac{\omega L^4}{8EI} \tag{2}$$

where y = deflection distance, ω = distributed load, L = length of the beam, I = moment of inertia, and E = modulus of elasticity.

The dimension of the clamp can be found in Figure 6. The analysis assumes a line pressure of 689.5 kPa and a cylinder bore size of 1.27 cm. The materials used in the analysis were Delrin, 6061-T6 Aluminum, and 304 Stainless Steel.

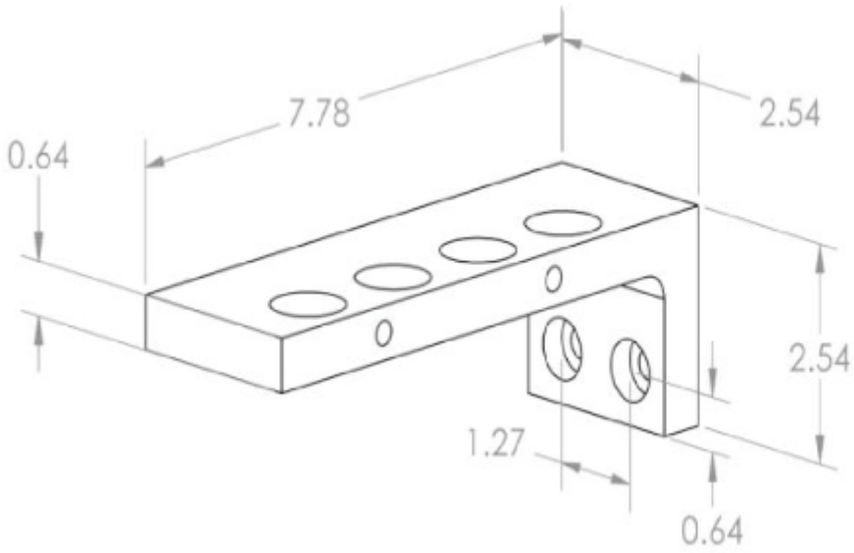

Figure 6. An overall dimensional drawing (in cm) for the cantilever bracket

2.2 Distal Clamp Analysis: The analysis was performed assuming that the four pneumatic cylinders form an even distributed load over the top face of the bracket. To simplify the analysis, the short leg of the bracket was assumed fixed to the wall. The beam length analyzed was 7.78cm. The summary of the analytical solution can be found in Table 1. From the three choices of material, Delrin is easy to machine but cannot sustain the required tensile strength. In addition, the amount of deflection is undesirable. Stainless steel would satisfy the tensile strength requirements and has very little deflection. However, it is harder to machine and is heavier than both Delrin and Aluminum. Aluminum also satisfies the strength requirement with little deflection. Given its strength to weight ratio [6], it is the most desirable material for the bracket.

Table 1. The summary of the analytical solution for the stress and deflection for the cantilever bracket

Material	Modulus of Elasticity	Yield Strength	Stress	Deflection
Delrin	2900 MPa	63 MPa	79.60 MPa	1.308 cm
6061 T6 Aluminum	69000 MPa	275 MPa		0.055 cm
304 Stainless steel	190000 MPa	206.81 MPa		0.020 cm

In order to confirm the analytical solution, a simple finite element analysis (FEA) was performed on the model with SolidWorks. The first analysis was performed with the same simplified assumption as the analytical solution: the entire right flat face of the model was assumed fixed. However, the forces modeled in the FEA were slightly different from the analytical solution. Instead of applying the load evenly over the entire length of the bracket, it was applied according to the actual size and location in the Y coordinate direction of the clamp contact. The applied loads were placed in the center of the bracket in the X coordinate direction in order to mimic the analytical model. The cross sectional areas of the pneumatic clamps were used to generate the area of the load applied to the bracket. The results from this analysis can be found in Table 2.

Table 2. The results of an FEA using SolidWorks: fixed location at the far right wall

Material	Stress	Deflection
Delrin	82.3 MPa	1.346 cm
6061 T6 Aluminum	82.7 MPa	0.056 cm
304 Stainless steel	81.2 MPa	0.021 cm

A second FEA was performed on the model according to the actual loads and constraints during use. The loads applied in this model were the actual size and location of the clamp contact on the bracket. The constraints in this analysis were applied to counter bored holes on the short leg of the bracket. The results of the analysis can be found in Table 3.

Table 3. The results of an FEA analysis using SolidWorks simulation: fixed location at the screw

Material	Stress	Deflection
Delrin	200.9 MPa	2.514 cm
6061 T6 Aluminum	193.9 MPa	0.107 cm
304 Stainless steel	197.7 MPa	0.039 cm

Although the numerical answers differ from the analytical solutions and the first FEA analysis, the general trends were observed to be the same. The stress does not change with material and the largest point of deflection is at the tip of the bracket. The actual stress and deflection in the bracket were higher in the second FEA due to the location of the constraints, as expected. An image of the model is shown in Fig. 7 and Fig. 8.

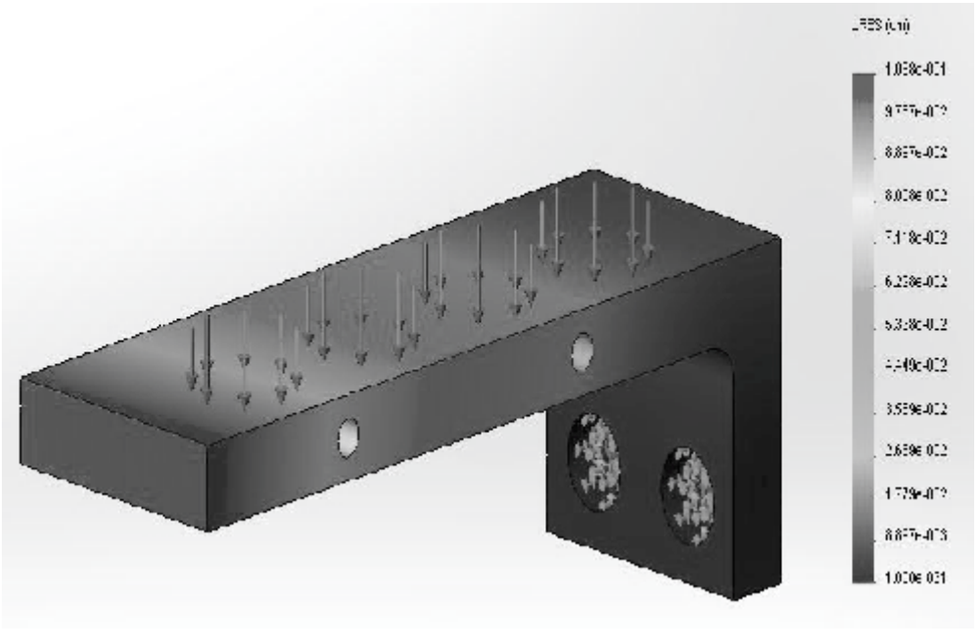

Figure 7. An image of the deflection in the bracket: the analysis was performed using an aluminum bracket

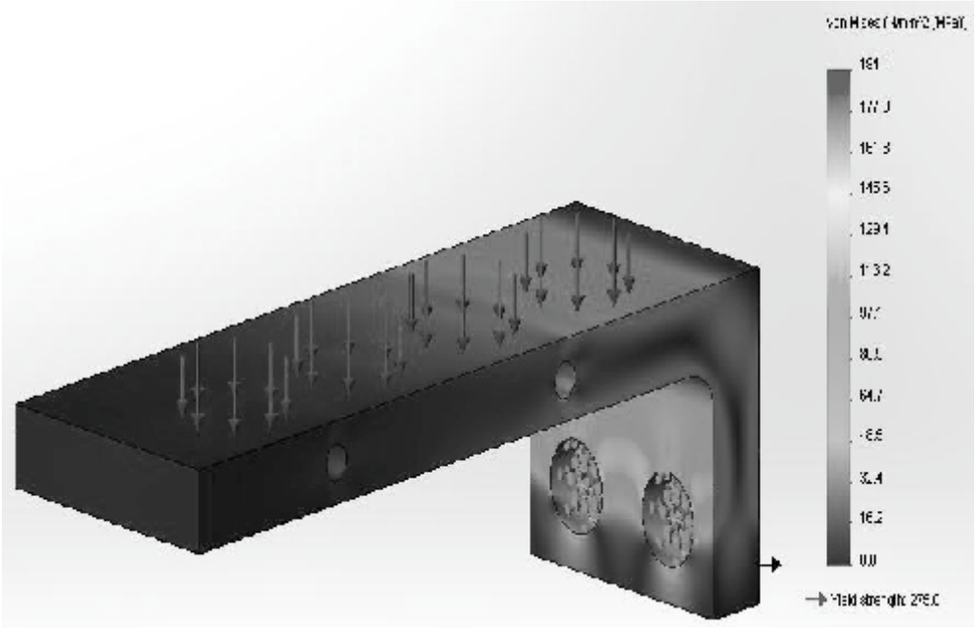

Figure 8. An image of the stress in the bracket: he analysis was performed on an aluminum bracket

2.3 Proximal Clamp Design: The requirements for the proximal clamp (right side clamp) were similar to the distal clamp (left side clamp). Therefore, the initial design was a duplicate of the distal clamps. However, after the initial assessment, this was not an efficient design due to the subtle complexity of the process. The process called for each assembly unit to be clamped into the distal clamp one at a time. Once the shrinking process started and the distal portion of the PTFE tube bonded with the distal end of the hypodermic tube, the operator would apply tension to the units to keep them straight and flat prior to securing them.The process of applying tension and securing the proximal ends of each assembly can be done at the same time. Therefore, it would only be necessary to have one clamp on the proximal end. The design illustrating this is shown in Figure 9. One slight concern with this is that if tension was applied to all four units at the same time with one hand, the proximal end of the unit would converge to the location of where tension is applied, which would cause misalignment with the heating nozzle. Therefore, a block

was designed that separates the individual units into their respective locations. The block was placed proximal of the proximal clamp but distal to where tension was applied. The proximal clamp is set up such that once each unit is clamped into the distal clamp, the proximal end of the unit is placed into its respective slot in the distal guide block then into the proximal guide block. Once the heater nozzle bonds the PTFE tube to the hypodermic tube, the operator would hold the units proximal of the proximal guide block and apply tension. Both guide blocks align the units into their respective locations prior to the operator activating the proximal clamp.

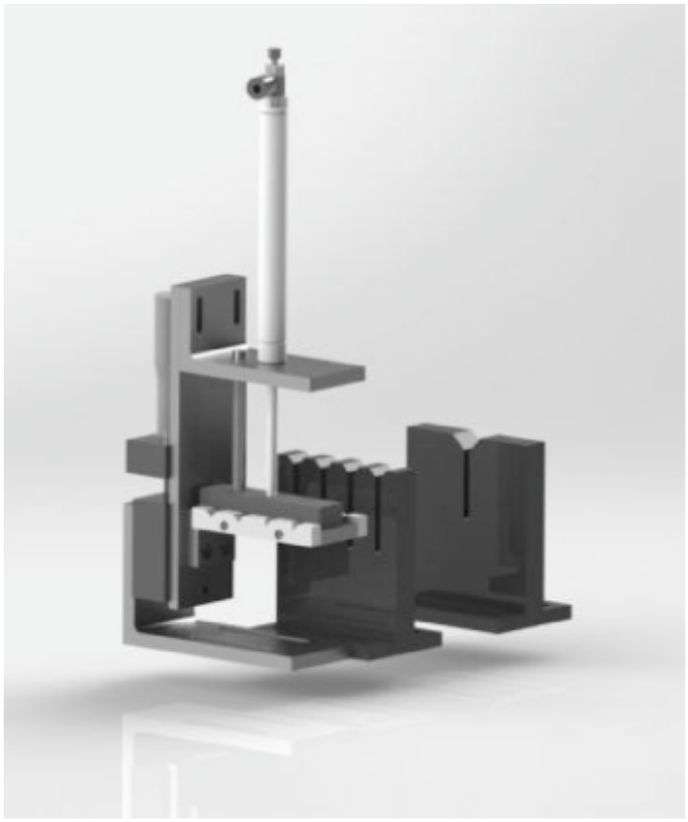

Figure 9. An image of the proximal clamp and guide blocks.

2.4 Proximal Clamp Analysis: Similar to the distal clamp bracket, the proximal bracket also forms a cantilever beam. The proximal bracket dimension and constraints are identical to the distal bracket. The only difference between the two is the load due to the clamps: instead of four pneumatic cylinders, there is only one. The analytical solution assumes that the right flat face of the bracket is fixed. The results for the stress and deflection for this bracket is organized in Table 4 for the three different materials.

Table 4. The summary of analytical solution for the stress and deflection for the cantilever bracket

Material	Stress	Deflection
Delrin	21.28 MPa	0.327 cm
6061 T6 Aluminum		0.014 cm
304 Stainless steel		0.005 cm

An FEA was performed in order to confirm the analytical solution. The FEA model was also simplified to show the correlations between the analytical solution with the FEA analysis. As expected, for the stress and deflection from FEA closely match the analytical solution. All materials analyzed are within the yield requirement of the bracket. However, the deflection in Delrin was

undesirable, as it will cause misalignment with the heating nozzle. For reasons similar to the distal bracket, stainless steel was not selected. Aluminum satisfies the yield requirement and has minimal deflection. Therefore, it was the material of choice.

Table 5. The results of FEA using SolidWorks: fixed location at the right wall

Material	Stress	Deflection
Delrin	22.0 MPa	0.313 cm
6061 T6 Aluminum	22.1 MPa	0.013 cm
304 Stainless steel	21.8 MPa	0.005 cm

A second FEA model was performed in order to determine the actual stresses and deflection during actual use. The forces applied in this model were identical to the first FEA. However, the constraints were applied to the counter bored holes instead of the right flat face. The results from this analysis can be found in Table 6.

Table 6. The results of FEA using SolidWorks simulation: fixed location at the screw

Material	Stress	Deflection
Delrin	44.9 MPa	0.548 cm
6061 T6 Aluminum	43.7 MPa	0.023 cm
304 Stainless steel	44.7 MPa	0.008 cm

The resulting stress and deflection are approximately double of the simplified model, which were similar pattern of results found in the distal clamp case. The difference in the results between the first and second FEA is due to the location of the constraints. By constraining the bracket at the location of the counter bored holes, the bracket is allowed to flex more and the moment arm is larger, which results in a higher displacement and stress.

3. CONCLUSION

The research presented in this paper was undertaken to increase the production capacity of heat shrink tubing operation, bonding PTFE tube over hypodermic tube and stainless wire under various constraints. Through reconfiguration of clamp mechanisms and heating nozzles, the production capacity increased by a factor of four. The advantages of the method presented in this paper are its simplicity of implementation and cost effectiveness in reconfiguration. In addition, the method also did not require increased space in the production process. The analytical solution for stress and deflection in the cantilever beam used in modeling clamping bracket and pneumatic cylinder agreed well with the FEA, enabling the selection of aluminum as the best material for the clamping bracket. To further increase the production capacity of the heat laminator, optimizing the programming logic controllers for pneumatic cylinders in the clamping mechanism or heating nozzle can be sought.

REFERENCES

1. Kraus, R. & Ryan, D., Advances in Heat-Shrink Technology, IEEE Electrical Insulation Magazine, Vol. 4, No. 3, May/June 2009, p. 31-34
2. Beahm, A., Catheter Bonding Technology Overview, BEAHM Designs, April, 20012
3. Beahm, B. & Ward, J., New Catheter Tipping Process Aids Tubing's Accuracy and Throughput, Medical Design Technology (online: www.mdtmag.com), June 30, 2005
4. Kucklick, T., The Medical Device R&D Handbook, CRC Press, Taylor & Francis Group, 2006
5. Beer, F., Johnston, E.R., Dewolf, J. & Mazurek, D., Mechanics of Materials, McGraw-Hill, 5th Edition, 2009
6. Askeland, D.R. & Fulay, P.P., Essentials of Materials Science and Engineering, CL Engineering, 2nd Edition, 2008

YTTERBIUM FIBER LASER PARAMETER OPTIMIZATION DURING DRILLING OF Al/15 wt%Al_2O_3-MMC

Arindam Ghosal*
Research Scholar, PEC, University of Technology, Chandigarh, India,
Email: er_ghosal@yahoo.co.in
Corresponding author

A. Manna
Associate Professor, PEC, University of Technology, Chandigarh, India

A. K. Lall
Professor, PEC, University of Technology, Chandigarh, India

ABSTRACT

This paper presents experimental study into the influence of machining parameters of Ytterbium fiber laser during drilling of Al/15wt%Al2O3-MMC. The response surface methodology (RSM) is used to achieve optimum responses i.e. minimum tapering and maximum material removal rate (MRR). A comprehensive mathematical model for correlating the interactive and higher-order influences of Ytterbium fiber laser machining parameters such as laser power, modulation frequency, gas pressure, wait time, pulse width on metal removal rate and tapering phenomena has been developed for achieving controlled over fiber laser machining process. Test results reveal that MRR is increased with decrease of wait time and laser power. At wait time 17.5 s and laser power 500 w the MRR is maximum i.e 0.23 g/s. Due to less wait time, the possibility of heat loss is less so MRR increases.

Key word: *Ytterbium fiber laser machining, MRR, Hole tapering.*

1.INTRODUCTION

An Ytterbium laser machine YLR 1000 with CNC system RP 3015 was used for experiments. The experimental scheme has been designed in such a way as to explore the influence of the various predominant laser machining process parameters, based on response surface methodology to obtain the optimal scheme for multi-variable experimentation and to perform investigations for exploring the interactive and higher order effects of the various parameters on the most important machining characteristics. Fig.1 shows Ytterbium laser drilling setup used for drilling of Al/15 wt%Al_2O_3-MMC work-piece.

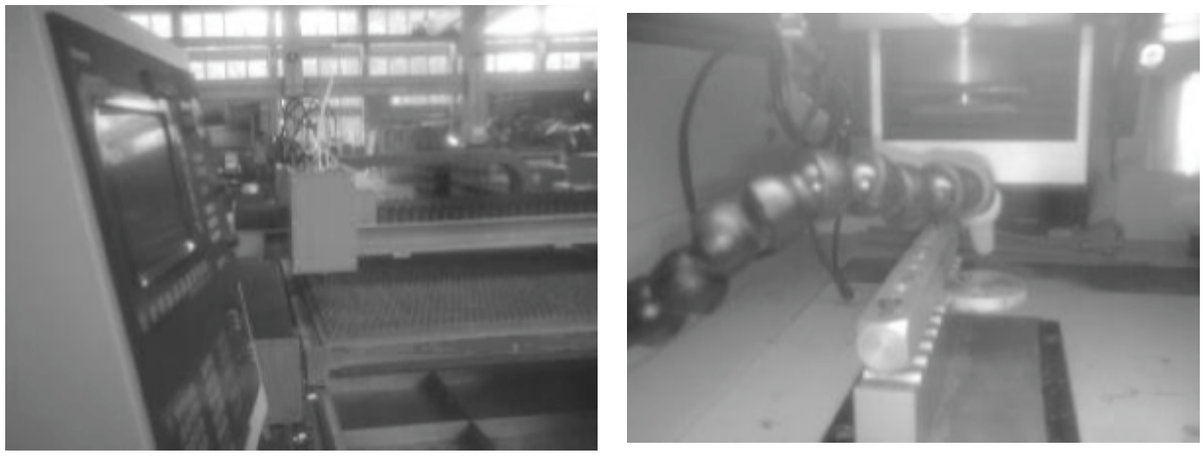

Fig. 1 Ytterbium laser drilling is done on Al- 15 wt % Al_2O_3 MMC

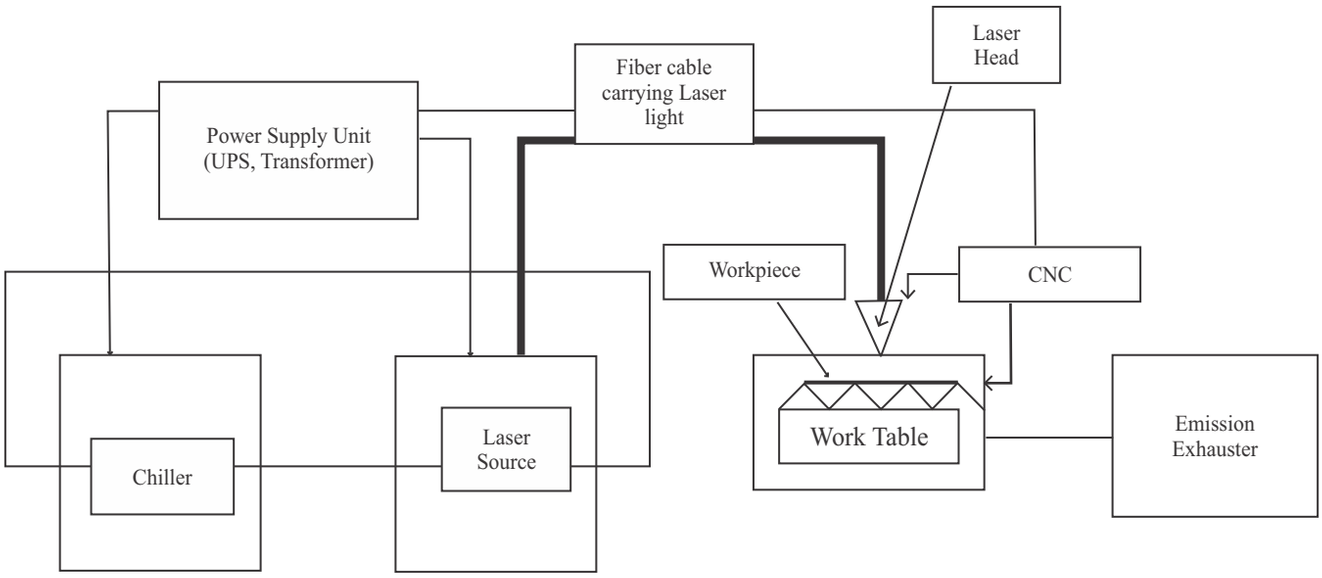

Figure 2: ytterbium fiber laser block diagram

Table 1 Machining parameters, actual setting values and their coded levels

Sr.No.	Machining Parameters	Symbol	Units	Level				
				-2	-1	0	1	2
1	Laser power (W)	x_1	Watt	400	500	700	900	1000
2	Modulation frequency(Hz)	x_2	Hz	600	700	800	900	1000
3	Gas pressure (bar)	x_3	bar	15	16	17	18	20
4	Wait time (s)	x_4	s	0.1	0.15	0.2	0.25	0.3
5	Pulse width (%)	x_5	%	75	80	90	95	100

Table 1 represents the different parameters such as laser power, modulation frequency, gas pressure, wait time, pulse width and their levels considered for experimental investigation. The range of input variables and their initial setting

values are coded for simplification of experimental data analysis. Based on few trail experiments the coded levels of different input variables are decided (Table 1).

$$Taper, radian = [Tan^{-1} \frac{(D - d)}{2.t}]. \frac{\pi}{180}. \quad \text{.....Eqn.1}$$

Where, D = Measured diameter at top of the machined hole, mm; d = Measured diameter at bottom of the machined hole, mm; t = Thickness of the work-piece, mm

2. MATHEMATICAL MODELING AND PROCESS OPTIMIZATION An experimental plan for studying the relationship between the controllable parameters and the various machining criteria has been made based on central composite second-order rotatable design is shown in Table 2. Table 2 also represents the experimentally obtained results for response 1 and response 2, i.e. MRR and hole taper respectively.

2. MATHEMATICAL MODELLING AND PROCESS OPTIMIZATION

Experiment no.	X_1	X_2	X_3	X_4	X_5	Response1 (MRR) g/s	Response2(Taper) rad
1	-1	-1	-1	-1	1	0.205	0.0006
2	1	-1	-1	-1	-1	0.218	0.0003

Experiment no.	X_1	X_2	X_3	X_4	X_5	Response1 (MRR) g/s	Response2(Taper) rad
3	-1	1	-1	-1	-1	0.217	0.0010
4	1	1	-1	-1	1	0.216	0.0011
5	-1	-1	1	-1	1	0.209	0.0012
6	1	-1	1	-1	1	0.208	0.0010
7	-1	1	-1	-1	1	0.192	0.0010
8	1	1	1	-1	-1	0.203	0.0011
9	-1	-1	-1	1	-1	0.210	0.0006
10	1	-1	-1	1	1	0.294	0.0005
11	-1	1	-1	1	1	0.204	0.0005
12	1	1	-1	1	-1	0.211	0.0005
13	-1	-1	1	1	1	0.211	0.0004
14	1	-1	1	1	1	0.211	0.0005
15	-1	1	1	1	-1	0.205	0.0008
16	1	1	1	1	1	0.205	0.0008
17	-2	0	0	0	0	0.209	0.0008
18	2	0	0	0	0	0.203	0.0009
19	0	-2	0	0	0	0.210	0.0010
20	0	2	0	0	0	0.203	0.0011
21	0	0	-2	0	0	0.205	0.0004
22	0	0	2	0	0	0.208	0.0006
23	0	0	0	-2	0	0.210	0.0011
24	0	0	0	2	0	0.203	0.0008
25	0	0	0	0	-2	0.203	0.0013
26	0	0	0	0	2	0.247	0.0009
27	0	0	0	0	0	0.203	0.0009
28	0	0	0	0	0	0.209	0.0012
29	0	0	0	0	0	0.203	0.0014
30	0	0	0	0	0	0.215	0.0012
31	0	0	0	0	0	0.203	0.0009

2.1 Mathematical Models for Mrr and Taper Considering five variables (Table 1) and utilizing the experimental results from 63 experiments (i.e. 31 experiments x 3-replication of each experiment), and according to the equation 4 the mathematical models for MRR and taper angle are developed. The developed mathematical model based on RSM for correlating the MRR with various predominant laser machining process parameters as considered in the experimental design as follows,

$$Y_{MRR} = 0.197 - .011.x_1 + .017\ x_2 - 0.012.x_3 - .015.x_4 - 0.024x_5 - .020.x_1.x_2 - .050x_1.x_3 + .009\ x_1.x_4 + .013\ x_1.x_5 + .066\ x_2.x_3 - .029\ x_2.x_4 - .017\ x_2.x_5 + .051.x_3.x_4 + 0.021\ x_3.x_5 + 0.017x_4.x_5 + .002\ x_1^2 + .002.x_2^2 + 0.007x_3^2 + 0.001.x_4^2 + 0.025x_5^2 \quad \text{.....Eqn.3}$$

Similarly, the developed mathematical model for taper is

$$Y_{Taper} = 0.001 - 7.7E\text{-}05.x_1 - 0.0001.x_2 + 0.0002.x_3 - 0.0004.x_4 - 0.0003.x_5 + 0.0002\ x_1.x_2 - 6.1E\text{-}05.x_1.x_3\ 0.00037.x_1.x_4 + 0.00037.x_1.x_5 - 0.0007\ x_2.x_3\ 9.5E\text{-}05.x_2.x_4 + 0.0003.x_2.x_5 - 0.0003x_3.x_4 + 0.0007.x_3.x_5 + 8.1E\text{-}05.x_4.x_5 - 0.0002.x_1^2 - 7.99E\text{-}05.x_2^2 - 0.0006.x_3^2 - 0.0001x_4^2 - 7.6E\text{-}05.x_5^2$$

2.2 Analysis of Variance and Model Fitment Test The analysis of variance (ANOVA) test has been performed to test the adequacy of the developed models for establishing the mathematical link between the response and the machining parameters of laser machining process. The ANOVA test module has been designed to estimate the sum of squares of the response into the contribution due to the second order and a lack of fit component which measures the deviations of the responses from the fitted surface as well as a measure of the experimental errors.

Table 3 Results of analysis of variance for MRR and Taper:

Source f o variation	Degree of freedom	Sum of squares		Mean square		F-value	
		Eqn. 3	Eqn. 4	Eqn. 3	Eqn. 4	Eqn. 3	Eqn. 4
Second-order terms	20	0.00869	2.361E-06	0.000434926	1.180E-07		
Lack of fit	6	0.00059	1.280E-07	9.975E-05	2.134E-08	6.0312	3.7352
Experimental errors	4	0.00012	0.000000188	3.064E-05	0.000000047		
Total	30	0.009419631	2.677E-06				

From Table 3, as per the second order term, it is concluded that the laser power, modulation frequency, gas pressure, wait time, pulse width are significantly influencing for controlling MRR and taper as their P-value 0.0029 and 0.0183 respectively, and both are less than 0.05. The F-test values for both the responses at 95% confidence level are 6.0312 and 3.7352 respectively. The R2 value for MRR is 0.92. The value of R2(adj) for MRR is 0.77. These values are above the average value and developed second order models fits the data, therefore, the data for both the response are well fitted in the developed second order models.

3. PARAMETRIC ANALYSIS ON MACHINING CHARACTERISTICS OF YTTERBIUM FIBER LASER

The influences of the various process parameters of Ytterbium fiber laser on both the responses i.e. MRR and taper during laser machining of 5 mm thick Al/15wt.%Al2O3-MMC have been analyzed based on the developed mathematical modes established utilizing response surface methodology (RSM).

3.1 Parametric influence on MRR From Fig-3 it is seen that MRR increases with increase of modulation frequency and decrease of laser power at modulation frequency. At 950 Hz modulation frequency and 500 W laser power MRR is maximum.

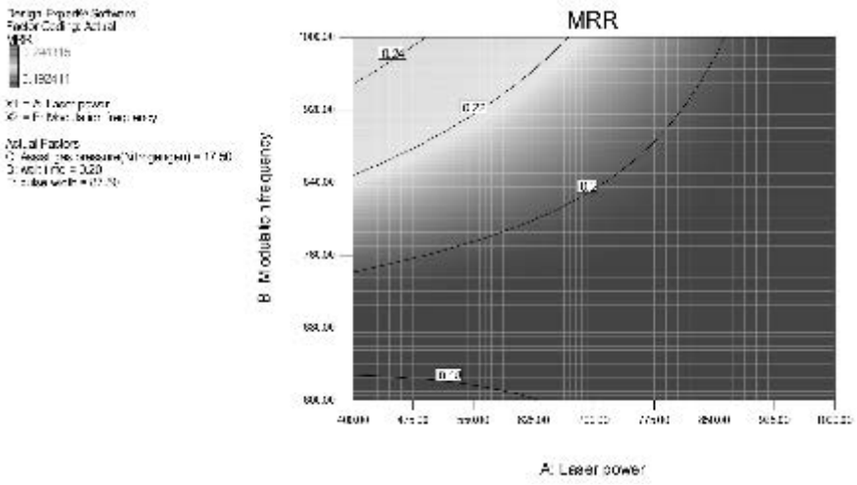

Fig3, effects of modulation frequency and laser power on MRR

Fig 3 shows that MRR is increased with decrease of wait time and laser power. At wait time 17.5 s and laser power 500 w the MRR is maximum i.e 0.23 g/s. Due to less wait time, the possibility of heat loss is less so MRR increases.

4. TAPER (MIN) OPTIMISATION

Fig 4 shows that, at high wait time and low laser power the hole taper is minimum. At wait time 0.28 s and laser power 500 W the hole taper is zero

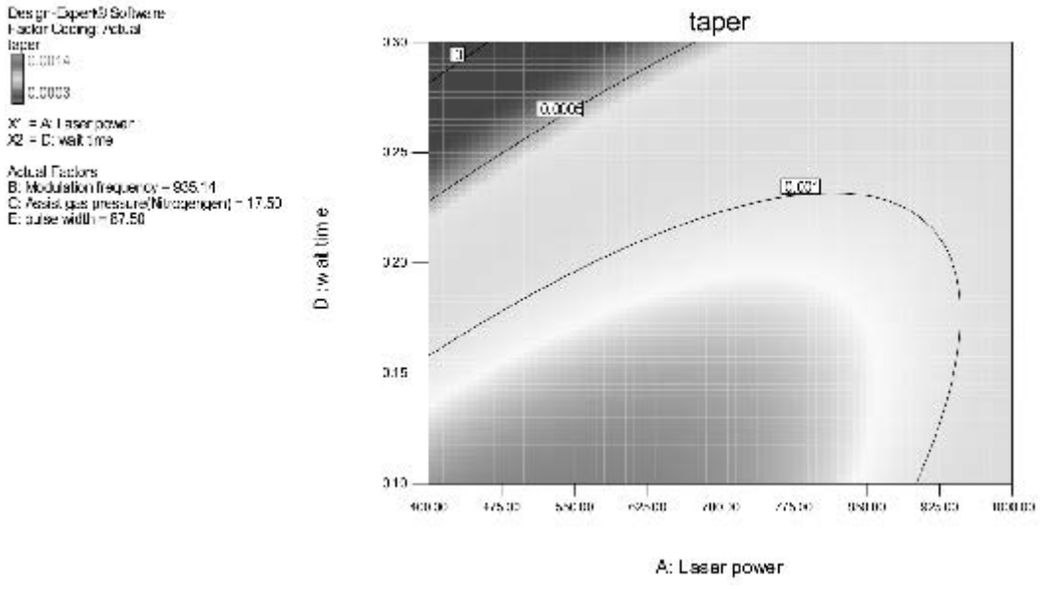

Fig 4, effects of wait time and laser power on taper

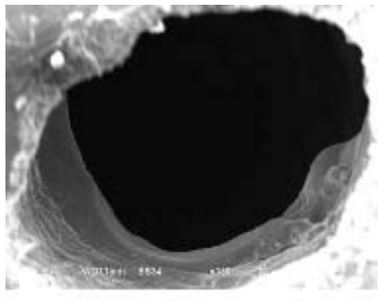

Fig5 SEM photograph of drilled laser hole

5. CONCLUSION

Based on the machining of Al/15wt%Al2O3-MMC by Ytterbium fiber laser the following outcome can be concluded on the basis of the developed mathematical relations as follows:

(I) It is seen that MRR is increased with decrease of wait time and laser power. At wait time 17.5 s and laser power 500 w the MRR is maximum i.e 0.23 g/s. Due to less wait time, the possibility of heat loss is less so MRR increases.

(ii) It is seen that MRR increases with increases of pulse width and modulation frequency. At 98% pulse width and 1000 Hz modulation frequency, the MRR is maximum i.e. 0.24g/s.

(iii) It is seen that, at high wait time and low laser power the hole taper is minimum. At wait time 0.28 s and laser power 500 W the hole taper is zero.

REFERENCES

1. Benyounis K.Y, Olabi A.G, Hashm M.S.J., Optimizing the laser welded butt joints of medium carbon steel using RSM, Journal of Materials Processing Technology, 164-165, (2005) 986-989.
2. Cronjager L.; Meister D.; (1992), Machining of fibre and particle-reinforced aluminum Ann.CIRP, 41(1), 63-66.
3. Kacer K.; Muthe M.; AKman E.; Demir A.; Candan L.; Canel T; Gunay V.; and Sinmazcelek T.; (2009) Characterization of drilling Alumina ceramic using Nd:YAG pulsed laser, "Journal of material processing technology", Vol-209 (4), pp 2008-2014
4. Manna.A. ; Bhattacharyya B.; (2003), A study on machinability of Al/SiC-MMC, Journal of Materials Processing Technology, 140, 711-716.
5. Miranda, R M., Structural analysis of heat affected zone of marble and lime stone tiles cut by CO2 laser, Materials Characterization, 53 (2004) 411-417. .

APPLICATION OF MADM USING AHP FOR THE JUSTIFICATION OF MATERIAL AND PROCESS SELECTION: A CASE STUDY

Dattatraya Bhise
Dronacharya Group of Institutions, Greater Noida, India
Email:dvbhise@rediffmail.com

ABSTRACT

Rapidly changing technology and shorter product life cycles are forcing small enterprises to invest in new products and processes that meet global competition. But due to the paucity of financial resources, lack of skills appropriate to the technology and inability to conduct a detailed information search significantly increases technical, financial, business and personal risk of these small enterprises. These organizations have neither the time nor the dedicated specialists available to investigate medium to long term investment alternatives as thoroughly as they would like under these conditions. The purpose of this paper is to provide a good insight into the use of multi-attribute decision model (MADM) that is analytic hierarchy process (AHP) in selection of material and manufacturing process while developing a new product. In this study AHP is used in decision making by an automobile manufacturing firm for material and manufacturing process selection for one of its components. Information on the use of AHP in decision making process for the selection of material and manufacturing technologies is provided and an AHP model is proposed.

Keywords: *Multi-attribute decision model; MADM; Analytical hierarchy process; AHP; Material selection,; Process selection; Decision making.*

1.INTRODUCTION

Many companies are currently strengthening their competitive position by updating the technology used for manufacturing. The selection of the appropriate technology that achieves or matches with the organization objective must be made on the basis of sound decision-making process [1]. The decision to implement new manufacturing technology is a major decision for many organizations. The success or failure of the organization could be due to this decision, and therefore it is very important that proper consideration be given to all aspects of implementation before a final commitment is made. This is necessary to ensure that all the expected benefits of the decision are realized [2].

Here a case of an automobile ancillary unit manufacturing several components of a bike like handlebar, side panels, front and rear rims, rear carrier etc. is taken up for study. Company supplies these parts to two major manufacturers of automobiles in India. Top level management of this company wants to improve the design of rear carrier (grip). Previously it was made from steel bars with welding as manufacturing process. Now the company has got an order to manufacture aerodynamically shaped, elegant looking, eye catching rear grip. Today with recent advances in materials technology there are several materials as well as variety of manufacturing processes available at the disposable of engineers. However the problem is how to select an appropriate material and process that suits the characteristics of the product as well as organizations overall strategy. So to solve this complex problem the company decided to hire the services of a consultant. The consultant after discussion with the engineers decided to use multi-attribute decision model (MADM) using analytic hierarchy process (AHP) to pick the appropriate material and manufacturing process for the rear grip.

Developing a decision making model for the material and process selection is particularly useful for small companies. The paucity of financial resources, lack of skills appropriate to the technology and inability to conduct a detailed information search significantly increases technical, financial, business and personal risks. Small companies have neither the time nor the dedicated specialists available to investigate medium to long term investment alternatives as thoroughly as they would like under these conditions. The small firms tend to have a flatter organizational structure, fewer strata and shorter chain of command and hands-on-managers who are occupied with the day to day operation and have less time than corporate planners to devote to medium and long term strategic planning [3]. Small firms do not have the knowledge or time to evaluate technology potential [4].

In large enterprises, the technological needs as well as the technological assets of the com any are the sole responsibility of persons and even a whole department, whereas in smaller companies similar activities are sometimes undertaken usually on ad-hoc basis (5). Improving the productivity of small companies can best be achieved by helping them make better techno-logical decisions [6]. The material and process selection decision making model can facilitate and expedite the decision making process.

2. MATERIAL AND PROCESS SELECTION: AN OVERVIEW

In the early stages of designing a component, the designer is faced with many decisions among which are the selection of the most appropriate material, and the most appropriate manufacturing route - meaning one that is capable of forming the selected material to the desired shape economically. Both have a major impact on performance and manufacturing cost. Process selection, however,

has received less attention.

The selection of a suitable manufacturing process often involves considering the complex coupling between characteristics of the design, the material and the process. Whilst most materials can be well described by a common set of properties, enabling selection for a given design on the basis of these properties alone, the same is only partially true for process selection. The most discriminating characteristics of processes are often specific to the class of process. For example, very different questions arise when selecting a casting process than when selecting a welding process, so the information needed to answer these questions is mostly specific to each process class. Furthermore, the data and information needed to capture these characteristics can be strongly influenced by the class of material being processed -there is limited scope for selecting a welding process for aluminium, or steel, or polymers from a generic welding selector that does not have material-specific data. [7].

M. Ferrante; S.F. Santos; J.F.R. de Castro (2000) [8] pointed out that materials selection is a multidisciplinary activity, which cuts across a large number of professional expertise. As a consequence, it draws together people with different backgrounds ranging from the essentially technical to the non-technical, such as marketing for instance.

N.A. Gjosten; (1995), [9] described motivation for material selection can be either the realization of a completely new product or, more frequently, the substitution of an existing material. In the latter case, better performance and cost reduction can be the main driving forces for the process, but malfunction, weight reduction, feasibility of recycling and processibility, are also frequent motivations. Taking weight reduction, for instance, its importance makes it one of the main targets for design improvements and materials selection, particularly in the automotive industry.

Generally any material selection event must consider a large number of materials candidates and premature exclusions have to be avoided. Also, when facing a materials selection problem, engineers are normally asked to choose a solution which fulfills more than one objective, that is, not only lower weight, but (for instance) low cost, good fatigue resistance and better fabricability, as well.

3. ANALYTIC HIERARCHY PROCESS

AHP is based on the innate human ability to make sound judgments about small problems. It facilitates decision-making by organizing perceptions, feelings, judgments and memories into a framework that exhibits the forces that influence a decision. The AHP has been applied in a variety of decisions and planning projects in nearly 20 countries [10].

3.1 Three steps of AHP methodology The AHP methodology is explained in Saaty's (1990) book. A general approach to enable the reader to follow the paper with ease is given below.

Step 1 (structuring the hierarchy). Group related components and arrange them into a hierarchical order that reflects functional dependence of one component or a group of components on another. The approach of the AHP involves the structuring of any complex problem into different hierarchy levels with a view to accomplishing the stated objective of a problem.

Step 2 (performing paired comparisons between elements/decision alternatives). Construct a matrix of pair-wise comparisons of elements where the entries indicate the strengths with which one element dominates another using a method for scaling of weights of the elements in each of the hierarchy levels with respect to an element of the next higher level. Use these values to determine the priorities of the elements of the hierarchy reflecting the relative importance among entities at the lowest levels of the hierarchy that enables the accomplishment of the objective of the problem, comments Albayrakoglu, M (1996), Chan, F.T.S. et all(2000) [11,12]. The scale used for comparisons in AHP enables the decision maker to incorporate experience and knowledge intuitively. and indicates how many times an element dominates another with respect to the criterion. The decision maker can express his preference between each pair of elements verbally as equally important, moderately more important, strongly more important, very strongly more important, and extremely more important. Reciprocals of these values are used for the corresponding transposed judgments [13].

Table 1: Pair-wise comparison values

1	Objectives i and j are of equal importance
3	Objective i is weakly more important than j
5	Objective i is strongly more important than j
7	Objective i is very strongly more important than j
9	Objective i is absolutely more important than j
2,4,6,8	Intermediate values

Step 3 (synthesizing results). Synthesize these priorities to obtain each alternative's overall priority. Select the alternative with the highest priority.

3.2 Development of analytic hierarchy process as applicable to the case situation Developing the performance hierarchy

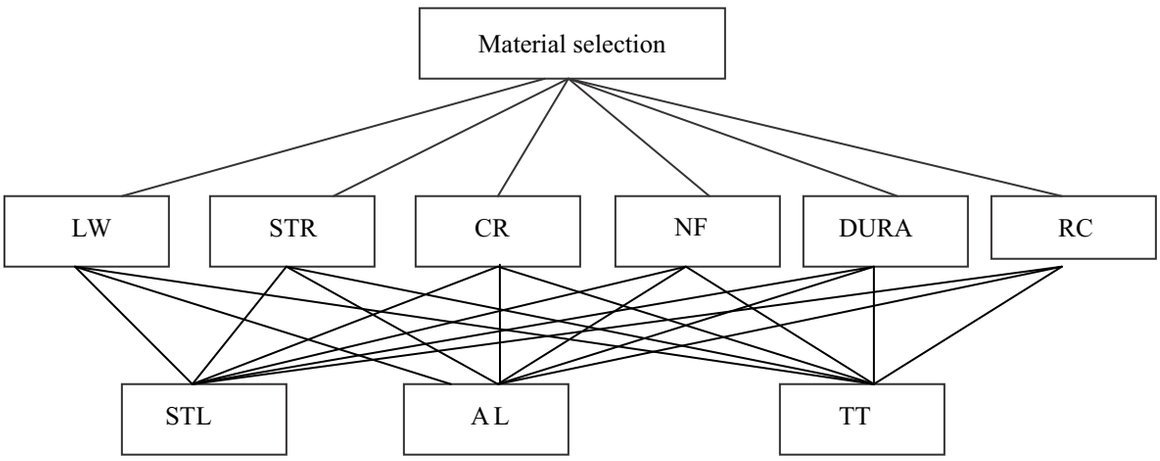

Figure 1: AHP model

Goal level: The first step of the AHP consists of developing a hierarchical structure of the assessment problem. In the case of material selection the overall objective is the selection of material from the different available materials.

Attributes level: The attributes are various factors on the basis of which the material will be selected.

Table 2: Attributes

Light weight (LW):	How light weight the material is?
Strength (STR):	How strong the material is?
Corrosion resistant (CR):	Indicates the corrosion resistant ability of the material
Nice finish (NF):	This is an indicator of the quality of the finished product that can be obtained
Durability (DURA):	This is an indicator of the durability of the material.
Reasonable cost (RC):	This is an indicator of the cost of the raw material

Alternatives level: The decision alternatives are the different materials that suit the requirements, the engineers want to compare and evaluate. Three alternatives were selected after discussion amongst the engineers, these are: Steel, Aluminum and Titanium

The attributes are compared with each other on a pair-wise comparison. The relative weights or priorities are obtained. Highly user-friendly software, the multi-attribute decision model (MADM), has been developed for the aid to the user for pair-wise comparison of the attributes as well as for the alternatives and for analyzing the user inputs. A questionnaire was developed with respect to the case situation described earlier. A cross- section of users were asked to respond to the questionnaire for selection of the appropriate material. These responses were used as an input to the AHP model.

Using the developed program, the data were processed for 9 user responses. The user responses have finally been aggregated for final results. The relative importance and consistency of each of these attributes are given in Table 4. Similarly, from the analysis, it appears that the aluminum (AL) option is the best under the circumstances of the developed case situation (Table 4-10). Thus, it appears that otherwise the justification for aluminum (AL) would have been very difficult because of the trade-offs between Steel, titanium and AL.

Table 3: Pairwise comparisons for different attributes

	1	2	3	4	5	6	eigen-vector
1 Light-weight	1	5	1	1	3	3	0.263
2 Strength	1/5	1	1/5	1/3	1	1/3	0.057
3 Corrosion resistant	1	5	1	3	3	3	0.316
4 Nice finish	1	3	1/3	1	3	1	0.168
5 Durable	1/3	1	1/3	1/3	1	1	0.081
6 Cost	1/3	3	1/3	1	1	1	0.116

eigen value = 6.221
C.I. = 0.044
C.R. = 0.036

Table 4: Comparing the alternatives with respect to the attribute lightweight

	1	2	3	4	5	6	eigen-vector
1 Light-weight	1	5	1	1	3	3	0.263
2 Strength	1/5	1	1/5	1/3	1	1/3	0.057
3 Corrosion resistant	1	5	1	3	3	3	0.316
4 Nice finish	1	3	1/3	1	3	1	0.168
5 Durable	1/3	1	1/3	1/3	1	1	0.081
6 Cost	1/3	3	1/3	1	1	1	0.116

eigen value = 3.039
C.I. = 0.019
C.R. = 0.033

Table 5: Comparing the alternatives with respect to the attribute strength

Strength

	1	2	3	eigen-vector
1 Steel	1	5	3	0.637
2 Aluminium	1/5	1	1/3	0.105
3 Titanium	1/3	3	1	0.258

eigen value = 3.039
C.I. = 0.019
C.R. = 0.033

Table 6 : Comparing the alternatives with respect to the attribute corrosion resistant

Corrosion resistant

	1	2	3	eigen-vector
1 Steel	1	1/3	1/5	0.114
2 Aluminium	3	1	1	0.405
3 Titanium	5	1	1	0.481

eigen value = 3.029
C.I. = 0.015
C.R. = 0.025

Table 7 : Comparing the alternatives with respect to the attribute nice finish

Nice finish

	1	2	3	eigen-vector
1 Steel	1	1/3	1/3	0.143
2 Aluminium	3	1	1	0.429
3 Titanium	3	1	1	0.429

eigen value = 3.000
C.I. = 0.000
C.R. = 0.000

Table 8 : Comparing the alternatives with respect to the attribute durability

Durability

	1	2	3	eigen-vector
1 Steel	1	3	3	0.600
2 Aluminium	1/3	1	1	0.200
3 Titanium	1/3	1	1	0.200

eigen value = 3.000
C.I. = 0.000
C.R. = 0.000

Table 9 : Comparing the alternatives with respect to the attribute reasonable Cost

Reasonable Cost

	1	2	3	eigen-vector
1 Steel	1	1/3	1/5	0.105
2 Aluminium	3	1	1/3	0.258
3 Titanium	5	3	1	0.637

eigen value = 3.039
C.I. = 0.019
C.R. = 0.033

Table 10: Final weightages for different alternatives

Material selection process ►

1 Steel	0.184
2 Aluminum	0.420
3 Titanium	0.396

↕ ↔move Edit matrix, ESC: exit, Report 3 figs in () are weights

The weightage for aluminum as seen from table 11 is slightly higher than titanium and so aluminum is selected as a material for manufacturing rear grip.

4. MANUFACTURING PROCESS SELECTION

Similarly for manufacturing process selection the AHP model is developed and the results are as follows:

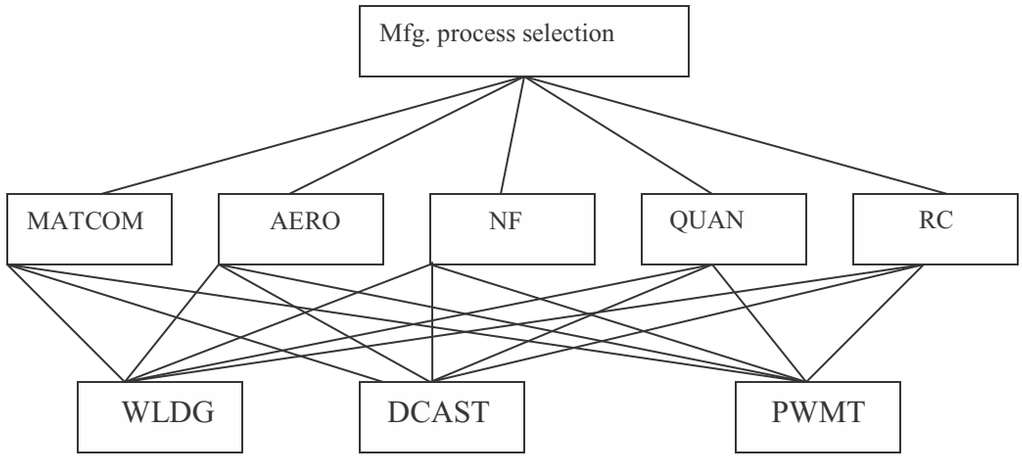

Fig 2: AHP model for mfg. process selection

Table 11: Pairwise comparisons for different attributes

	1	2	3	4	5	eigen-vector
1 Material compatibility	1	1	1	5	3	0.296
2 Aerodynamic look	1	1	1	3	3	0.267
3 Nice finish	1	1	1	3	3	0.267
4 Quantity	1/5	1/3	1/3	1	1	0.080
5 Cost	1/3	1/3	1/3	1	1	0.089

eigen value = 5.031
C.I. = 0.008
C.R. = 0.007

All the three alternatives are evaluated for different attributes, the weights and consistencies are as follows:

Material compatibility

	1	2	3	eigen-vector
1 Welding	1	1/5	1/3	0.105
2 Die casting	5	1	3	0.637
3 Powder metallurgy	3	1/3	1	0.258

eigen value = 3.039
C.I. = 0.019
C.R. = 0.033

Aerodynamic look

	1	2	3	eigen-vector
1 Welding	1	1/5	1/3	0.105
2 Die casting	5	1	3	0.637
3 Powder metallurgy	3	1/3	1	0.258

eigen value = 3.039
C.I. = 0.019
C.R. = 0.033

Nice finish

	1	2	3	eigen-vector
1 Welding	1	1/5	1/3	0.105
2 Die casting	5	1	3	0.637
3 Powder metallurgy	3	1/3	1	0.258

eigen value = 3.039
C.I. = 0.019
C.R. = 0.033

Quantity

	1	2	3	eigen-vector
1 Welding	1	1/5	1	0.156
2 Die casting	5	1	3	0.659
3 Powder metallurgy	1	1/3	1	0.185

eigen value = 3.029
C.I. = 0.015
C.R. = 0.025

Cost

	1	2	3	eigen-vector
1 Welding	1	3	5	0.659
2 Die casting	1/3	1	1	0.185
3 Powder metallurgy	1/5	1	1	0.156

eigen value = 3.029
C.I. = 0.015
C.R. = 0.025

Table 12 : Final weightages for different alternatives

Manufacturing process ►

1 Welding	0.158
2 Die casting	0.598
3 Powder metallurgy	0.243

↕ ↔ move Edit matrix, ESC: exit, Report, 3figs in () are weights

From table 12 it is quite evident that the weightage for die casting is more than the other two options, so the rear grip is produced from aluminum die casting.

5. RESULTS AND RECOMMENDATIONS

With this paper an attempt is made to develop a multi-attribute decision model using AHP for selection of material and manufacturing process for a case situation. AHP software is developed for this analysis. The model developed here can be used by organizations for solving complex, multi-attribute level problems. By defining the goal and feeding the importance of different attributes to the model, it can solve complex problems quite well.

There are few limitations associated with the model developed here.

(I The goal and objective of the end user should be clear.

(ii) While making pairwise comparisons a questionnaire should be developed so that multi user responses can be obtained, these responses then can be converted to single user input. (As the model gives output depending on single user input only.)

(iii) The number of attributes and alternatives can not be too large, otherwise the pairwise comparisons will increase and the process becomes time consuming.

REFERENCES

1. Obeidat MA, Benaldy AM. (1990) An integrated model for the management of new technology. In: Karwowski W, Ra imi M, editors. Ergonomic of Hybrid Automation 11. Amsterdam: Elsevier Science, 1990, 171–9.
2. Mohd MY. Strategic approaches to CNC adoption and implementation for Malaysian Industries. Jurutera (IEM bulletin) 1996; 10:33–8.
3. Coward DG, Schott E. In: Towill DR, Cherrington JE, editors. Organizational factors Affecting the Introduction and Efficiency of AMT Operation in Small firms. A Systems Approach to AMT Deployment. London: Springer, 1993. 19–34.
4. Noori H, Radford RH. Technology transfer: challenges facing smaller companies in readings and cases in the management of between design and utilization. Homewood 11: Irwin, 1988.
5. Dankbaar, B. Technology management in Technology Contingent SMEs. International journal of Technology Management 1998;15(1/2):70–80.
6. Lefebvre LA, Harvey J, Lefebvre E. Technological experience and the technology adoption decisions in small manufacturing firms. R&D Management 1991; 21 (3):241–9.
7. Shercliff H. R. & Lovatt A. M. (2001), Selection of manufacturing processes in design and the role of process modeling, Progress in materials science, vol. 46, no. 3-4, pp. 429-459.
8. M. Ferrante; S.F. Santos; J.F.R. de Castro. Materials Selection as an interdisciplinary technical activity: basic methodology and case studies, Materials Research, 3, no.2, 1-9, 2000.
9. N.A. Gjosten; The next generation of vehicles - a materials challenge, American Institute of physics Corporate meeting, October 1995, pg 1.
10. Saaty, T.L. (1990), The Analytic Hierarchy Process, McGraw-Hill, RWS Publications, Pittsburgh, PA.
11. Albayrakoglu, M. (1996), "Justification of new manufacturing technology: a strategic approach using the analytic hierarchy process", Production and Inventory Management Journal, Vol. 37 No. 1, pp. 71-7.
12. Chan, F.T.S., Bing, J. and Nelson, T.K.H. (2000), "The development of intelligent decision support tools to aid the design of flexible manufacturing systems", International Journal of Production Economics, Vol. 65 No. 1, pp. 73-82.
13. Harker, P.T. and Vargas, L.G. (1990), "Reply to remarks on the analytic hierarchy process", Management Science, Vol. 36, pp. 269-73.

SELF BALANCED TWO WHEELED PENDULUM

Aman Verma
Mechanical Engineering, Dronacharya
College Of Engineering, Greater Noida
E-mail: verma_aman1992@ovi.com, Ph: 9999672856

T.Bothichandar*
Associate Professor, Mechanical Engineering, Dronacharya
College Of Engineering, Greater Noida
E-mail: bothi_chandar@rediffmail.com, Ph:9891627680
Corresponding author

G.R. Tyagi
Asistant Professor, Mechanical Engineering, Dronacharya
College Of Engineering, Greater Noida
E-mail: tyagi.gr@gmail.com, Ph:7838584105
Address: Dronacharya College Of Engineering, B-27, Knowledge Park-3,
Greater Noida-201308

ABSTRACT

It is a two wheeled battery powered self-balancing pendulum mechanism which can be utilized for self-balancing of two wheeled moving robots. The system is based on an inverted pendulum design in which microcontroller and motors in the base of the device keep the pendulum upright .When powered on and made balancing enabled, it will sense tilt and correct the wheel's drive to make the pendulum erect. To adjust the pendulum upright, it needs to adjust the "balance angle" by adjusting an error to the angle, the pendulum will swing a little backwards and forward to maintain the "balanced angle". To accomplish the balancing requirements the methodology and technology uses gyroscope and accelerometer for navigation and corrections.

A Microcontroller AVR ATMega328, which is a member of ATMEL family in mega series, with flash memory of 32 Kb, a 8 bit microcontroller, running frequency of 16 MHz, operating voltage of 5V and an in-built ADC with resolution of 10 bits is used for sensing and control.Motor Driving IC will be used to drive the motors. It will be a H-Bridge based IC which allows DC motors to run forwards and backwards. The device could also be planted alongwith distance sensors which could sense the distance and produce sounds or vibrations for alerting the operator and make it possible to work wherever such application needed.

Keywords: *Self-Balancing, Pendulum, Navigation*

1.INTRODUCTION

Accelerometer is an analog input device that sends X-axis values to the controller. The controller receives these values and gives command to the motor driving IC to move the motors. The motors are made to move forward or backward depending upon the values received from controller so as to balance the robot.

1.1 Microcontroller [4] Microcontroller, as the name suggests, are small controllers. They are like single chip computers that are often embedded into other systems to function as processing/controlling unit. They are used in automobiles, washing machines, microwave ovens, toys etc, where automation is needed. Here we are using AVR AT Mega 328 microcontroller based on Arduino Platform.

1.2 Description [1] Arduino is an open-source electronics prototyping platform based on flexible, easy-to-use hardware and software. It's intended for artists, designers, hobbyists, and anyone interested in creating interactive objects or environments. Arduino can sense the environment by receiving input from a variety of sensors and can affect its surroundings by controlling lights, motors, and other actuators. The microcontroller on the board is programmed using the Arduino programming language and the Arduino development environment. The hardware reference designs (CAD files) are available under an open-source license, you are free to adapt them to your needs.

1.3 Hardware An Arduino board consists of an 8-bit Atmel AVR microcontroller with complementary components to facilitate programming and incorporation into other circuits. An important aspect of the Arduino is the standard way that connectors are exposed, allowing the CPU board to be connected to a variety of interchangeable add-on modules known as shields. Some shields communicate with the Arduino board directly over various pins, but many shields are individually addressable via an I^2C serial bus, allowing many shields to be stacked and used in parallel. Official Arduinos have used the MegaAVR series of chips, specifically the ATMega8, ATMega168, ATMega328, ATMega1280, and ATMega2560. A handful of other processors have been used by Arduino compatibles.

1.4. Arduino Uno Platform [2]The Arduino Uno is a microcontroller board based on the ATmega328 (datasheet). It has 14 digital input/output pins (of which 6 can be used as PWM outputs), 6 analog inputs, a 16 MHz ceramic resonator, a USB connection, a power jack, an ICSP header, and a reset button. It contains everything needed to support the microcontroller; simply connect it to a computer with a USB cable or power it with a AC-to-DC adapter or battery to get started. The Uno differs from all preceding boards in that it does not use the FTDI USB-to-serial driver chip. [3]Instead, it features the Atmega16U2 (Atmega8U2 up to version R2) programmed as a USB-to-serial converter.

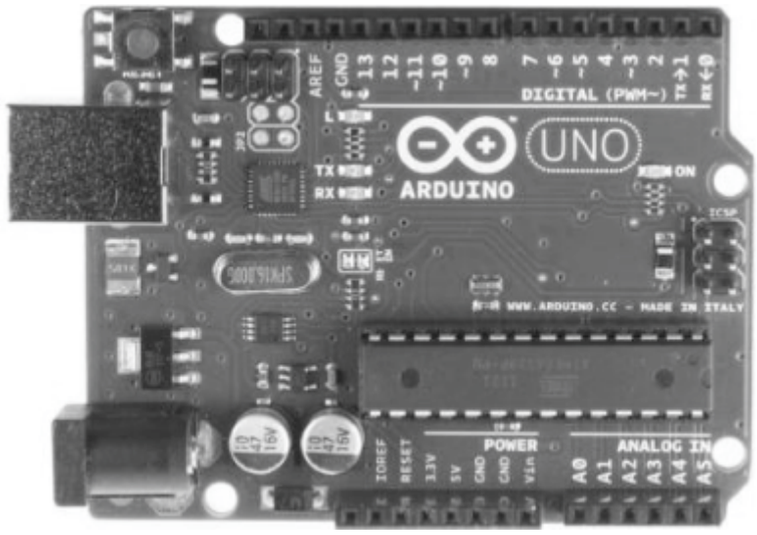

Fig. I. The Arduino UNO Board

2. ACCELEROMETER – ADXL 335

[5]The ADXL335 is a small, thin, low power, complete 3-axis accel-erometer with signal conditioned voltage outputs. The product measures acceleration with a minimum full-scale range of ±3 g. It can measure the static acceleration of gravity in tilt-sensing applications, as well as dynamic acceleration resulting from motion, shock, or vibration. Bandwidths can be selected to suit the application, with a range of 0.5 Hz to 1600 Hz for the X and Y axes, and a range of 0.5 Hz to 550 Hz for the Z axis.

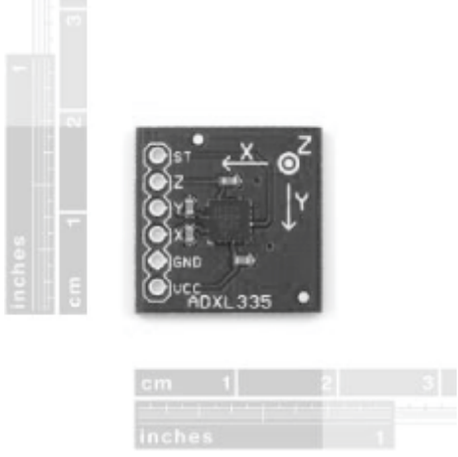

[6]Fig. II. ADXL 335

2.1 Operation The ADXL335 is a complete 3-axis acceleration measurement system. The ADXL335 has a measurement range of ±3 g mini-mum. It contains a polysilicon surface-micromachined sensor and signal conditioning circuitry to implement an open-loop acceleration measurement architecture. The output signals are analog voltages that are proportional to acceleration. The accelerometer can measure the static acceleration of gravity in tilt-sensing applications as well as dynamic acceleration resulting from motion, shock, or vibration.

2.3 Motor Driver Circuit – L293d The Device is a monolithic integrated high voltage, high current four channel driver designed to accept standard DTL or TTL logic levels and drive inductive loads (such as relays solenoides, DC and stepping motors) and switching power transistors. To simplify use as two bridges each pair of channels is equipped with an enable input. A separate supply input is provided for the logic, allowing operation at a lower voltage and internal clamp diodes are included. This device is

suitable for use in switching applications at frequencies up to 5 kHz

2.4 H Bridge An H bridge is an electronic circuit that enables a voltage to be applied across a load in either direction. These circuits are often used in robotics and other applications to allow DC motors to run forwards and backwards. H bridges are available as integrated circuits, or can be built from discrete components.

2.5 Lcd (Liquid Crystal Display) [7]Frequently, a program must interact with the outside world using input and output devices that communicate directly with a human being. One of the most common devices attached to a controller is an LCD display. Some of the most common LCDs connected to the 8051 are 16x2 and 20x2 displays. This means 16 characters per line by 2 lines and 20 characters per line by 2 lines, respectively.

[8]Fortunately, a very popular standard exists which allows us to communicate with the vast majority of LCDs regardless of their manufacturer. The standard is referred to as HD44780U, which refers to the controller chip which receives data from an external source (in this case, the UNO) and communicates directly with the LCD.

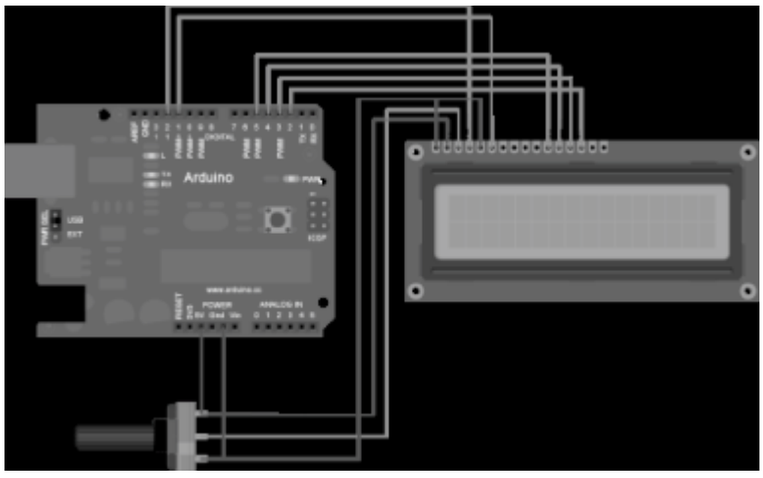

[8]Fig. III. LCD-Microcontroller Interfacing

2.6. Combined Circuitry

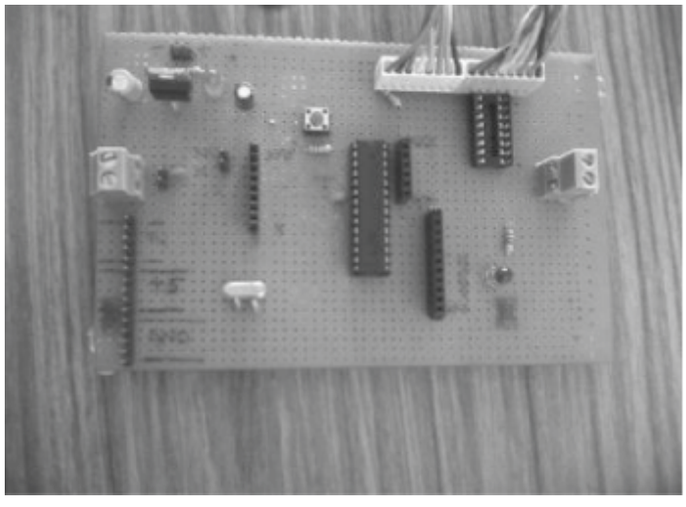

Fig.IV. Self Prepared Arduino Board With Motor Driving Circuit

3. SOFTWARE

Connecting hardware according to the circuit diagram doesn't work really. You need to program the components accordingly so as to work according to the algorithm you have designed in order to make the project work properly as required. Following is the description of software used.

3.1 Arduino Ide [9]The Arduino IDE is a cross-platform application written in Java, and is derived from the IDE for the Processing programming language and the Wiring project. It is designed to introduce programming to artists and other

newcomers unfamiliar with software development. It includes a code editor with features such as syntax highlighting, brace matching, and automatic indentation, and is also capable of compiling and uploading programs to the board with a single click. There is typically no need to edit makefiles or run programs on a command-line interface. Although building on command-line is possible if required with some third-party tools such as Ino. The Arduino IDE comes with a C/C++ library called "Wiring" (from the project of the same name), which makes many common input/output operations much easier.

3.2 Serial [10]Used for communication between the Arduino board and a computer or other devices. All Arduino boards have at least one serial port (also known as a UART or USART): Serial. It communicates on digital pins 0 (RX) and 1 (TX) as well as with the computer via USB. Thus, if you use these functions, you cannot also use pins 0 and 1 for digital input or output. You can use the Arduino environment's built-in serial monitor to communicate with an Arduino board. Click the serial monitor button in the toolbar and select the same baud rate used in the call to begin.

3.3 Schematic Diagram

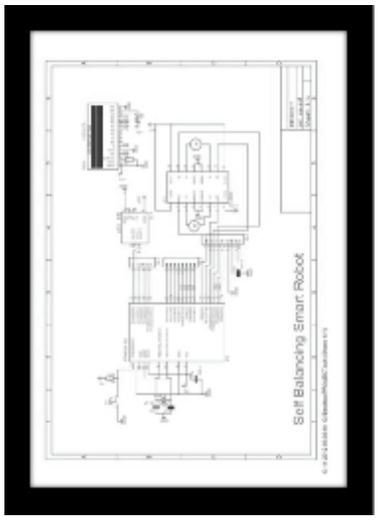

Fig. V. Schematic

4. CONCLUSION

The device can be used as a cheaper, purposeful, working and environmental friendly robot which can balance itself on two wheels without any physical or mechanical interference. This may also be used as a transportation tool, indoors as well as outdoors such as transportation for military applications, warehouses, corporate campuses, industry etc.

REFERENCES

1. http://www.arduino.cc/
2. http://www.google.co.in/imgres?imgurl=http://www.digikey.com/Web%2520Export/techzone/microcontroller/article 2011november-arduino-open-source-
3. http://www.google.co.in/imgres?imgurl=http://computerpr0n.com/wp content/uploads/2012/04/Atmega168PinMap2.pn
4. http://docs-asia.electrocomponents.com/webdocs/0e8b/0900766b80e8ba21.pdf
5. http://www.sparkfun.com/datasheets/Components/SMD/adxl335.pdf
6. http://www.google.co.in/imgres?imgurl=https://dlnmh9ip6v2uc.cloudfront.net/images/products/9/2/6/9/09269-2.jpg
7. http://www.multyremotes.com/lcd-interfacing.htm
8. http://arduino.cc/en/Tutorial/LiquidCrystal
9. http://arduino.cc/en/Tutorial/HomePage
10. http://arduino.cc/en/Tutorial

DESIGN OF A DIELECTRIC FREE METALLIC BALANCE ANTIPODAL VIVALDI ANTENNA FOR X-BAND

Dr Sanjay Kumar*
Defence Avionics Research Establishment (DARE)
C.V.Ramannagar, Bangalore-560 093, India.
Tel/Fax: 91-80-25347705
E-mail: tnksk@yahoo.co.in
Corresponding author

Saurabh Shukla
Defence Avionics Research Establishment (DARE)
C.V.Ramannagar, Bangalore-560 093, India.
Tel/Fax: 91-80-25347705
E-mail:saurabh.dare@gmail.com

ABSTRACT

A novel design of dielectric free metallic Balanced Antipodal Vivaldi Antenna for X-band is proposed in this paper.Balanced Antipodal Vivaldi Antenna is a special class of Taper Slot Antenna (TSA) element which is capable enough to provide symmetric beamwidths along with large bandwidth.Considering these properties, a Coaxial line fed dielectric free metallic Balance Antipodal Vivaldi Antenna has been designed and simulated to serve as an Antenna element over a large bandwidth from 8 to 12 GHz. This Antenna Element exhibits some attractive features like return loss better than -10dB over 8-12 GHz, cross polarization, compactness and moderate gain. The simulated radiation pattern and VSWR have been presented and discussed in this paper. The Antenna element has been designed and optimised in CST Microwave.

Keywords: *Balanced Antipodal Antenna, Cross polarization, Coaxial Line, Gain, VSWR.*

1.INTRODUCTION

The Balanced Antipodal Vivaldi Antenna belongs to the group of endfire traveling wave antennas. It was presented by Langley, Hall and Newman [1]. Traveling wave antennas have demonstrated wide bandwidth, moderate gain, and symmetrical E- and H-plane beam patterns. Balanced Antipodal Vivaldi Antenna consists of a feed line, which is usually a stripline and transitions occurs from stripline to the radiating structures. Radiating structures are known as fins and these are exponentially tapered but linear, parabolic, hyperbolic or elliptical tapers can be employed to achieve the requirement. The continuous scaling and gradual curvature of the radiating structure ensures theoretically unlimited bandwidth, which is, in practice, constrained by the mechanical dimensions.There are two fundamental types of Balanced Antipodal Vivaldi Antenna, which can be used as the radiating structure. These types are Dielectric based Balanced Antipodal Vivaldi Antenna and Dielectric free Balanced Antipodal Vivaldi Antenna.

This paper describes a unique dielectric free Balanced Antipodal Vivaldi Antenna Element designed for X-band with gain ranging between 6-10 dB. This is a new Antenna in which only metal is used to carve out the Balanced Antipodal antenna. This antenna can be used for high power transmission applications with $\pm 35^0$ beamwidth in H plane and $\pm 15^0$ in E plane. The fabrication of this antenna is quite easy as no dielectric is used for realization. Also due to its compactness, it can be used on any platform. The advantage of balanced Antipodal configuration is that it provides high cross polarization as compared to Antipodal configuration and exhibits linear polarization.The thickness of each fin in Antenna Element is kept as 1mm so that it can withstand the load. Also sidewalls are provided to hold the fins with screws. The mechanical models have been shown in Fig 1 & Fig 2

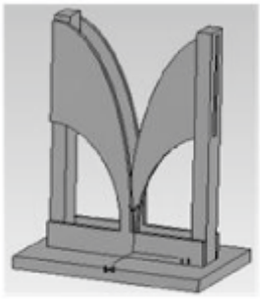

Fig.1 Balanced Antipodal Vivaldi Antenna

2. VIVALDI ELEMENT

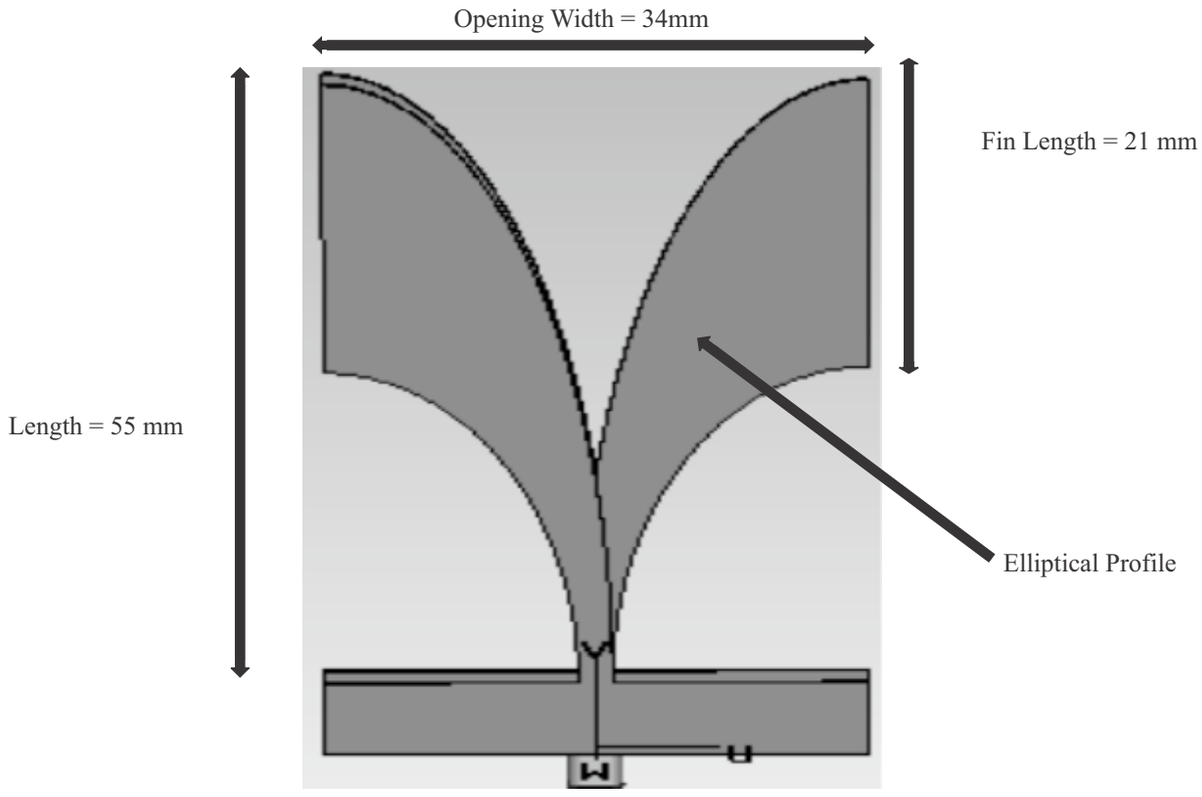

Fig.2 Fins and coaxial feed arrangement

There are two types of transitions in the Balanced Antipodal Vivaldi Antenna. One is the coaxial feed to stripline transition and other is the stripline to free space transition [2]. Both transitions have their effect on the bandwidth and the return loss of the Balanced Antipodal Vivaldi Antenna. The gradual opening of the fins depends upon the selected taper profile and it provides a matching between stripline to free space transition and thus minimizes the reflection at the transition region. Hence an elliptical taper profile has been chosen for the Antenna Element (as shown in Fig 1) to provide broad bandwidth as well as Beamwidth

3. DESIGN PARAMETERS & DETAILS

The relationship between Balanced Antipodal Antenna directive gain and length can be given as:

$D = 10\log(10L/\lambda_0)$ (1)

Where

λ_0 is the free space wavelength at any frequency of operation.

L = Length of the Balanced Antipodal Antenna

Thus for a high gain Balanced Antipodal Antenna, length is generally taken as 2 to 3 times of the wavelength of the lowest frequency of operation. But, for a wide beam Balanced Antipodal Antenna, the length has been chosen and optimised to almost one wavelength. The optimised length is approximately $1.5 * \lambda_L$ where λ_L is the free space wavelength at lowest frequency of operation.

For efficient transition from slotline to free space, Opening width of the Balanced Antipodal Vivaldi Antenna should be greater than $0.5 * \lambda_L$. Therefore, optimised Opening width for Balanced Antipodal Antenna is chosen as λ_L at 8 GHz. The stripline width is taken as 2 mm for ease in fabrication.

4. EQUATION OF THE FLARE

The Beamwidth and the VSWR of Balanced Antipodal Vivaldi Antenna depends upon the type of flare provided for the widening of the fins. The flare can be exponential, linear, parabolic or some other equation based curve. The TSA flare is designed as [3]

$$x^2/a^2 + y^2/b^2 = 1 \quad (2)$$

Where, a = half major axis

b = half minor axis

The equation (2) represents the general equation of an ellipse. The elliptical flare helps in achieving wide bandwidth with returnyloss better than -10 dB. Moreover the beamwidth in E & H plane are different due to elliptical taper. The fin flare is selected as an elliptical profile and major and minor axes are optimized for wide 3-dB beamwidth for H & E-plane as compared to other profiles of Balanced Antipodal Antenna. The flare is provided on the both radiating fins of the antenna which makes it Balanced radiating structure.

5. FEED PARAMETERS AND DETAILS

The Feeding technique plays an important role in impedance matching. Ultra wideband performance of a Balanced Antipodal Antenna depends upon the transition from feed to free space.Hence a large bandwidth can be obtained by proper impedance matching. Various techniques have been developed for efficient coupling of field waves from the input to the free space. Some of the commonly used techniques are microstrip, coaxial, stripline and coplanar waveguide feeding. In this paper a stripline feeding technique has been presented to give better matching over 8-12 GHz band [4] [5]. The designed stripline with radial stub is shown in Fig 3.

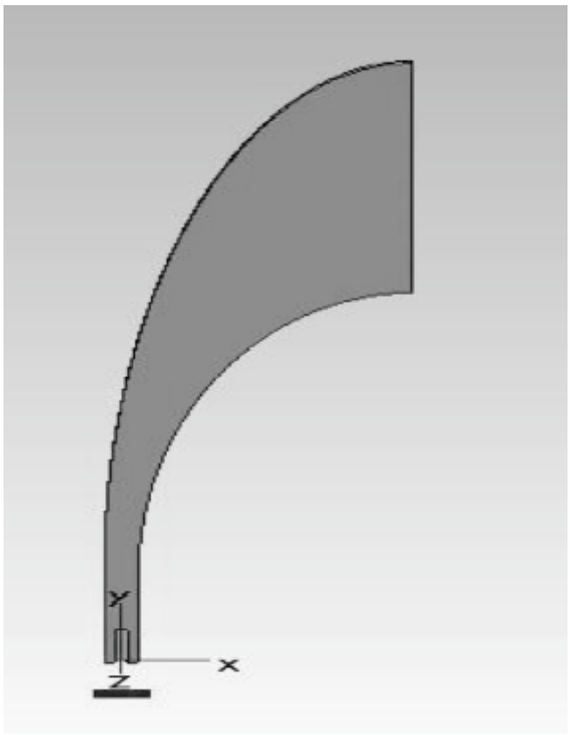

Fig.3 Feed for Balanced Antipodal Vivaldi Antenna

The stripline has a constant width of 2 mm for efficient transition from stripline to radiating fins.

6. RADIATING ELEMENT PERFORMANCE

A model has been designed and optimized in CST Microwave studio 2011 to achieve the goals. The optimized results for Return Loss, gain and 3-dB beamwidth in E& H-planes are presented in Fig 4. to Fig 8. The results are matching with the theoretical calculations and a further study can be done on a fabricated model to find out the effect of manufacturing defects over the Balanced Antipodal Vivaldi Antenna.

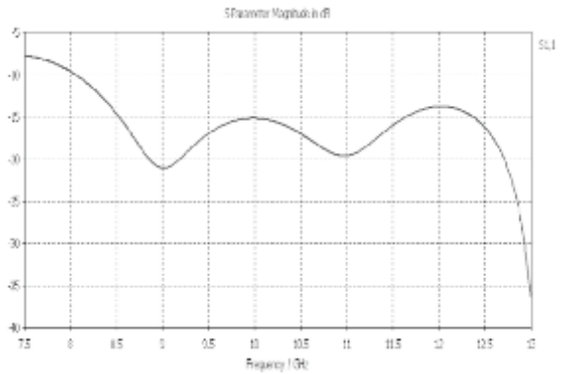

Fig.4 Simulated Return Loss of the Vivaldi Antenna Element.

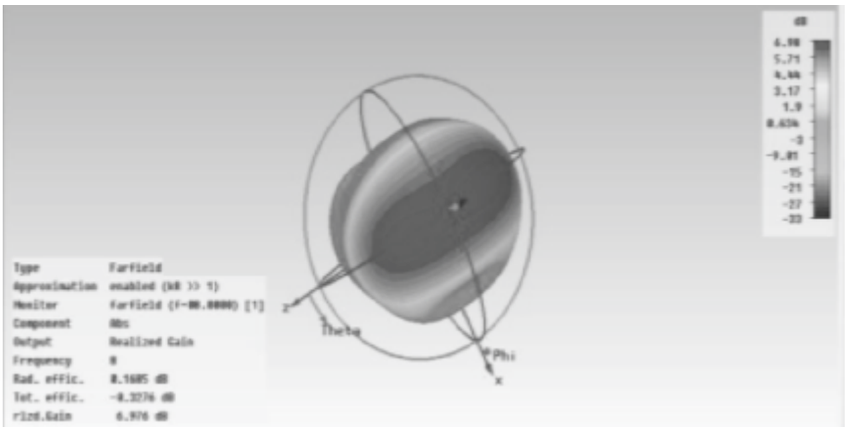

Fig5 Simulated Radiation Pattern at 8 GHz

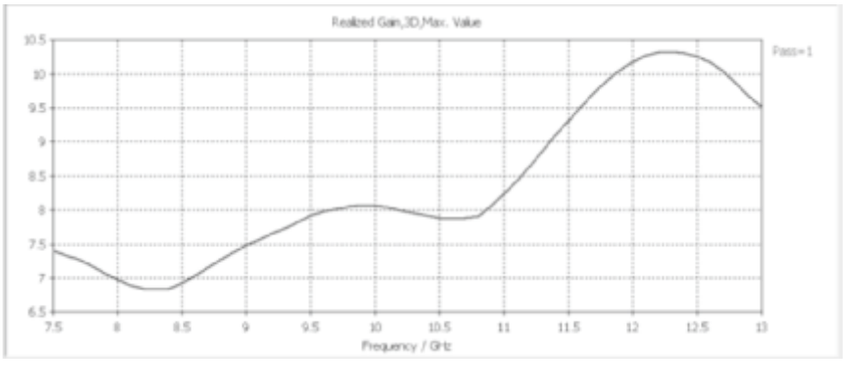

Fig.6 Simulated Gain Pattern

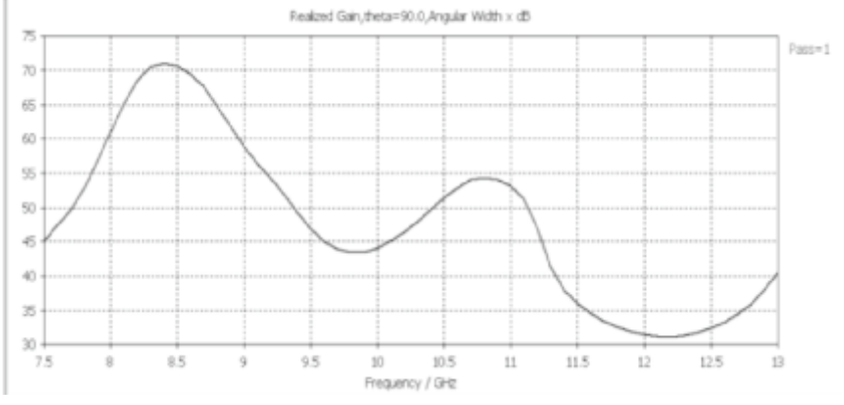

Fig.7 Simulated E-plane 3-dB beamwidth

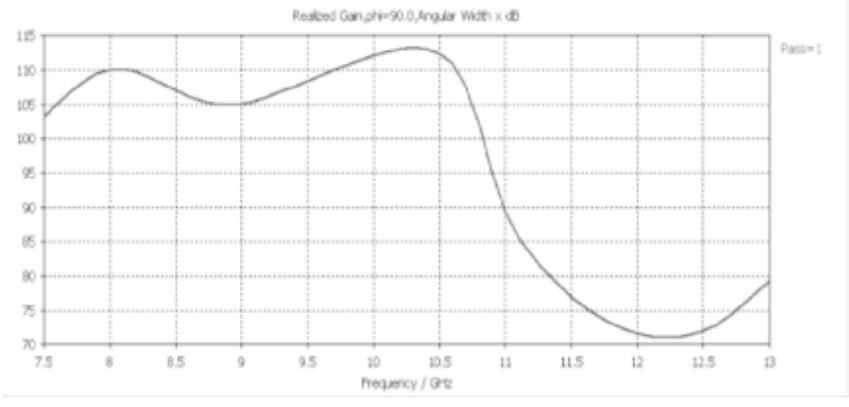

Fig.8 Simulated H-Plane 3-dB beamwidth

7. CONCLUSION

In conclusion, a novel Dielectric free Balanced Antipodal Antenna has been designed and optimized. The Antenna offers a almost symmetrical E& H-plane beam width .The Stripline to free space Transition provides a better matching over the whole band of operation i.e. 8-12GHz. The simulated VSWR is observed to be less than 2:1 over the entire band. The Antenna also has a Gain of 6 to 10dB over the entire band [6]. Also the thickness of the Antenna is small enough for easy fabrication and makes it preferred choice of antenna for the High Power Transmission application.

Acknowledgement The authors would like to thank Director, DARE for his continuous support and encouragement for this work.

REFERENCES

1. J.D.S. Langley, P.S. Hall & P. Newman, "Balanced Antipodal Antennas for wide bandwidth phased Arrays". ". IEEE Proc,Microwave and Antenna Prop. Vol 143, April, 1996.
2. Lewis, L.R., Fasset, M., and Hunt, J.: „A broadband stripline array element ", IEEE Syrnp. Antennas and Propagation,Atlanta,USA, 1974, pp. 335-337
3. P. J. Gibson, "The Vivaldi Aerial", Proc. 9th European Microwave Conference, Brighton, U.K., 1979, pp. 101-105.
4. D. H. Schaubert and J. Shin, "Parameter study of Tapered Slot antenna array", IEEE international antennas and propagation,symposium digest, new port beach, CA, June 1995, pp 1376-1379.
5. R. N. Simons and R. Q. Lee, "Linearly Tapered Slot Antenna Impedance Characteristics," in 1995 IEEE AP-S International Symposium, Vol. 1, Newport Beach, CA, pp. 170-173,1995.
6. Kai Fong Lee, Wei Chan, "Advances in microstrip and printed antennas," page 465-466, John Wiley & Sons.

MEASUREMENT SETUP AND PERFORMANCE ANALYSIS OF DIGITAL RECEIVER SYSTEM WITH MULTIPLE SIGNAL DETECTION AND EXPANDABLE BANDWIDTH CAPABILITIES ON A MULTI-PROCESSOR HARDWARE PLATFORM

Kiran George*
kgeorge@fullerton.edu; 657-278-2640
Computer Engineering Program
California State University
Fullerton, CA 92831, USA
Corresponding author

Chien-In Henry Chen
henry.chen@wright.edu; 937-546-9270
Department of Electrical Engineering
Wright State University Dayton,ohio45435

ABSTRACT

In the past, digital wideband receiver implementations were primarily on pipelined single-processor hardware platforms. However, these implementations have many drawbacks such as inability to process the sheer volume of signal data entering the receiver and limited bandwidth. A multi-processor 3 giga-samples per seconds (GSPS) receiver system with expandable bandwidth, that utilizes Nvidia Tesla C2050 GPUs to handle the computational complexity and a Xilinx Virtex-5 FPGA to perform signal formatting, is presented. The receiver design combines several wideband receivers to achieve a much wider bandwidth for improved performance. This work also presents a multi-carrier RF signal generation, measurement setup and performance analysis of the multi-processor receiver system.

Keywords: *Digital receivers, fast Fourier transform (FFT), multiple signal detection, GPU, FPGA, multi-processor receiver system.*

1.INTRODUCTION

The fundamental function of a modern radar receiver is to intercept radio frequency signals to identify and locate its source. To meet stringent operational requirements, high instantaneous dynamic range (IDR) is indispensable, as the complex nature of electromagnetic emissions requires the radar receiver to rapidly search a large frequency range with maximum sensitivity in real time. Furthermore, detection of multiple incoming signals of any carrier frequency and bandwidth (BW) is central to the working of a modern radar receiver, unlike the narrow-band communication receiver, which usually receives one signal at any given time and is designed for a known signal. Desirable characteristics of a modern digital radar receiver include 1) fine frequency resolution in reduced response time in wide bandwidth, 2) multiple signals detection, and 3) high IDR for detecting weak signals in the presence of strong signals, in addition to external and internal noise.

In the past, most radar receivers were designed using analog technology in which an input RF signal is converted into video signals by heavy weight analog hybrids, power dividers, and crystal video detectors. The video signals are processed to determine the frequency of the input signal. But using digital technology the receiver uses directly digitized signals without the analog delay lines and video detectors. The input RF signal is down converted into intermediate frequency (IF) and digitized using a high-speed analog to digital converter (ADC). This process retains all information and the digital receiver produces an overall better performance than the analog counterpart [1].

In the past, digital wideband receiver implementations were primarily on pipelined single-processor platforms. However, these implementations have many drawbacks such as inability to process the sheer volume of signal data entering the receiver and limited BW. In this paper, we present a design of 3 GSPS multi-signal digital wideband receiver system on a multi-processor hardware platform with expandable BW capability and its performance measurement using a multi-carrier RF signal generation and testing setup. Section II presents background and limitations of single processor receivers. Section III presents the proposed receiver system and its implementation on multi-processor platform. A bandwidth expandable receiver system for multiple signals detection is presented in Section IV. Section V presents performance evaluation of the implemented design. Section VI concludes remarks.

2. DIGITAL WIDEBAND RECEIVER IMPLEMENTATIONS ON SINGLE-PROCESSOR PLATFORMS

In the past, implementation of digital wideband receivers was primarily on pipelined single-processor platforms [2] [3][4][5]. However, these implementations had severe performance limitations:

(a) Higher-length of the FFT operation: A higher-precision data format and a higher-length of the FFT operation have a higher impact on receiver's IDR as it dictates the effective channel width of the receiver. However, FFT is a computationally intensive block in digital receiver systems. Increasing length of the FFT operation and higher-precision data format will require large computational power, which limits the performance of single-processor receivers. The length of FFT of single-processor receivers is in general limited to 256 points to meet the time-resolution requirement [2][3][4][5].

(b) Larger volume of signal data produced by ADC: The ADC is a critical subsystem of a digital radar receiver, which affects receiver's BW and IDR. As the ADC technology advances and the resolution of the ADCs improve, the processing and memory requirements of the digital signal processor that follows it also increases dramatically [6]. Currently, operating speeds of single processor-based systems are not on par with state-of-the-art ADCs and this disparity is an impediment in radar receiver design implementation. Many practical digital receivers compensate the high sampling rate of ADCs to accommodate the speed at which the detection logic in the processor can process the data [2][4]. However, for real-time and more efficient operation, processors in digital radar receivers of the future will need to process larger volume of signal data at a rate commensurate with the improvement of ADC's sampling speed.

(c) Multiple signals detection: Multiple signal detection is a highly desirable characteristic of wideband receivers. The bottlenecks of multiple signal detection are noisy signal environment, signal interferences, and computational complexity involved in real-time implementation. Several multiple signal detection schemes have been proposed. The detection problem for multiple signals embedded in noisy environment is treated as a multiple hypothesis test based on log-likelihood ratios [7]. Multiple signal detection using the atomic decomposition and the expectation maximization (EM) algorithms was proposed in [8]. The receiver design proposed in [9] is based on the time-frequency analysis. It uses an extension of the short time Fourier transform (STFT) consisting of a set of smoothed spectrograms obtained by non-coherent integration of the representation generated by the STFT. A configurable receiver was first proposed in [10] which employ a hardware configurable scheme to detect multiple signals before next set of buffered data arrives for processing. However, these techniques are computationally intensive and hence its real-time implementation on single-processor systems faces challenges.

3. MULTIPLE-PROCESSOR PLATFORM FOR DIGITAL WIDEBAND RECEIVERS [11]

Today, high performance computing (HPC) certainly allows us to ask questions on a scale that we have not been able to ask before. The complexity of HPC applications is partly defined by the number of processors and the amount of memory required in executing them. Researchers are looking at different ways to offload the computationally intensive tasks to specialized hardware accelerators such as Nvidia's Tesla GPU cards and FPGAs. FPGA can be compared to an escalator with deeper pipelines and flexible architectures, while a GPU can be compared to an elevator with fixed architecture and multiple fast streaming cores. By combining both platforms a truly multi-processor platform which is more efficient can be realized, where the challenge is in the intelligent partitioning of the HPC application to benefit from both the architectures. These specialized processors offer hardware acceleration and can be configured using Cell Software Development Kit (SDK), NVIDIA Compute Unified Device Architecture

Receiver Implementations		Two Sig. IDR (dB)	Five Sig. IDR (dB)	Max. NO:OF signals	False Alarm (%)	Freq. Resol. (MHz)	Freq. Sep. (MHz)	FFT Size	Platform
	Single-Processor Implementations								
1	(2)	4	-	2	1	10	10	256	ASIC
2	(3)	22	-	2	1	10	10	256	FPGA
3	(4)	24	-	2	1	10	10	256	ASIC
4	(5)	22	-	2	1	10	10	256	FPGA
	Multi -Processor Implementation								
5	(11)	44.5	42.5	5	1	0.75	10	4K	HPC Server (comprising of two GPUs each with 440 streaming processors)

(CUDA) or Hardware Description Languages (HDL) such as VHDL/Verilog. The IBM Cell processor is used as a hardware accelerator in Los Alamos National Lab's (LANL) petaflop supercomputer and Roadrunner. The Theoretical and Computational Biophysics (TCB) group at University of Illinois at Urbana Champaign (UIUC) is involved in molecular modeling and

simulations using the NVIDIA's Tesla cluster [12][13]. The second fastest supercomputer, Nebulae, with a theoretical peak performance of 2.98 petaflops per second, uses NVIDIA Tesla C2050 GPUs as accelerators.

Table 1. Comparative performance of wideband digital receiver systems

Comparative performance of single and multi-processor implementations wideband digital receivers are given in table 1. Single-processor implementations 1 - 4 adopted 256-point fixed-point kernel function FFT that replaced general multipliers with shifters, adders and subtractors to reduce the computational complexity. However, by doing so bit truncation errors are introduced in FFT stages, which in turn limits IDR of the receivers. Multi-processor receiver implementation [11], which replaced 256-point fixed-point kernel function FFT with 4096-point FFT, demonstrated drastic improvement in IDR, frequency resolution and the number of signals it can process. This multi-processor system utilized Nvidia Tesla C2050 GPUs to handle the computational complexity and a Xilinx Virtex-5 FPGA to perform signal formatting.

3.1 Digital Wideband Receiver Implementation on Multi-Processor Platforms

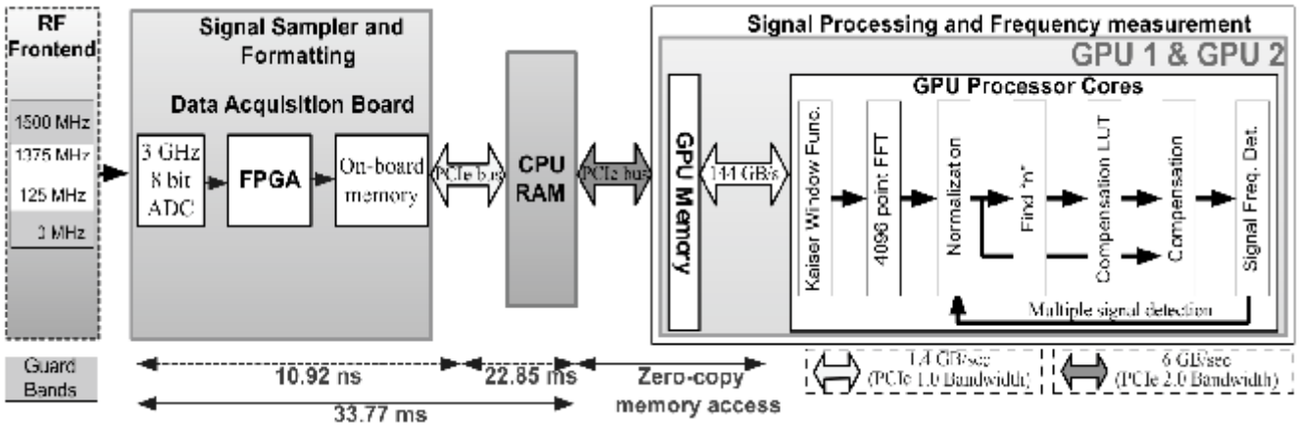

Fig. 1. Receiver Block Diagram with Timing Information (11)

As shown in Fig. 1, the digital wideband receiver system [11] utilized a multi-processor computing platform, which composed of two Tesla C2050 GPUs and a Virtex-5 FPGA. The design development focused on hand-written VHDL/Verilog cores on the FPGA platform with the computational complexity handled by the GPUs. By utilizing the GPU as a coprocessor, the signal frequency data was transferred as a text file from the GPU memory to the CPU memory once the computational steps are completed.

(1) Signal Sampling and Formatting (Implemented on DAQ board with FPGA)

The signal sampling and formatting was performed using a data acquisition (DAQ) board. The DAQ board has one 8-bit ADC (3000 MSPS), 4GB of DDR2 DRAM memory and a Virtex-5 FPGA chip (XC5VLX50T) on-board. The on-board ADC has a signal-to-noise ratio of 42 dB, analog input range of -350mV to +350mV, and analog input BW of DC to 3 GHz (-3dB BW). In order to achieve a 1.25 GHz input bandwidth, the Nyquist sampling frequency required is at least 2.5 GHz. The usable input frequency range of 1.25 GHz allows for guard bands at 0–125 MHz and 1.375–1.5 GHz. To take the finite slope of the input filter into consideration, the ADC on the DAQ board will operate at 3 GHz. The RF signal was first passed to the ADC, which samples the signal every 0.3 ns to produce 8-b amplitude measurements.

The windowing circuitry in the FPGA latches up the A/D data in its FIFO registers, and transfers bursts of 128-b LVDS data vectors at 8GB/sec to two 8GB DDR DIMM modules. Between these forward bursts of A/D data, the FPGA transfers 32 MB of data samples to the CPU (host) RAM via PCIe bus interface (at 1.4 GB/sec), allowing for uninterrupted high speed data acquisition. This acquired digitized data in host RAM will be available to the GPU streaming processor cores using the data path shown in Fig. 1. The transfer of 32 MB data samples to the CPU RAM using the PCIe interface (data transfer rate of 1.4 GB/s) takes 22.85 ms. The two GPUs utilized the zero-copy memory access technique of the CUDA mapped host memory feature to access the sampled data. The output data, allocated in page-locked CPU memory, are directly mapped to the device's (GPU) address space so no explicit host-GPU memory transfer is needed. Thus the total time for the GPUs processor cores to receive the acquired digitized data for processing was 33.77 ms, which includes time taken for data sampling and collection.

(2) Windowing, Super-Resolution and Frequency Measurement (Implemented on two GPUs)

Fast streaming cores in the GPUs was utilized to the fullest to achieve maximum performance acceleration in processing the acquired 8000 data sets (each data set with 4096 8-b data elements). The main blocks of each GPU are: 1) Window function (calculates the product of the data samples and the Kaiser window coefficient), 2) 4096-point 8-b FFT: (FFTW, a C subroutine library for computing the FFT), 3) Normalization (normalizes the 2048 FFT output amplitudes and the maximum value is 1), 4) Find "n" (find the row of highest amplitude (strongest) signal frequency spectrum in the compensation table using the super-resolution algorithm [4]), 5) Compensation LUT and Compensation (Extract the strongest signal frequency spectrum from the compensation table an subtract it from the original FFT outputs), and 6) Signal Frequency Detection (closely estimate the detected signal frequency using the super-resolution algorithm).

4. DIGITAL RECEIVER SYSTEM IMPLEMENTATION WITH EXPANDABLE BANDWIDTH CAPACITY

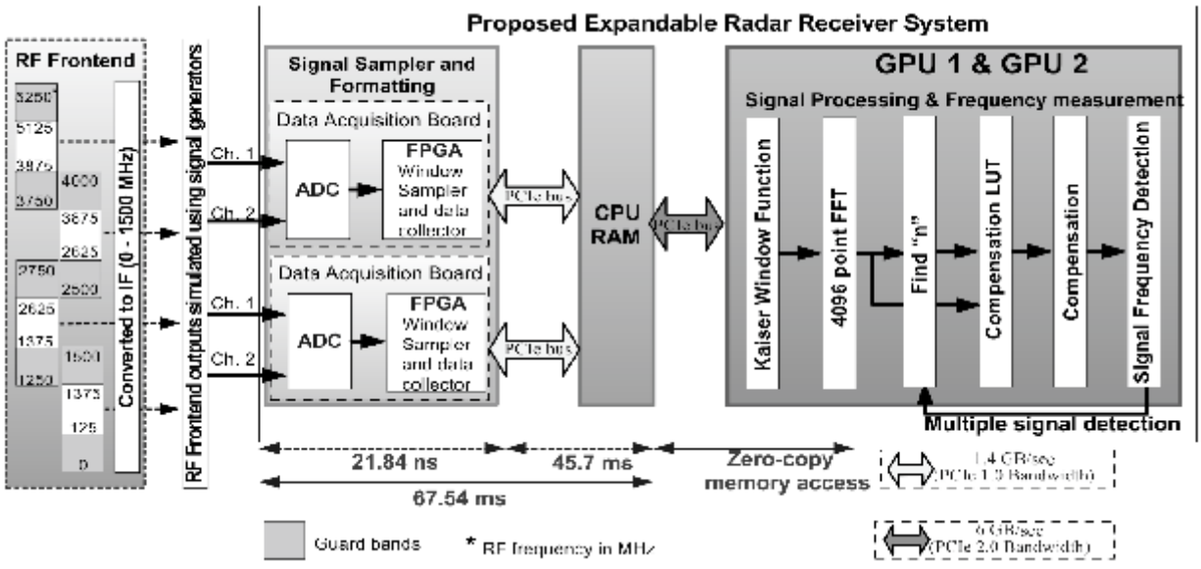

Fig. 2. Functional block diagram of the proposed receiver system with expandable bandwidth

As a radar receiver must rapidly search a large frequency range (up to 18 GHz), the BW of the modern digital receiver should be as wide as the ADC and DSP technology permits. Currently, operating speeds of digital hardware are not on par with state-of-the-art ADC. This disparity is the primary impediment in radar receiver design implementation. For real-time and more efficient operation, signal processors in digital radar receivers of the future must process data at a rate commensurate with the ADC. A definitive and more feasible approach would be to combine several wideband receivers to achieve a much wider BW for improved performance [14]. This section presents an expandable radar receiver system comprising of four 1.25 GHz wideband receivers (Receiver 1, 2, 3 and 4) to achieve a maximum combined instantaneous bandwidth (BW) of 5 GHz (Fig. 2).

The signal sampling and formatting is performed using two DAQ cards described in section III.A.1. Each of the DAQ cards is capable of sampling two channels concurrently at a sampling rate of 3 GHz. The four input RF signals are passed to the ADC on the DAQ cards. The ADC samples the signal every 0.3 ns to produce 8-b amplitude measurements. The FPGAs on both the DAQ cards transfer 64 MB (for two channels) of data samples to the CPU (host) RAM via PCIe bus interface (at 1.4 GB/sec), allowing for uninterrupted high-speed data acquisition. The transfer of 64 MB data samples from DAQ cards to the CPU RAM takes 45.7 ms. The two GPUs utilize the zero-copy memory access technique of the CUDA mapped host memory feature to access the sampled data. The output data, allocated in page-locked CPU memory, are directly mapped to the device's (GPU) address space so no explicit host-GPU memory transfer is needed. Thus the total time for the GPUs processor cores to receive the acquired digitized data for processing is 67.54 ms, which includes time taken for data sampling and collection. The computation of signal processing and frequency measurement is handled by two Nvidia C2050 GPUs.

The proposed system is configurable with three configurations based on the desired performance requirement. They are shown in Fig. 3. Configuration-1 (CN1) utilizes two parallel ADC channels in two DAQ boards, thus implementing four 1.25 GHz receivers (Receiver 1, 2, 3 and 4) covering a combined BW of 5 GHz. Configuration-2 (CN2) utilizes one ADC channel in both DAQ boards, thus implementing two 1.25 GHz receivers (Receiver 1 and 2) covering an BW of 2.5 GHz. And, configuration-3 (CN3) utilizes one ADC channel in one DAQ board, implementing a single receiver (Receiver 1), covering an BW of 1.25 GHz. Furthermore, the proposed system can also be expanded by combining more of the signal sampler and formatting blocks to cover a wider BW.

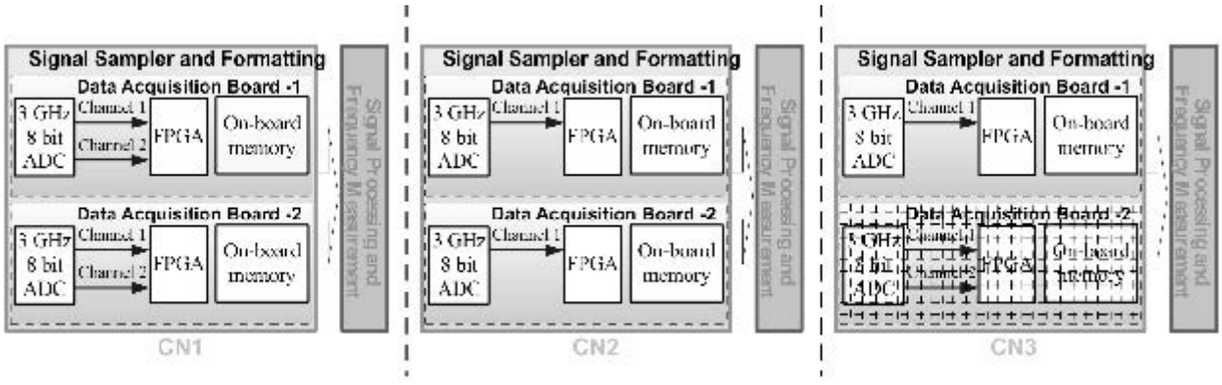

Fig. 3. CN1 implements four 1.25 GHz receivers (BW: 5 GHz); CN2 implements two 1.25 GHz receivers (BW: 2.5 GHz); CN3 implements Single 1.25 GHz receiver (BW: 1.25 GHz)

The usable RF input frequency ranges of receiver 1, 2, 3 and 4 are 125 - 1375 MHz (guard bands at 0-125 MHz and 1375-1500 MHz), 1375 - 2625 MHz (guard bands at 1250 - 1375 MHz and 2625 - 2750 MHz), 2625 - 3875 MHz (guard bands at 2500 - 2625 MHz and 3875 - 4000 MHz), and 3875 MHz - 5125 MHz (guard bands at 3750 - 3875 MHz and 5125 - 5250 MHz) respectively. The guard bands are used to account for the non-linearity associated with the input filters, limiting amplifiers and ADC in the receiver system. The signal frequency in the guard bands is not used for signal detection and frequency calculations. The RF frequency ranges of receiver 2, 3 and 4 are down converted to IF (0 -1500 MHz).

As digital hardware implementation of the radar receiver is the primary focus of the proposed receiver system, the four IF signals from the RF frontend to the receiver is simulated using signal generators. According to the preliminary simulation results, the design can accurately calculate the frequencies of 5 signals with a frequency resolution of 0.5 MHz, IDR of 40 db, and frequency separation of 3 MHz. The combined effectiveness of the multiple signal detection techniques adopted for the proposed system is illustrated using simulation for CN1, as shown in Fig. 4. There are five valid signals in the data. Data windowing, FFT, super-resolution block, and frequency calculation operations are performed on the IF signal data from four receivers independently. Out of the total 20 signal frequencies calculated, only the first five signal frequencies

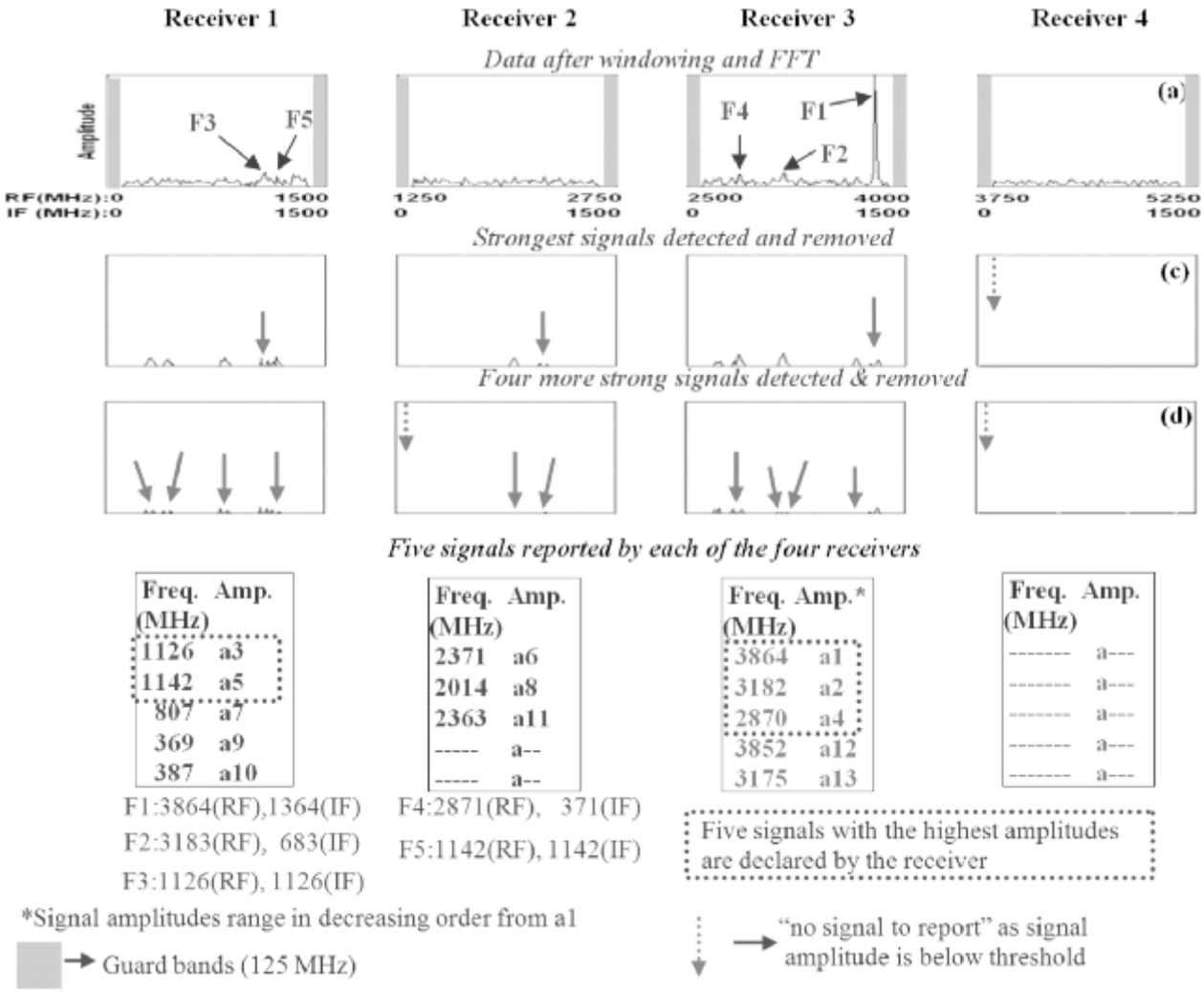

Fig. 4. Simulation example for CN1

(3864 MHz, 3182 MHz, 2870 MHz, 1126 MHz, and 1142 MHz) with the highest signal amplitudes are reported as detected signals by the receiver. In terms of the computational performance of the proposed expandable receiver system, the two GPUs are able to process the 8000 data sets in 36.2 ms before the next set of digitized data arrives.

5. PERFORMANCE MEASUREMENT OF A DIGITAL RECEIVER SYSTEM IMPLEMENTED ON A MULTI-PROCESSOR HARDWARE PLATFORM

5.1 Measurement Setup (using multi-carrier continuous wave signal generator, DAQ board and GPUs) Traditionally, multi-carrier RF signal generation and testing is cumbersome as most of the signal generators only generate single RF signal. For multi-carrier generation, the RF outputs of the signal generators are mixed using a RF power combiner (Fig. 5) before the signals are passed onto the DAQ and the DSP module for processing as discussed in section III.

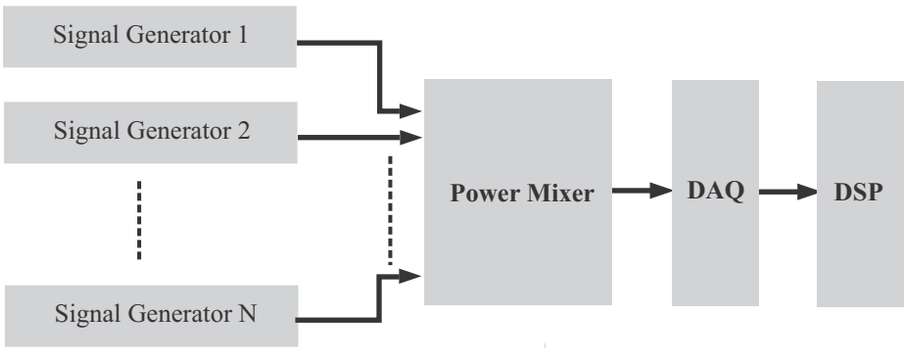

Fig. 5. Traditional multi-carrier signal testing setup

However, for analyzing the multi-carrier behavior of the proposed receiver, the multi-carrier continuous wave option of the R&S SMBV100A Vector Signal Generator (bandwidth: 9 Hz – 6 GHz) is utilized (Fig. 6), which generates multi-carrier signals with user-definable offset from carrier, based on a selection of up to 8192 carriers. Each carrier can be separately set and switched on; multiple carriers can be jointly configured. Using the carrier-setup menu (Fig. 7), the number of carriers, carrier spacing (spacing between carriers for the Multi Carrier CW signal), carrier start (start index of the carrier range), carrier stop (stop index of the carrier range), power start (power of the starting carrier) and power step (width of the step with which the power will be changed from carrier to carrier) are preset. The carriers are arranged symmetrically around the middle carrier. The total bandwidth, calculated as (number of carriers – 1)*carrier spacing, should not exceed the system bandwidth of the instrument (6 GHz). The carrier power, calculated as power start + number of carriers *power step, must be within the valid value range -80 dB to 0 dB.

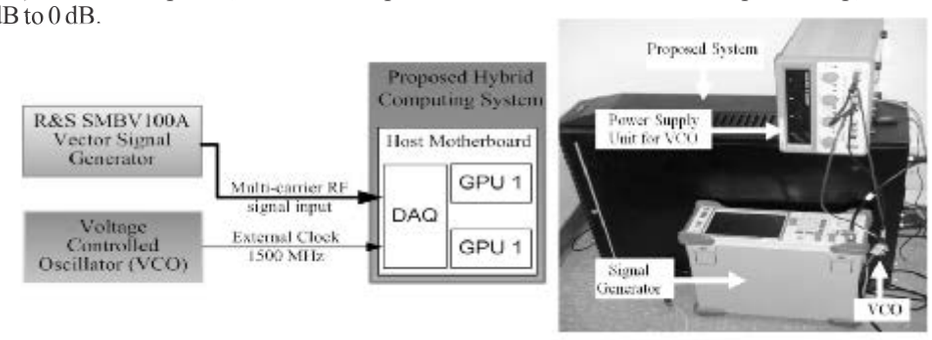

Fig. 6. Multi-carrier signal generator generation and measurement

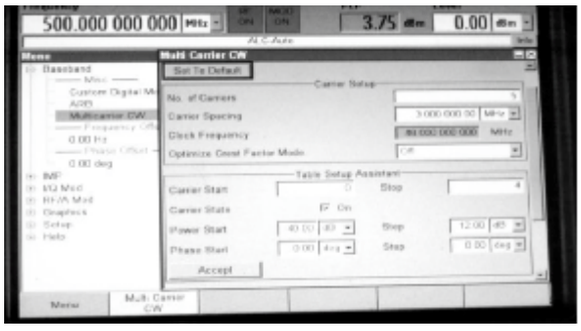

Fig. 7. Inputs for multi-carrier setup

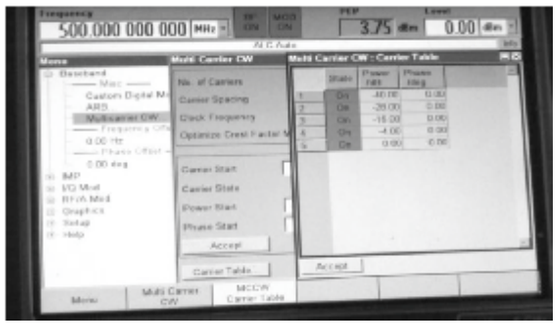

Fig. 8. Carrier table signal power displayed

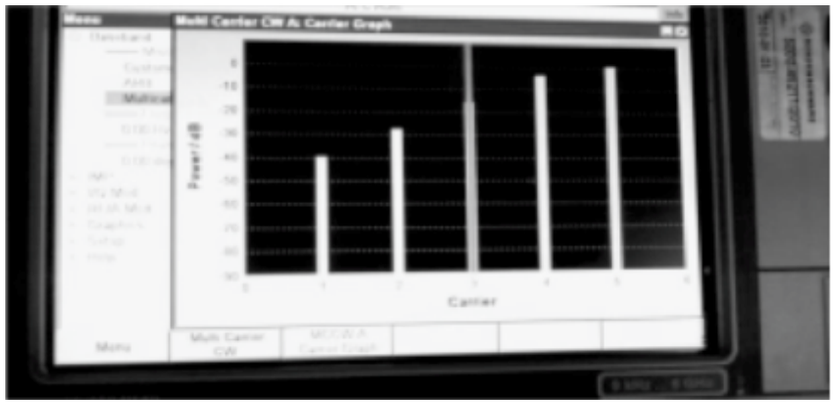

Fig. 9. Graphical display of relative powers of multiple carriers generated

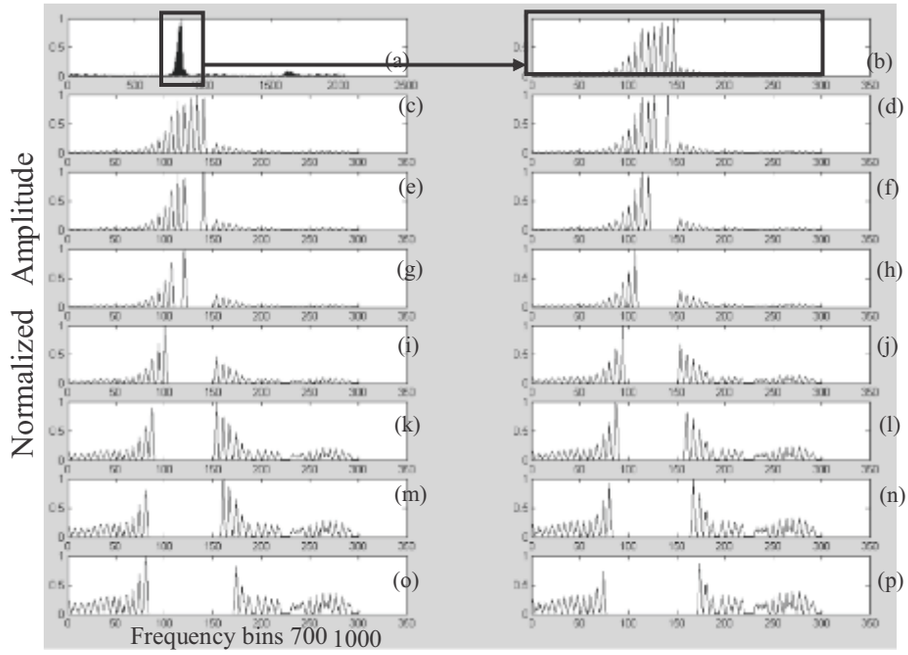

Fig. 10. Multi-signal (15 signals) detection with maximum IDR of 25 db and frequencies ranging between 576 MHz and 630 MHz

The Carrier Table (Fig. 8) displays the settings of all available carriers. Carriers in the "On" state are highlighted. The Carrier Graph (Fig. 9) gives a graphical representation of the chosen carrier configuration. The carriers are on the X-axis and the colored bars represent those carriers in the "On state". The Y-axis is Power, and the height of the bars corresponds to the power of each individual carrier.

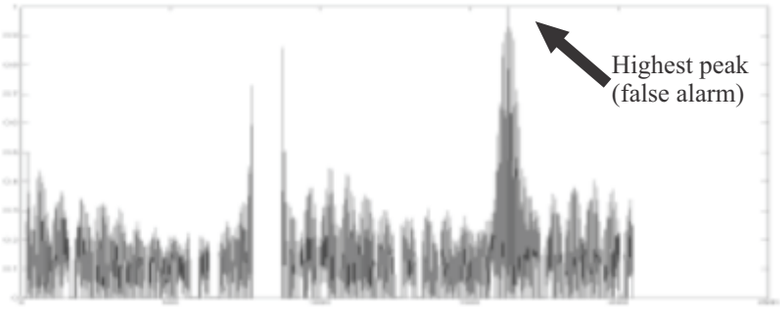

Fig. 11. Depiction of 2048 frequency bins of subplot Fig. 10(p)

5.2 Performance Analysis The procedure to ascertain the maximum IDR for 15 signals is described next. The signal generation using the Multi-Carrier Continuous Wave option of the R&S SMBV100A Vector Signal Generator (described above) and detection is illustrated in Fig. 10. The frequency spectrum (2048 frequency bins) of the digitized data is shown in Fig. 10(a). A total of 15 signals were generated with a carrier spacing (frequency separation) of 4 MHz with carriers between 576 MHz and 630 MHz. The IDR between the first (strongest) signal and the fifteenth (weakest) signal is 25 db. Fig. 10(b) - (p) shows only the frequency bins between 700 and 1000 for more clarity. Fig. 10(c) - (p) depict the detection and removal of the strongest signal in the dataset. The fifteen signals detected were 616.16 MHz, 608.39 MHz, 604.21 MHz, 612.22 MHz, 596.14 MHz, 599.58 MHz, 592.06 MHz, 588.13 MHz, 583.89 MHz, 620.04 MHz, 580.31 MHz, 624.17 MHz, 628.11 MHz, 575.8 MHz, and 1192.01 MHz. The weakest signal (fifteenth signal) is a false alarm (signal detected as 1192.01 MHz instead of 632 MHz). From the 2048 frequency bin plot (Fig. 11) it is was observed that the highest peak is a spurious signal, not the actual signal (632 MHz). Next, the same experiment was conducted by dropping the IDR between first and the fifteenth by 1 db to 24 db. The signal detections are shown in Fig. 12. From Fig. 13 it can be observed that the highest peak was the actual signal (632 MHz) and was successfully detected.

Exhaustive simulations were conducted to identify the IDR for multiple signals with frequency separation as a variable. Up to 20 signals were generated using the setup described in the above section. As shown in Table 2, it is observed that as the number of signals detected increases, the achievable IDR decreases. Also, as the frequency separation is reduced the achievable IDR also decreases. By varying the signal amplitudes and frequencies in full scale BW of 1.25 GHz for the receiver that can detect up to 20 signals, the maximum SFDR, frequency separation, frequency resolution, and maximum IDR were measured as 40.2 dB, 3 MHz, 0.5 MHz and 22 dB, respectively. In terms of the computational performance of the proposed receiver implementation, the two GPUs are able to process and identify 20 signals in each of the 8000 data sets within 33.77 ms (before the next set of digitized data arrives).

Table 2. Comparison of maximum achievable IDR for multiple signal data (measured) with different frequency separations

Freq. Separation	# Signals	IDR (db)
4 MHz	2	4 4.5
	3 to 4	37
	5 to 14	31
	15 to 20	24
3 MHz	2	36
	3 to 4	29
	5 to 14	27
	15 to 20	22

6. CONCLUSION

The design and performance evaluation of multi-processor 3 GSPS receiver with expandable BW implemented on a multi-processor hardware platform was presented. The receiver, with a hardware platform that utilizes Nvidia Tesla C2050 GPUs to handle the computational complexity and a Xilinx Virtex-5 FPGA to perform signal formatting, combines four wideband receivers to achieve an effective BW of 5.125 GHz. The work also presented a multi-carrier RF signal generation and testing setup, and performance analysis of the receiver implementation on the multi-processor hardware platform. The proposed receiver system, detecting up to 20 signals with the SFDR, the frequency separation, the frequency resolution and the IDR of 40.2 dB, 3 MHz, 0.5 MHz and 22 dB respectively, outperforms the predecessor single-processor receiver designs.

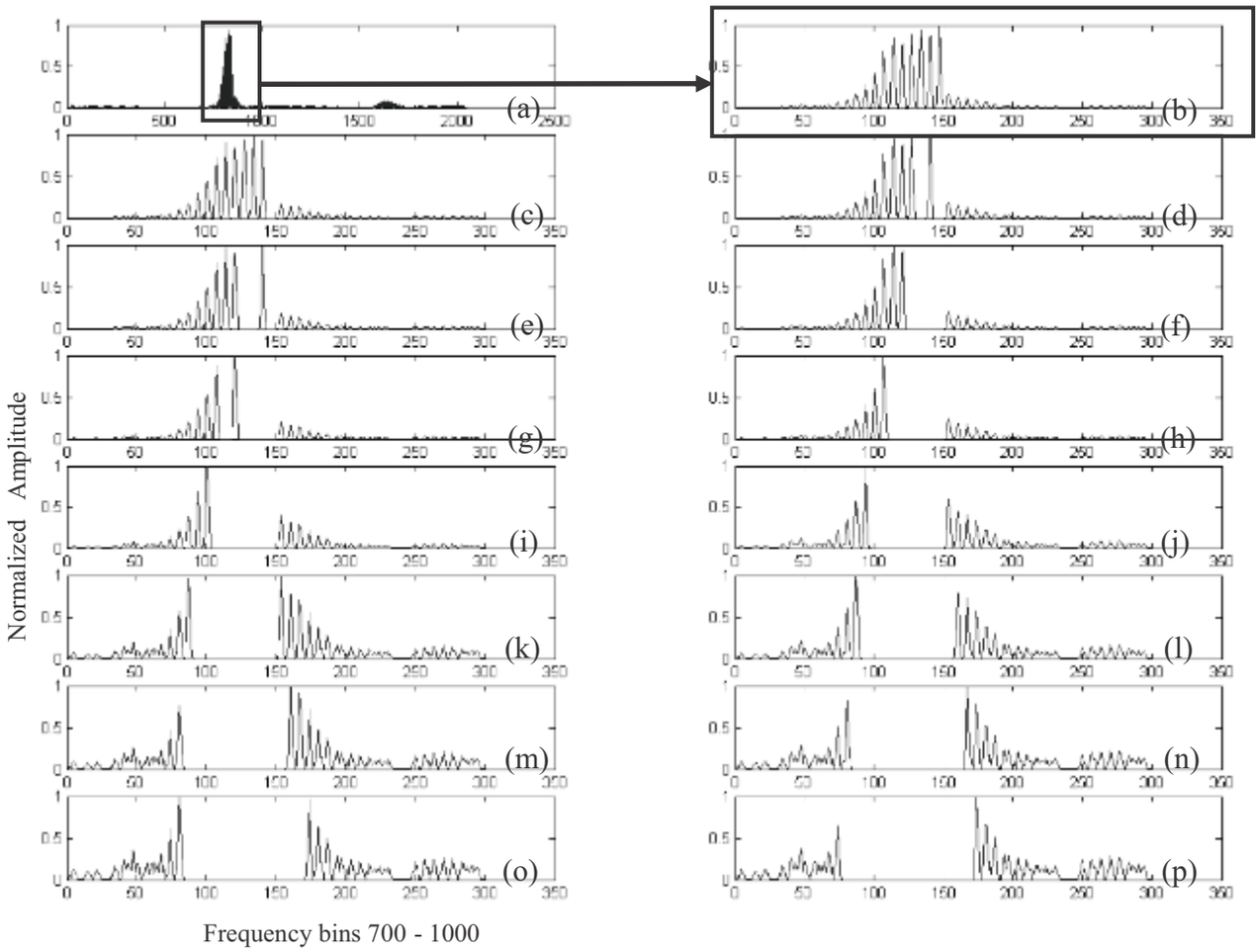

Fig. 12(a) – 8(p) Multi-signal (15 signals) detection with maximum IDR of 24 db and frequencies ranging between 576 MHz and 630 MHZ

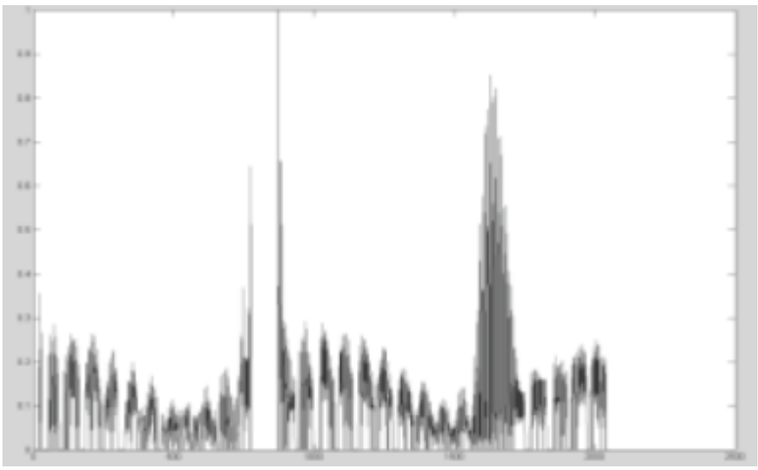

Fig. 13. Depiction of 2048 frequency bins of subplot Fig. 12(p)

REFERENCES

1. J. B. Y. Tsui and J. P. Stephens, "Digital microwave receiver technology," IEEE Trans. Microw. Theory Tech., vol. 5 0 , no. 3, pp. 699–705, Mar. 2002.
2. D. Pok, C.-I. H. Chen, J. Schamus, C. Montgomery, and J. B. Y. Tsui, "Chip design for monobit receiver," IEEE Trans. Microw. Theory Tech., vol. 45, no. 12, pp. 2283–2295, Dec. 1997.
3. J. M. Emmert, J. A. Cheatham, B. Jagannathan, and S. Umarani, "An FFT approximation technique suitable for on-c h i p generation and analysis of sinusoidal signals," in Proc. IEEE Int. Symp. Defect Fault Tolerance VLSI Syst., pp. 361–368, Nov. 2003.
4. K. George, C.-I. H. Chen, and J. B. Y. Tsui, "Extension of two-signal spurious-free dynamic range of wideband digital receivers using Kaiser window and compensation method," IEEE Trans. Microw. Theory Tech., vol. 55, no. 4, pp. 788–794, Apr. 2007.
5. Y.-H. G. Lee and C.-I. H. Chen, "Dynamic kernel function fast fourier transform with variable truncation scheme for wideband coarse frequency detection," IEEE Trans. Instrum. Meas, vol. 58, no. 5, pp. 1555–1562, May 2009.
6. D.M. Lin and L.L. Liou, "Two signal high dynamic range and high resolution wideband digital receiver using beat frequency," Proc. IEEE Military Comm. Conf., pp. 1- 6, Nov. 2008.
7. P-J Chung, J. F. Bohme, C. F. Mecklenbrauker, and A.O. Hero, "Multiple signal detection using the Benjamini-Hochberg procedure", IEEE Int. Work. Computational Advances in Multi-Sensor Adaptive Processing, pp. 209-212, Dec. 2005.
8. J. Grajal and G. Lopez-Risueno, "Multiple signal detection and estimation using atomic decomposition and EM", IEEE Trans. Aerospace and Electronic Systems, Vol. 42, No. 1, pp. 84-102, Jan. 2006.
9. G. Lopez-Risueno, J. Grajal, and A. Sanz-Osorio, "Digital channelized receiver based on time-frequency analysis for signal interception", IEEE Trans. Aerospace and Electronic Systems, Vol. 41, No. 3, pp. 879-898, Jan. 2005.
10. K. George and C.-I. H. Chen, "Multiple signal detection and measurement using a configurable wideband digital receiver," Proc. IEEE Int. Instrum. Meas. Tech. Conf., pp.1-5, May, 2007.
11. K. George and C. Chen, "Design and Performance Evaluation of a Digital Wideband Receiver on a Hybrid Computing Platform," Proc. IEEE Int. Instum. Meas. Tech. Conf., pp. 16-20, May 2011.
12. J. D. Owens, M. Houston, D. Luebke, S. Green, J. E. Stone, and J.C. Phillips, "GPU computing," Proc. IEEE, vol. 96, no. 5, 879-899, Apr. 2008.
13. J. E. Stone, J. C. Phillips, P. L. Freddolino, D. J. Hardy, L. G. Trabuco, and K. Schulten, "Accelerating molecular modeling applications with graphics processors," Jour. Comp. Chemistry, vol. 28, no. 16, pp. 2618-2640, Dec. 2007.

(14) J. B. Y. Tsui, Digital Techniques for Wideband Receivers, 2nd Edition, Artech House, 2001.

TMS320C6713 DSK AND VM3224k2 DSP DEVELOPMENT PLATFORMS: A REVIEW

Varun Sharma
Department of Electronics and Communication, JIIT Noida ,India
Email: varun.sharma010991@gmail.com
Contact Num: +91-7503797183

Priyanka Arora
Department of Electronics and Communication, JIIT Noida ,India
Email: arora.pri02@gmail.com
Contact Num: +91-9310749333

Harshul
Department of Electronics and Communication, JIIT Noida ,India
Email: pkg1410@gmail.com
Contact Num: +91-9911803667

Tanuj Chauhan*
Department of Electronics and Communication, JIIT Noida ,India
Email: tanuj.chauhan@jiit.ac.in , Senior Lecturer
Contact Num:+91-9871221050,
Corresponding author

A-10,Sector-62,Jaypee Institute Of Information Technology, Noida , Uttar Pradesh,201307

ABSTRACT

The paper provides an overview of the TMS3206713 DSK and its interfacing with the VM3224K2 Daughter Card which enhances the time and speed deterministic operations related to Digital Speed Algorithms. The implementation and computation of the paper is done in C language and compilation using CCS (Code Composer Studio) Integrated Development Environment. Embedded Daughter Card is used to display the images captured by the analog camera on to the LCD.The paper is an attempt to enhance the reader's horizons towards implementation of various digital signal processing techniques using the kit and the daughter card as the user gets an insight into the practical implementation of the theoretical concepts.

Keywords: *DSP, TMS320C6713, VM3224K2, CCS, RTDX, IDE, POST.*

1.INTRODUCTION

In the last four decades Digital Signal Processing has become a core technology in the rapidly growing areas such as real time signal processing, audio, video processing and communication, making it a very well established discipline. The ease with which complex linear or non linear algorithms can be implemented along with high reliability, ease of manipulation and availability of low cost practical implementations make the digital signal processing a preferred choice while handling continuous time signals. To bridge the gap between theoretical understanding and implementation of real time DSP algorithms many Digital Signal Processing Kits have been developed that focuses on improving high precision operations. In this paper one such kit TMS320C6713 which was developed by Texas Instrument in collaboration with Spectrum Digital is being discussed. To develop video processing algorithms on TMS320C6713 in we use VM3224K2 daughter card which is an extension to the DSK kit and is further discussed in the paper.

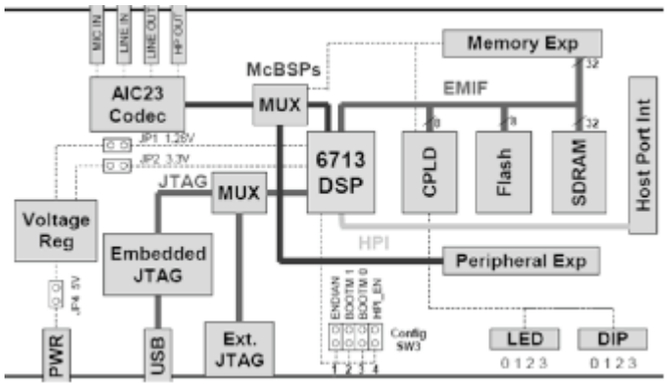

(Figure 1-Block Diagram Of TMS320C6713)

- 32 Bit floating point processor
- Operating Frequency 225 MHZ
- (very long instruction word)architecture
- 264 KB of internal me,ory
- 16 Mb of external SDRAM
- 512 KB of flash memory
- JTAG EMULATION THROUGH ON-board JTAg emualator with USB host
- single voltage power supply (+5v)
- on board peripherals includes
  - 32 bit EMIF and
  - External peripheral interface (daughter card Vm3224k2)
  - HPI (HOST PORT interface)
  - 32 bit stereo codec AIC23

(Figure 2-Key Features of DSKC6713)

2. INTERFACING

2.1 Hardware Interfacing

VM3224K2 LCD Display Daughter Card

The DSP STAR TFT LCD Video Daughter Card (VM3224K2) is a hardware module that allows video in/out and facilitates video processing algorithm based on TMS320C6000 DSP in a cost efficient manner. The video module acquires NTSC (National Television System Committee) /PAL (Phase alternating line) signals as input that are transmitted at 30/25 frames per second respectively and displays digital video data on TFT LCD display. The daughter card is compatible with image processing algorithms but is only used to display the input and output images and the whole processing is done in TMSC6713.It has a 3.5 inch TFT LCD display and a resolution of 320X240 which is displayed in l a landscape/portrait pixel arrangement.

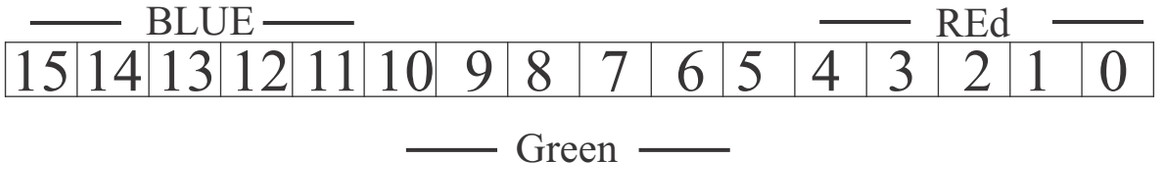

(Figure 3-RGB565 Bit Representation)

The TFT LCD uses a RGB565 pixel expression and has 16 bits per pixel. The LCD panel receives pixel data periodically according to the pixel array pattern which is in sync with the horizontal and the vertical signals. Hence, the video module contains memory that can store 320x240 pixel data. The module also contains an LCD controller that conveys memory data to the LCD panel in synchronization with the horizontal and vertical sync signals. The LCD controller generates signals to drive the LCD, and the 18-bit address generator generates pixel data addresses directed to the LCD [3]. The image is stored in the DSK in the RGB565 format.

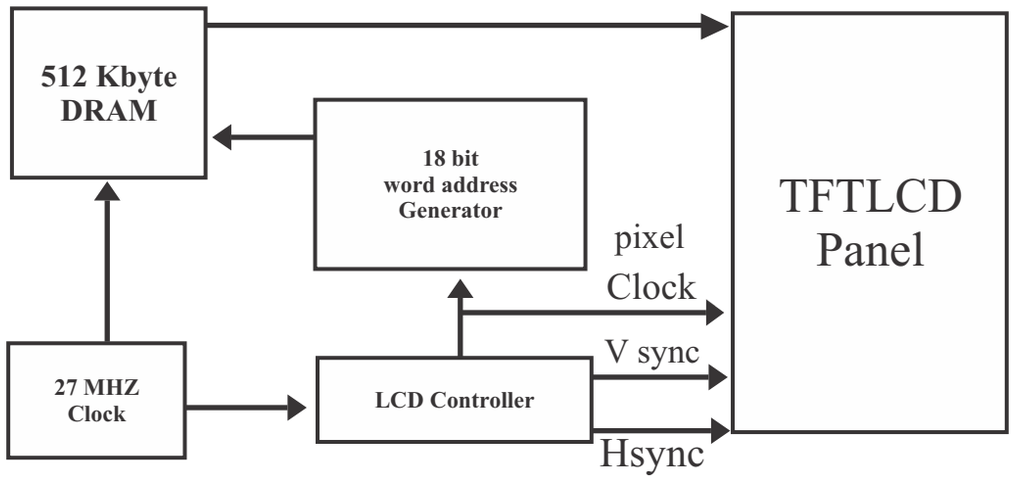

(Figure 4- Block Diagram Representing Camera Interfacing)

The four CPLD registers for control and data processing of the video module namely CNTL (Control),ADDH (High Address register),ADDL (Low Address Register),DATA Register. The image capture speed is determined by Rate field of the CNTL register and is then stored in the screen buffer. Other parameter such as backlight intensity and Reset are also controlled by the control Register.

Screen buffer enclosed in the VM3224K2 takes 512K bytes in size. Half of these (256K bytes) are used for the input buffer and the other half (256K bytes) is used for the output buffer. The DSP processor accesses the screen buffer through ADDH and ADDL registers. Therefore, the screen buffer data can be read by putting the data address in ADDH and ADDL registers and then reading it from the DATA register. At this time, the address registers value increments automatically.

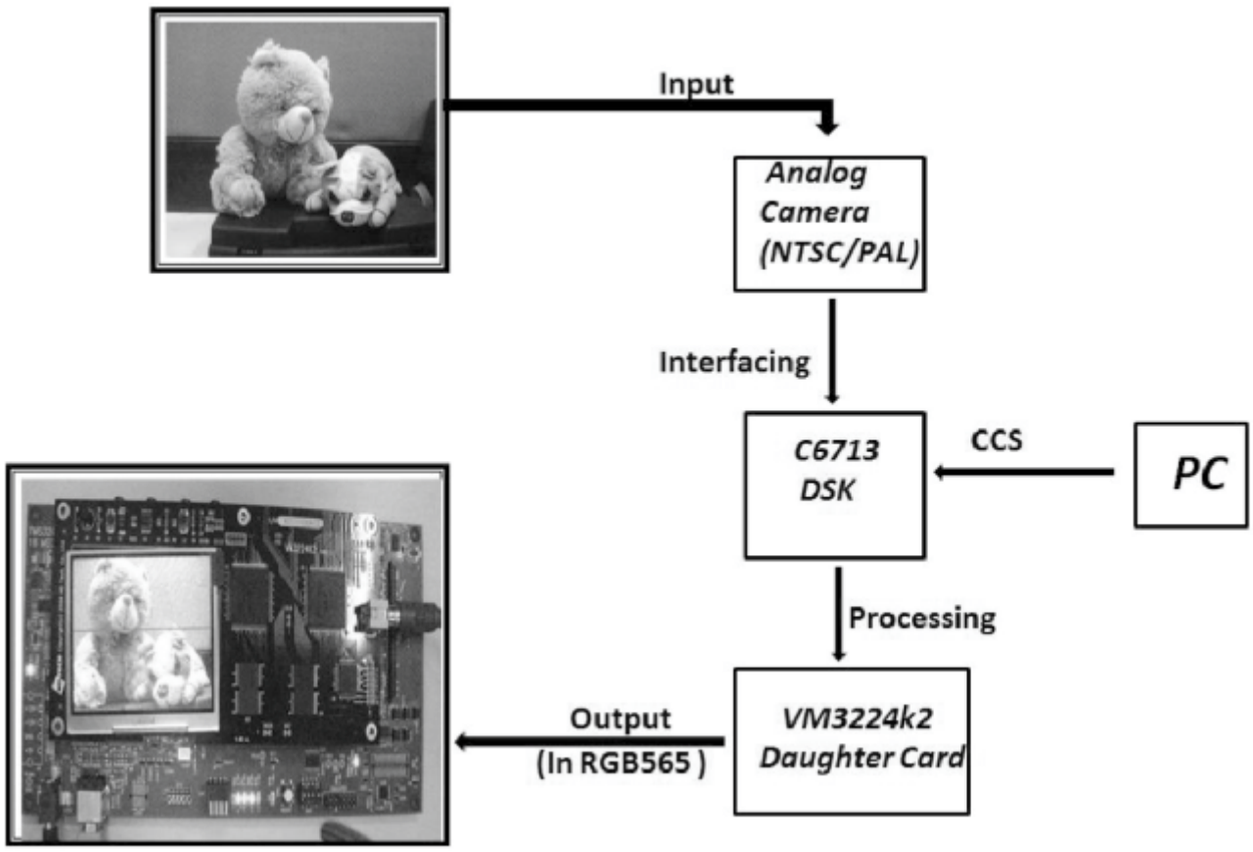

(Figure 5- Daughter Card VM3224K2 Interfacing)

2.2 Software Interfacing The coding is done in C-language in CCS(Code Composer Studio). It helps in compilation, real time debugging, and linking programs in an integrated development environment (IDE).The software helps in converting High level C language into machine understandable and executable out file to be loaded and run on the C6713 processor. The intuitive IDE provides a single user interface taking the user through each step of the application development flow which helps the user to get acquainted to the sophisticated productivity tools much faster. CCS includes with it SYS/BIOS, which is an advanced real time operating system and is used for hardware extraction, memory management and multitasking of TMS320C6713.

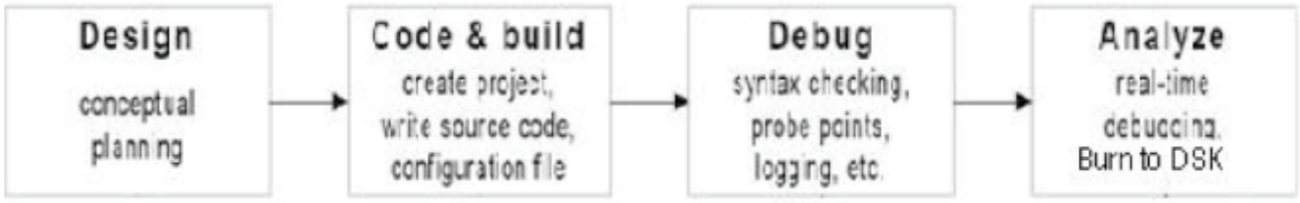

(Figure 6 : Block Diagram Representation (CCS))

Real time data analysis can be performed using real time data exchange (RTDX), a well notified feature of CCS that allows exchange between C6713 and the host computer, via the Joint Test Action Group (JTAG).

POST(Post power on self test) and diagnostic utility uses the board support library to test the DSK before it can be used for any further use and implementation .POST which is stored in onboard flash memory is used to check the Direct memory access, Internal, external and flash memories ,Onboard codec, Two channel buffered serial ports ,LEDs and DIPs.

Once the POST completes successfully the booting operation of the system is initialized. There are three LEDs to provide the user

with feedback from the test procedure. The test program (stored in the FLASH memory, code available on the DSK CD-ROM) runs every time DSK is powered on and reset. The successfulness of POST is determined by the generation of the 1 KHz tone and simultaneous blinking of all the LED three times.

(Figure 7: POST)

3. CONCLUSION

The paper presents a simple approach towards TMS320C6713 Kit hardware peripherals and interfacing the kit with VM3224K2 Daughter card and reading and displaying video data to the LCD .It enhances the opportunity for real time implementation of DSP algorithms related to image processing. We have also shown a great implementation of our objective in DSP hardware using C-programming language. The relevant code for the same can be obtained from the authors.

REFERENCES

1. Rulph Chassaing, "Digital Signal Processing and Applications with the C6713and C6416 DSK," Ed. New Jersey: John Wiley & Sons, Inc Ch 1-3.
2. Texas Instruments, DSP STAR TFT LCD Video Daughtercard (VM3224K2)User's Manual Revision 2.4, 2009.
3. Texas Instruments, Spectrum Digital TMS320C6713 DSK Technical reference Rev. B November 2003.
4. Neeraj Kumar, Sushree Mahapatro, Sukanti Pal, Implementation of Color Image Enhancement using DCT on TMS320C6713 presented at International Journal of Electronics and Computer Science Engineering.
5. T Sreekanth Rao, B Prathyusha, P Nagarjuna Reddy ,Implementation of Graphical Equalizer using LabVIEW for DSP Kit DSK C6713 presented at Journal of information and communication technologies, VOLUME 2, ISSUE 6, June 2012

A TECHNIQUE TO INDICATE THE QUALITY OF CIGARATTE FILTER USING FUZZY LOGIC

Santhosh K V
kv.santhu@gmail.com
Research Scholar, Dept of Electrical Engineering, NIT Silchar, Assam

ABSTRACT

A cigarette filter has the purpose of reducing the amount of smoke, tar, and fine particles inhaled during the combustion of a cigarette. Filters also reduce the harshness of the smoke (Nicotine) and keep tobacco flakes out of the smoker's mouth. This paper proposes a technique to check the quality of filter, so as to choose a proper filter which can restrict the amount of harmful smoke entering the human body. The whole system is implemented physically using capacitive sensor, NI DAQ cards; analysis is made with the help of LabVIEW software.

Smoking is injurious to health. But it is practically impossible to make everyone quit smoking. Through this paper an attempt is made to reduce the amount of hazardous chemical entering the human body by choosing a proper filter. The proposed technique is subjected to test with various samples and to validate the proposed technique, the samples were subjected to chemical tests. Results showed the proposed technique achieved its objective.

Keywords : *Capacitive sensor, Cigarette filter, Fuzzy logic, Industrial automation, LabVIEW.*

1.INTRODUCTION

Nicotine is a powerful insecticide and among the deadliest of all plant products in its pure form. According to the US Department of Health and Human Services, it raises blood pressure, affects the central nervous system, and constricts blood vessels in humans. Nicotine is a colorless liquid that is highly soluble in water, and is readily absorbed through the skin in its pure form. Nicotine is found in Cigarette.

Cigarette filters are specifically designed to absorb vapors and to accumulate particulate smoke components. Filters also prevent tobacco from entering smoker's mouth, and to provide a mouthpiece that will not collapse as the cigarette is smoked. Filters generally have the following components: 95% of cigarette filters are made of cellulose acetate and the balance are made from papers and rayon. The cellulose acetate tow fibers are thinner than sewing thread, white, and packed tightly together to create a filter; they look like cotton. Filters vary in filtration efficiency, depending on whether the cigarette is to be „light " or „regular ". Filtration efficiency can be defined as the percentage of absorption of vapors, and accumulate particulate smoke components. The efficiency of cigarette filter depends on the density of cellulose acetate tow fibers. Then by measuring the density of cellulose acetate tow fibers one can indicate the quality of cigarette filter. To compute the density of cellulose acetate tow fibers, we make use of its dielectric property [1-14]. This property of cellulose acetate is made use and a capacitance sensor is designed. By measuring the value of capacitance one can find the density of cellulose acetate. The output capacitance of capacitance sensor is converted to frequency using a timer circuit, and to voltage using a frequency to voltage converter circuit. This data is transmitted to PC using the DAQ cards. LabVIEW is used to process the data and display the quality of cigarette filters. This paper aims at design of one such Instrumentation system which will check the quality of the cigarette filter.

The paper is organised as follows: After introduction in section –I, a brief description on block diagram is given in section-II. Section-III discusses about the problem statement followed by problem solution in Section- IV. Section-V deals with the results and analysis. Finally, conclusion and discussion is given in section-VI

2. BLOCK DIAGRAM

The block diagram representation of the proposed instrument is given in Fig.1

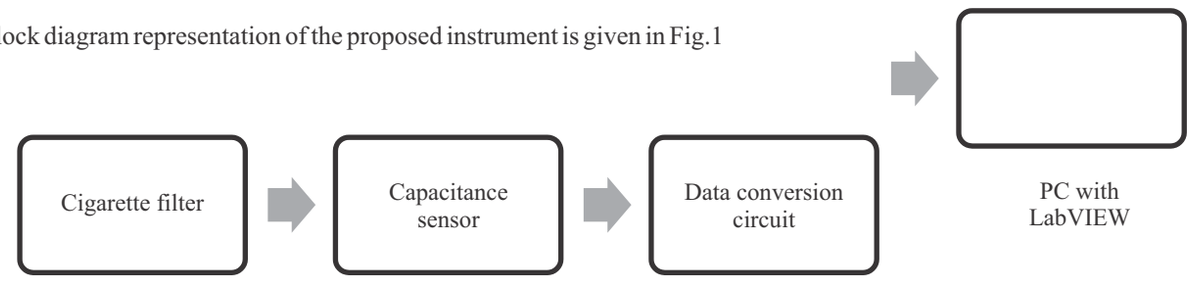

Figure. 1. Block diagram of the proposed instrument

A: SENSOR

The quality of the filter depends on the amount of cellulose acetate, so by measuring the amount we can know the quality of the

filter. To measure the amount of cellulose acetate we use the property of cellulose acetate, which says it is a good dielectric. The capacitance is given by eqn.1 [15-17]

(1) ————

Where:

o= Permittivity of free space

r = Permittivity of dielectric

A = Area of the plate

D = Distance between plates

From eqn.1 we can design a capacitance sensor to measure the dielectric constant of cellulose acetate as shown in Fig.2. Two cylindrical plates are placed parallel so as to form a capacitance plates. These plates are used to measure the dielectric constant of cellulose acetate present in cigarette filter. The value of the capacitance which is measured using these plates will be indication of the density of cellulose acetate tow fiber and indirectly the quality of cigarette filter.

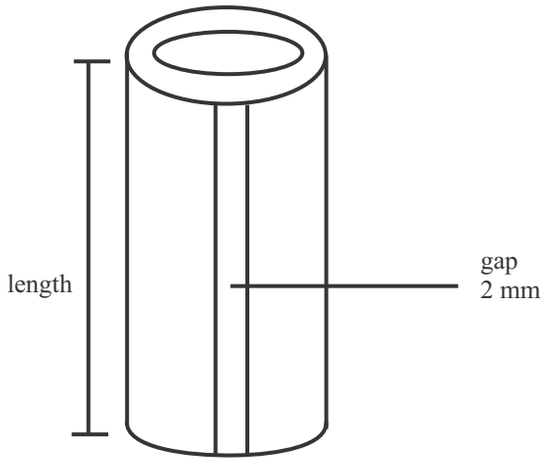

Figure.2. Graphical representation of Capacitance sensor

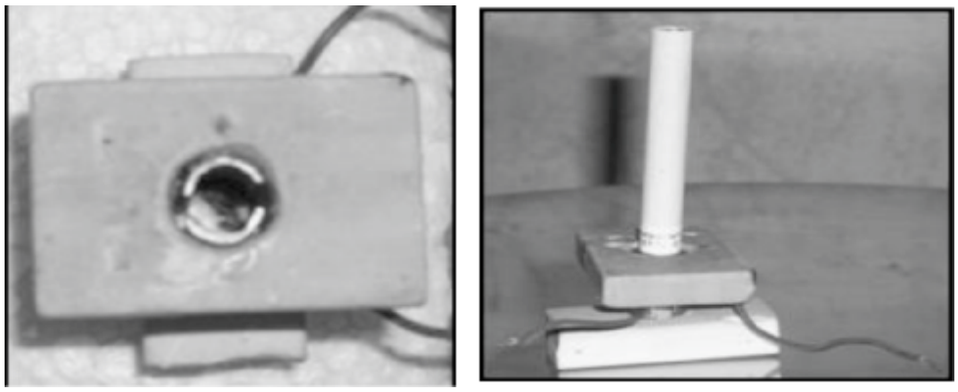

Figure.3. Picture of Capacitance sensor without and with cigarette

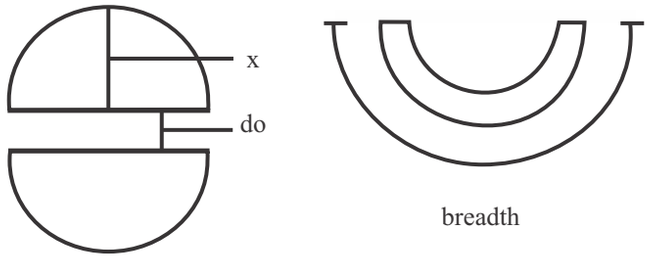

Figure.4. Top view of capacitance sensor

D is found out using integration, since its value is not same at all points as in Fig. 4

do = 2mm,

xis taken as 3.5mm

$D = do + 4 * \int 3.5mm\ X$ (2)

D = 2.0245mm

Equating the result of eqn.2 in eqn.1

——————————— F (3)

On substituting the known values for the constant present in eqn.3. We ge

——————————— F

The capacitance obtained is further converted to frequency using a timer circuit. A brief description on ti mer circuit is discussed in following topic.

B: Timer Circuit In Astable mode, the 555 timer (shown in Fig.5) puts out a continuous stream of rectangular pulses having a specified frequency. Resistor R1 is connected between VCC and the discharge pin (pin 7) Resistor R2 is connected between the discharge pin (pin 7) and the trigger (pin 2). Threshold pin (pin6) is connected with trigger pin. Hence the capacitor is charged through R1 and R2, and discharged only through R2, since pin 7 has low impedance to ground during output low intervals of the cycle [18-19].

The frequency (f) of the pulse stream depends on the values of R1, R2 and Co, as in eqn. 4.

——————————— Hz (4)

( ) ( )

Thus the capacitance from the sensor corresponding to the density of cellulose acetate tow fiber in cigarette filter is converted to frequency given by eqn.5.

——————————— Hz (5)

( ) ( ) ( )

On substituting the values of R_1 and R_2 we get

——————— Hz

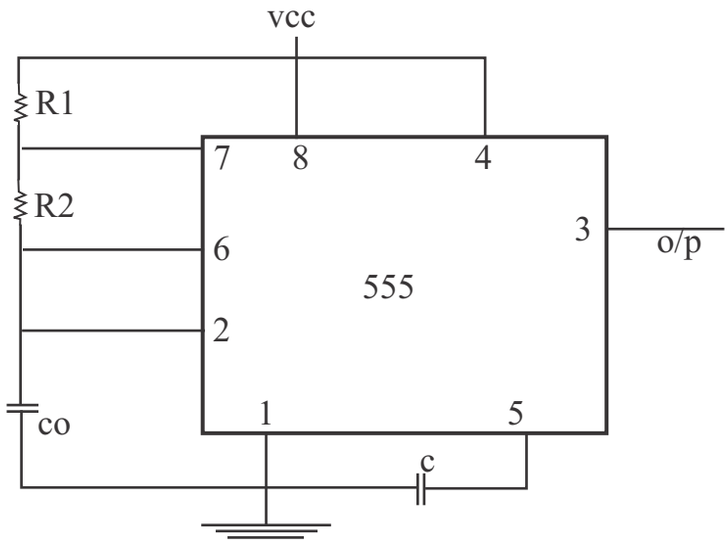

Figure.5. 555 as astable Multi vibrator

C: Frequency To Voltage (f/v) Converter TC 9400 frequency to voltage converter circuit is shown in Fig.6. When used as a F/V converter, the TC9400 generates an output voltage linearly proportional to the input frequency waveform. Each zero crossing at the threshold detector's input causes a precise amount of charge (q = CREF * VREF) to be dispensed into the operational amplifier ‟s summing junction. This charge in turn flows through the feedback resistor, generating voltage pulses at the output of the operational amplifier. A capacitor (CINT) across RINT averages these pulses into a DC voltage which is linearly proportional

to the input frequency [20].

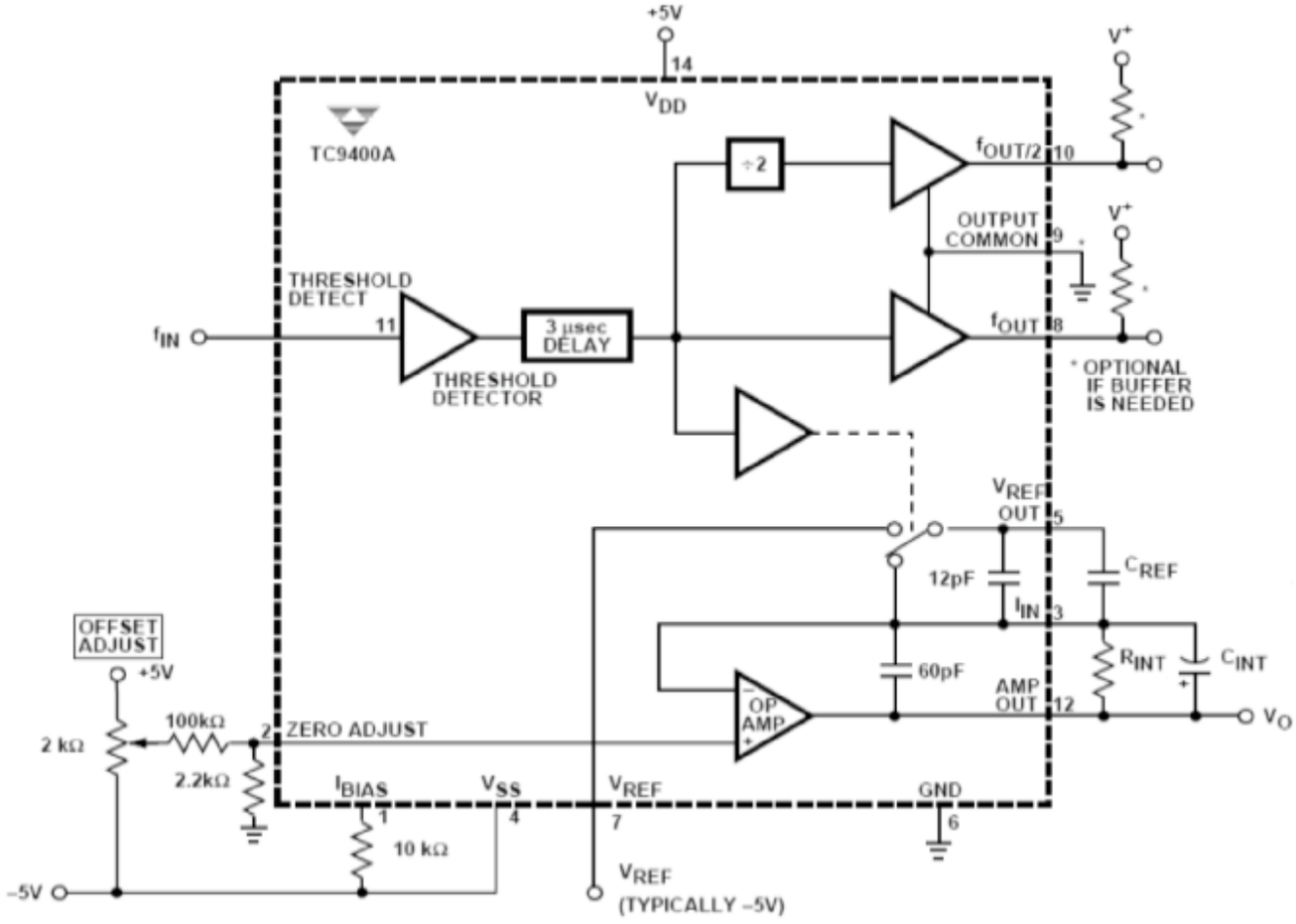

Figure.6. TC9400 Frequency to voltage converter

The output voltage in volts is related to the input frequency (f) by the eqn.6:

$V_o = (V_{REF} * C_{REF} * R_{INT}) * f$ Volts (6)

On substituting the values of RINT, COUT, and f we get

——— V

D: DAQ PCI NI 6024E Data acquisition is the process of sampling signals that measure real world physical conditions and converting the resulting samples into digital numeric values that can be manipulated by a computer. Data acquisition systems (abbreviated with the acronym DAS or DAQ).

The 6024E Series board is high-performance multifunction analog, digital, and timing I/O boards for PCI, PXI, PCMCIA, and CompactPCI bus computers. Supported functions include analog input, analog output, digital I/O, and timing I/O. The 6024E features 16 channels of analog input, two channels of analog output, a 68-pin connector and eight lines of digital I/O [21].

E: LabVIEW

LabVIEW is a fully featured programming language produced by National Instruments. It is a graphical language quite unique in the method by which code is constructed and saved. There is no text based code as such, but a diagrammatic view of how the data flows through the program. Thus LabVIEW is a much loved tool of the scientist and engineer who can often visualize data flow rather than how a text based conventional programming language must be built to achieve a task. LabVIEW programs are called virtual instruments, or VIs, because their appearance and operation imitate physical instruments, such as oscilloscopes and multimeters. LabVIEW contains a comprehensive set of tools for acquiring analyzing, displaying, and storing data, as well as tools to help you troubleshoot your code.

LabVIEW VI "s contains three components - the front panel, the block diagram, and the icon, and connector panel. In LabVIEW, you build a user interface, or front panel, with controls and indicators. Controls are knobs, push buttons, dials, and other input devices. Indicators are graphs, LEDs, and other displays. After you build the user interface, you add code using VIs and structures to control the front panel objects. The block diagramcontains this code. In some ways, the block diagram resembles a flowchart [22-24].

3. PROBLEM STATEMENT

The digital data corresponding to the density of cellulose acetate tow fibre in the cigarette filter is acquired through data converter and acquisition system to the PC which is loaded with LabVIEW software. Now, the LabVIEW software is programmed to perform the following objectives.

(I Acquire data using DAQ cards and display the voltage output of capacitance sensor.

(ii) Process the signal using fuzzy logic algorithms and indicate the quality of cigarette filter using fuzzy variables using LED ‟s and string data.

4. PROBLEM SOLUTION

The objectives of the proposed work are very clear from the earlier sections. In this section we discuss the program written on LabVIEW to achieve the proposed objectives. LabVIEW contains two window called as front panel and block diagram. Front panel window is where the user can control the program and visualize the outputs. Fig. 7 shows the front panel VI of the proposed work [26-28].

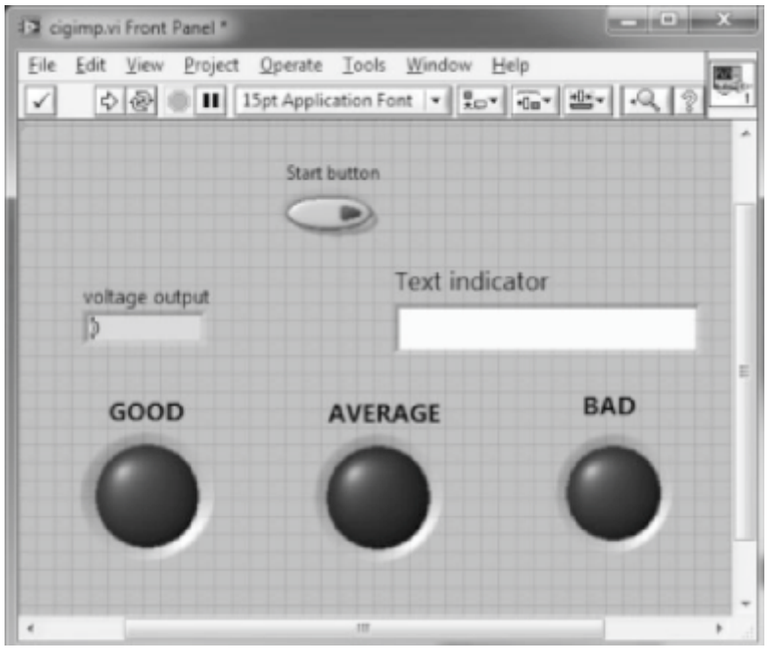

Figure.7. Front panel of the proposed work

Front panel consists of start button to control the starting and stopping of process. One numerical indicator to display the voltage output corresponding to the density of cellulose acetate tow fibre in cigarette filter, which is a direct indication of filter quality. One text indicator displaying string data, indicating the quality of cigarette filter. Front panel also consists of three LED coloured green, blue, and red. These LED ‟s are used indicate the quality of cigarette filter in terms of fuzzy variables like „GOOD ‟, „AVERAGE ‟, and „BAD ‟. To achieve the proposed target program is written in block diagram VI. The program written is shown in Fig.8.

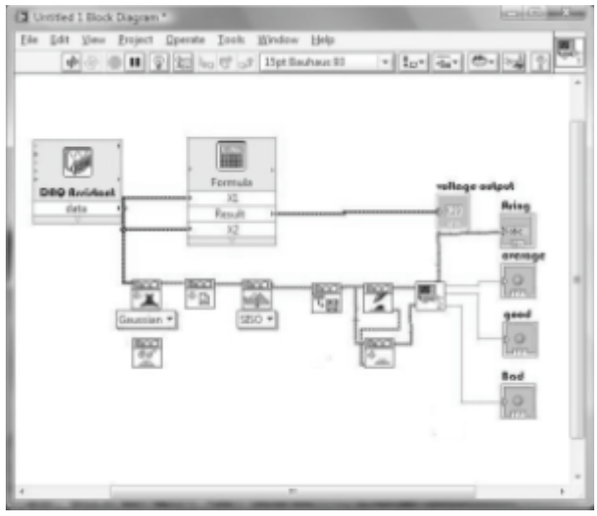

Figure.8. Front panel of the proposed work

Block diagram VI consists of an input DAQ Assist. Input DAQ Assit is used to acquire the signal from DAQ card 6024E. The DAQ Assit is connected with data conversion circuit from which signal is acquired from the capacitance sensor, which is used to measure density of cellulose acetate tow fibre in cigarette filter. The data once acquired is processed to display the actual voltage using a numerical indicator which will also be an indication of quality of cigarette filter. Further, fuzzy logic algorithm is applied on this signal. Based on then input and output of the proposed technique, input and output membership function is created. The fuzzyfication and defuzzyfication rule base is also created. Now processing is done using the fuzzy logic algorithm to display the quality of cigarette filter in terms of three LED ''s used on the front panel. Fig. 9 and Fig. 10 shows the input and output membership function of the fuzzy logic algorithm used for the proposed technique. Fig. 11 shows the defuzzyfication surface view of the proposed technique. Fig. 12 shows the surface graph for the proposed fuzzy logic algorithms. Table -1 shows the rule base of the proposed fuzzy logic algorithm [29-30].

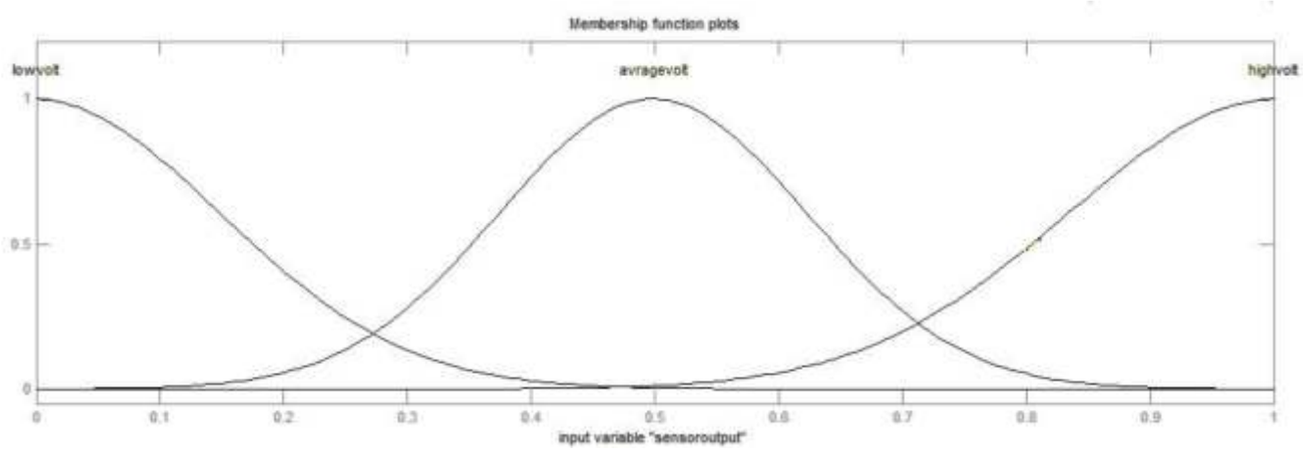

Figure.9. shows the input membership function

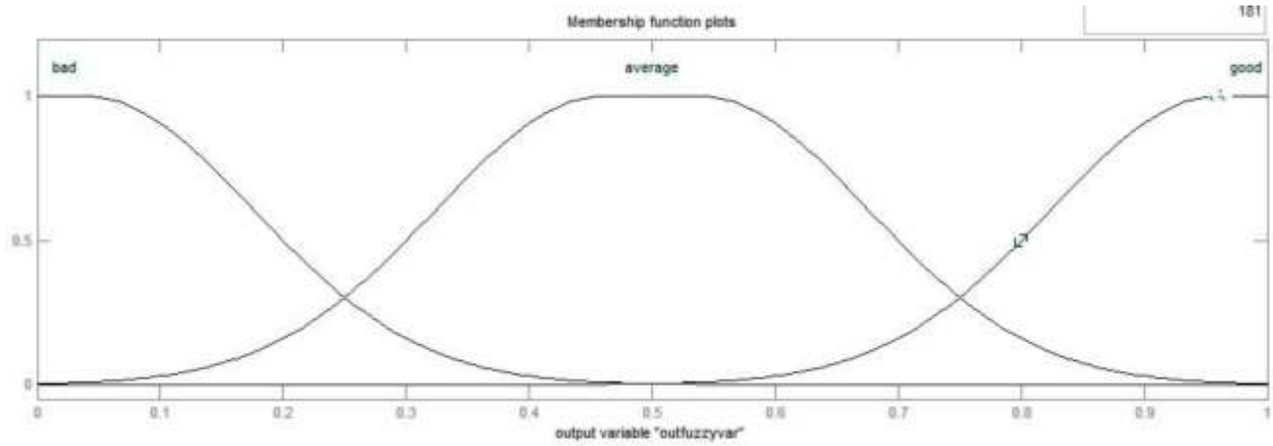

Figure.10. shows the output membership function

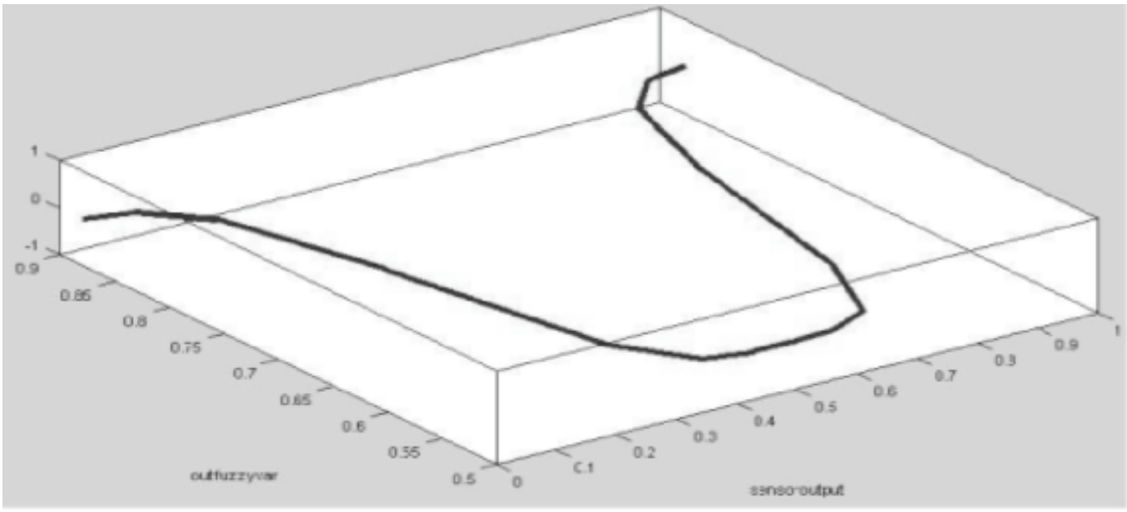

Figure.11. shows the defuzzyfied graph

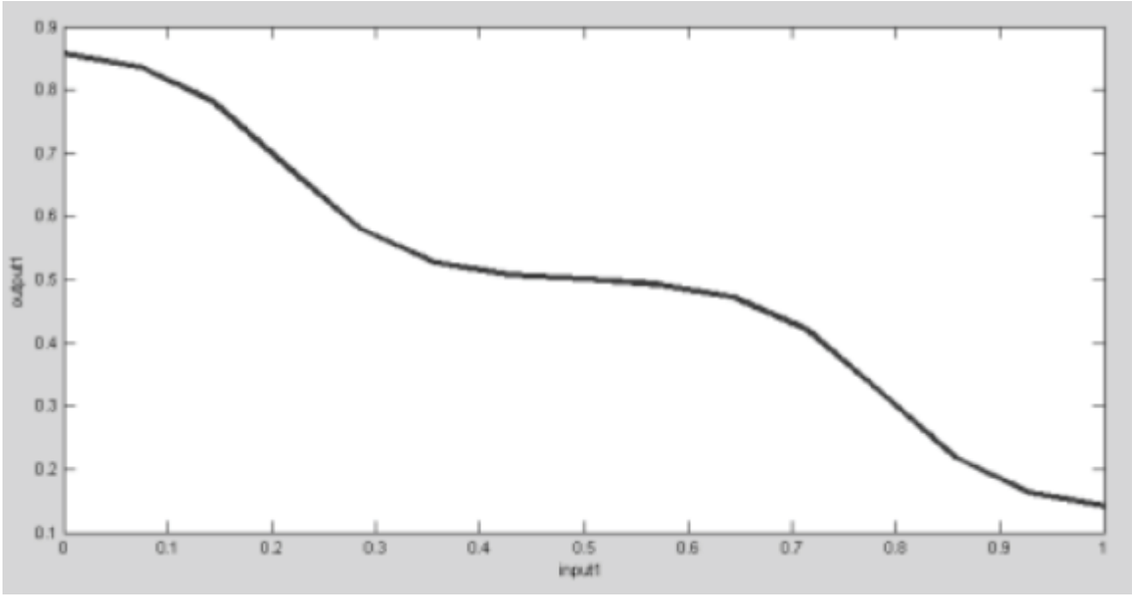

Figure. 12. Shows the surface graph

Sl.no	Rule
1.	If (input1 is lowvolt) then (output1 is good)
2.	If(input1 is averagevolt) then (output1 is average)
3.	If(input1 is highvolt) then (output1 is bad)

Table-1 Rule base of proposed fuzzy system

5. RESULT AND CONCLUSION

The proposed system was tested with different test. Samples of around 30 taken and were subjected to test, results of which is shown in Table-2, Fig. 13, Fig.14 and Fig.15 The good cigarette filter showed the low voltage values as its capacitances were more due to denser cellulose acetate tow fiber, whereas in the case of bad the voltage were high as the capacitance would be less due to less denser cellulose acetate tow fiber. The table -2 below shows the numerical indicator readings. Fig. 13, Fig. 14, and Fig.15 shows the results of fuzzy variables for good, average and bad cigarette filters.

Table-2 results from the proposed technique of different brands

Type of Cigarette		Voltage in V		
		Good	Average	Bad
1	Indian King	1.18	2.68	4.11
2	Gold Flake	0.97	2.44	4.02
3	Flake Premium	0.68	2.10	3.87
4	Berkeley	1.22	2.79	4.23
5	Charms 1.12	2.69	4.02	
6	Gold Coast	0.77	2.16	3.95

Figure. 13. Output as seen in front panel VI for a good cigarette filter.

Figure. 14. Result as seen on front panel VI for average cigarette filter

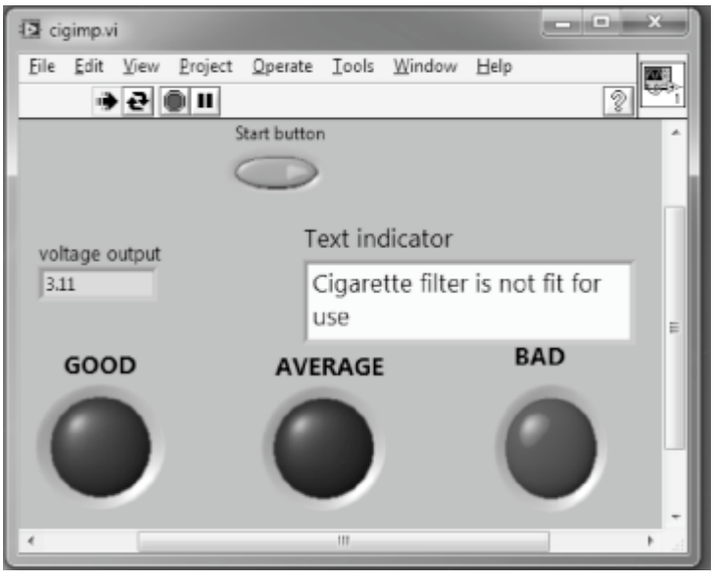

Figure 15.Result as seen on front panel VI for bad cigarette filter.

6. CONCLUSION AND DISCUSSION

Using the proposed technique the quality of six brands of cigarette were found using sample pieces. The results found by the system matched with the present industrial grading of cigarette filter. To validate the results of the proposed technique the samples were again subjected to chemical test. The chemical tests were carried out by collecting the vapors of cigarette at combustion of cigarette. This absorbed vapor was tested, the amount of nicotine, and other chemicals percentages were calculated. Results proved that the cigarette filter which was detected as bad by the proposed technique had a high percentage of nicotine on conduction of chemical tests, and on contrary the cigarette filter which was detected good by the proposed technique had a low percentage of nicotine.

The above results clearly indicated the results obtained by the proposed technique meet the desired objective. There is always a scope of improvement in this technique that is the proposed work considered static measurement method involving only one cigarette filter at a time, which can be improved to achieve dynamic measurement.

Smoking itself is injurious to health, but it ''s practically impossible to make everyone quit smoking. So an attempt has been made in this system to at least regulate the amount of harmful gas entering the human body.

REFERENCES

1. Farr WK, Revere A, Examination of whole cigarette smoke by light and electron microscopy. The Life Extensio Foundation, New York. 1958.
2. Bednarczyk NE. Tobacco smoke filters. Park Ridge, New Jersey: Noyes Data Corp, 1972:1–263, 1972.
3. Memo to Dr Larry Sykes from Pat Walford.. "Cigarette Filter Development." Bates No. 2021601017 – 2021601023, March 9, 1979.
4. US Department of Health and Human Services. The health consequences of smoking: the changing cigarette. A report of the Surgeon General, Rockville, Maryland: Public Health Service, Office of the Assistant Secretary for Health, Office on Smoking and Health, 1981:43. (DHHS Publication No (PHS) 81-50156.) , 1981.
5. Browne CL, The design of cigarettes, Filter Products Division, Hoechst Cellanese Corporation, Charlotte, North Carolina, 3rd ed.. 1990.
6. Wynder EL, Hoffmann D. Smoking and lung cancer: scientific challenges and opportunities. Cancer Res1994; 54:5284–95, 1994.
7. Hoffmann D, Djordjevic MV, Brunnemann KD, Changes in cigarette design and composition over time and how they influence the yields of smoke constituents. J Smoking-Related Disorders. 1995; 6:9–23, 1995.
8. Kluger R. Ashes to ashes: America's hundred-year cigarette war, the public health, and the unabashed triumph of Philip Morris. New York: Alfred A Knopf, 1996.
9. Davis DL, Nielsen MT, Norman A, Cigarette design and materials in Tobacco: production, chemistry and technology, Blackwell Science, Inc., Malden, Massachusetts, pp. 353–387, 1999.
10. Hoffmann D, Hoffmann I, El-Bayoumy K. A less harmful cigarette: a controversial issue. Chem Res Toxicol 2001;14:767–90, 2001. [11] J L Pauly, A B Mepani, J D Lesses, K M Cummings, R J Streck, "Cigarettes with defective filters marketed for 40 years: what Philip Morris never told smokers", Journal for health professionals and others in tobacco control, vol. 11, issue. 1, 2002.
12. D.C. Mariner, M. Ashley, C.J. Shepperd, G. Mullard, M. Dixon, "Modeling the diffusion of carbon monoxide and other gases from the paper wrapper of a cigarette during puffing" , Journal of Analytical and Applied Pyrolysis, vol. 66, No. 1–2, , Pages 263-280, January 2003.
13. Mouth level smoke exposure using analysis of filters from smoked cigarettes: A study of eight countries Original Research Article Regulatory Toxicology and Pharmacology, Volume 61, Issue 3, Supplement 1, pages S39-S50, December 2011.
14. Norman A. Cigarette manufacture: cigarette design and materials. In: Davis DL, Nielsen MT. Tobacco – production, chemistry and technology. Oxford: Blackwell Science, 353–87.
15. Manfred Brotherton, Capacitors, their use in electronic circuits, D.Van Nostrand Company, 1946. [16] William F Mullin, ABC ''s of Capacitors, H W Sams Publishers, 1971.
17. Alexander L Schulz, Capacitors: Theory, Types and Applications, Nova Science Publishers, 2010.
18. Howard M Berlin, 555 Timer Applications Sourcebook with Experiments, Sams Publishing, 1979.
19. Walter G Jung, IC Timer Cookbook, 2nd Ed, Sams Publishing, 1983.
20. www1.microchip.com/downloads/en/DeviceDoc/21483d.pdf
21. www.ni.com/pdf/manuals/370719c.pdf
22. Gary W Johnson, LabVIEW Graphical Programming: Practical Applications in Instrumentation and Control, 2nd Edition, Mc-Graw Hill, 1979.
23. Rick Bitter, Taqi Mohiuddin, Matt Nawrocki, LabVIEW: Advanced Programming Techniques, 2nd Edition, CRC Press,2006.
24. www.ni.com/labview/

25. Jovitha Jeroma, Virtual Instrumentation by LabVIEW, Prentice Hill, 2005.
26. Lisa K. wells, Jeffrey Travis, LabVIEW for everyone, Prentice Hall, New Jersey, 1997.
27. Kevin James, PC Interfacing and Data Acquisition: Techniques for Measurement, Instrumentation and Control, Newnes, 2000.
28. Sanjay Gupta, Joseph John, Virtual Instrumentation using LabVIEW, Tata Mcgraw Hill Publishing Co Ltd, 2005.
29. Harris J, An Introduction to Fuzzy Logic Application, Springer Publisher, 2000.
30. Timothy J Ross, Fuzzy Logic with Engineering Applications, John Wiley & Sons, 2004.

MANAGEMENT OF CONFLICT IN PHARMA CHANNEL SALES: A CRITICAL ANALYSIS ON BRANDED PHARMA PRODUCTS

Dr. Makarand Upadhyaya*
Associate Professor
Marketing at College of Business Administration
Jazan University, Jazan
Saudi Arabia.
Corresponding author

ABSTRACT

India is the 2nd largest producer of pharma products in the world where many of the world players have made their presence. Larger part of the business is trade oriented which makes the role of channel partners very important. Supremacy and politics is a kind of magnet between company and channels in channel sales. It could work either way depending upon the handling and relative positioning. Ideally it should help in aligning partner's interest in the channel with the overall vision of the organization. In monopolistic kind of products the relative supremacy of the channel partners remain subdued but in competitive products supremacy shifts towards channel partners. In this paper the study is done on trade sales in pharma products business in North India which is reasonably competitive in present scenario with a presence of number of small, large and even multinational players. The paper discusses about the existence of supremacy and political factors of channel partner in the Pharma products trade and probable solutions of countering its negative impact on companies.

Keywords: *Supremacy, Politics, Pharma products, Channel, Trade*

1.INTRODUCTION

Supremacy is the ability to get partner's to do things they wouldn't do naturally (Fedor&Bettenhausen, 2008). Collaboration and cooperation between partners vis a vis company policies is important, especially in global trade where geography, demography, different cultures and languages adds to the diversity (Porter & Mayes, 1979). Politics can be described as the use of supremacy to influence the environment to better achieve personal and commercial goals (Coopey& Burgoyne, 2000). The selection or use of supremacy types like personal, legitimate, expert, reward or coercive depends on the situation, relative stakes and the environment (Brass &Burkhardt, 1993). A political pyramid exists when people compete for supremacy. The individual will not get supremacy as he wishes but have to enter into the decisions on how to distribute authority in a supply chain. There is scarcity of supremacy when individuals gain supremacy in absolute terms at others expense and also when there is relative shift in the distribution of supremacy (Zaleznik,1971).In this study a survey of over 100 pharma channel partners and working executives were interviewed across 15 locations including rural, semi urban, urban and metro cities and analysis revealed that dealer development and management is very crucial for pharma products manufacturers. The study shows the differential behaviors and business pattern of channel partners in different areas namely rural, semi urban, urban and metro cities (Cropanzano&Grandey, 1997). In metro cities an increase in direct sales by pharma products producers is posing a lot of challenge to trade channel partners in recent times. This is despite of the fact that pharma products production recorded continuous growth in last few years. "Sub-dealers, who are serviced by front line dealers, are disappointed and not satisfied because they are of opinion that the pharma products companies do not recognize & appreciate their role in the structure of the channel sales.

Another matter of concern for retailers is that front line dealers do-not pass the appropriate benefits deserved by them. At the same time the concern of Dealers is the conversion of quality retailers into Dealership of their own company or the competitor resulting into their direct loss of volumes and profits. This clearly indicates that this segment has a huge growth prospects in the years to come. It will challenge the role & position enjoyed by the channel resulting in reduced margin and aggressive competition.

2. ANALYSIS OF SUPREMACY AND POLITICS

In channel sales the role of the channel partners is very important. There are different layers of channels in different businesses and in pharma products industry normally trade vertical has two to three layers. The top most layers exist in many companies which is generally the most important and supreme. In few companies the role played by this layer is handled by the company itself. If it is the external agency in this layer, it is called by different names like sales promoters/ CFA/ Marketing organizers, etc. Their role is defined clearly by all companies but still they are much more supreme than their position. The second layer which is also first layer in some companies is called as stockiest/dealer. They remain in direct touch with the company and directly do the business with the respective company. There is another layer of channel partners normally known as retailers. They do the transactions with the respective dealer/stockiest and are indirectly associated with the company. Role of a dealer/stockiest is to buy the product from the company and sell it to the retailers and/or to the customers. Dealers are managed by the company officials and/or by the upper layer depending upon the system being followed by the respective company. Different dealers have different sizes of business and enjoy different supremacy.

3. FINDINGS FOR CHANNEL SALES

In today's competitive environment there is a lot of volume selling pressure and companies, employees as well as dealers are under stretched target pressure (Cropanzano& Li, 2006). In managing those business requirement there are various factors. The factors which impact the supremacy of dealers are:

1. Size of business of the dealer – It means the business turnover of channel partner with the company.
2. Association with the company (Longevity) – It represents the number of years of business association of the dealer with the company.
3. Stakes of the company in that respective market – It represents as how important that particular market is for the company. Is it primary, secondary or tertiary market?
4. Total market size in which respective dealer operates and the respective market share – It represents the total market potential vis a vis the market share of that particular dealer.
5. Competitor's position in respective market – It represents company's position as compared to competitor's position in that market.
6. Strength of secondary network of the dealer – It represents the dealer's own network of sub dealers/retailers.
7. Investment capacity of the dealer in the market – It represents the financial soundness and investment capacity of the dealer.
8. Strength of customer bases of the dealer – It represents the market presence and regular customer base of the dealer with good footfall.
9. Approach and appetite of the dealer for growth – It is about the attitude of the dealer with respect to present and future business.
10. Pharma products business has a limited piece of total business pie – It means the cases where the dealer's total business size is too big as compared to our business. In other word the dealer has other businesses which are much larger than our business.
11. Individual/Firm goodwill – The goodwill of dealer and its firm is too good which enhances the image of the company as well.
12. TINA or limited alternative – This represents the situation where the company has no alternative.
13. Strong infrastructure – This represents the situation where the dealer has a good infrastructure to support the business.
14. Availability of other options/opportunities – This represents the situation where dealer has other better options available.

Apart from this there are some other factors by virtue of which a dealer becomes more supreme. These are the political factors which enhance the supremacy of channel partners.

1. Relationship with senior management of the company – This represent the situation where dealer has good rapport with the senior management of the company.
2. Networking with other dealers and capacity to influence them – This represents the leadership style of the dealer where he has the capacity to influence other dealers to support his thoughts.
3. Proximity to the people in dominance – It means where dealer has connection with those people who are in supreme.
4. Position or supremacy to influence the people in position at local bodies – This represents the position where dealer may influence the business with the help of local bodies.
5. High nuisance value – This represents those dealers who have big nuisance value and have the capacity to escalate small issues and even non issues.
6. Capability to exploit weakness of systems/individuals – This represents those dealers who have expertise in taking advantage of weakness of individual officers or sometimes systems.
7. Limited authority of dealing officials – It means when dealing officials have small authorities in taking decisions, respective dealers, at times take advantage of this.
8. Strong/Influential personality – It means some dealers have a strong persona and they take advantage of this.

Further, there are various reasons to exercise supremacy and use of politics by dealers and the most common are:

1. To get extra benefit in the business.
2. To satisfy their ego.
3. To exhibit the supremacy.
4. To pressurize respective officers and company to keep them on back foot.
5. To hide his weakness.
6. To improve bargaining supremacy.
7. To draw attention and priority.
8. To extract better services.

Though there is no readymade solution with organizations for countering these supremacy and politics issues of channel partners, as each dealer has different combination of these factors and so need to be handled separately but there are certain ways by which several factors may lose its negative impact. These are:

1. Strong and transparent system with minimum deviation- If the company is system oriented and does not deviate from this in

routine, individual dealers would not try to take chance.

2. Importance of front line executives – Companies should portray its front line executives as the face of the company and show good respect for them.
3. Less interference of seniors on day to day business – Day to day business should be dealt by the front line executives only and there should not be any interference of the senior management.
4. Seniors to build strong brand equity of the product – Seniors should spend more time and energy in uplifting the brand equity of the products and company. This will improve the importance of the product and company. The dealer would always have a fear of losing that brand if he does not work as per company policy.
5. Effective value system of the company – Strong value based companies have very little impact of supremacy and politics of dealers.
6. Strong two way communication with in organizational hierarchy – Effective communication between front line executives and seniors would reduce the impact of supremacy and politics of dealers.
7. Periodical training and development of employees as well as dealers – Value addition would make them more focused about their business and so the role of supremacy and politics would be diluted.
8. Relatively better retained margins to the dealers – If the retained margin in the business remains good, the focus of the dealer would always be more towards business and he would have fear in doing politics.
9. Information flow must maintain hierarchy – All the decisions and information should follow the hierarchy. This will keep frontline executive as well as seniors always updated and there will not be the scope of communication gap.
10. Complaints should be handled on merit basis and not on as who lodged it – There needs to be proper analysis of problems and solution should come on the basis of merits.
11. Conducive work environment – There needs to be conducive work environment both for the dealers as well as company officials. This will utilize the energy in a productive way.
12. Good back end support to front line executives – Since front line executives are face of the company, they must get good back end support not only from marketing department but also from other support functions like accounts, MIS, logistics etc.
13. Strong supply chain management – The role of supply chain is very important as the market is highly demanding w.r.to services. The expectation level is increasing day by day and if the company has the supply chain system efficient and effective, it will be a big support to have a command in the market.
14. Maintaining desired and designed service standards – Each business desire certain service standard and if they are maintained, it reduces the irritants of the market.
15. Delivery of agreed quality and proper handling of complaints – Quality of product and timely complaint handling adds on to the brand equity.
16. Visible growth opportunities both for employees and channel – When dealers as well as company employee see the growth opportunity in the business, both remain focused and reduce the chance of deviation towards other things.
17. Timely decision making – It is very important to make timely decisions. At times even saying no timely is better than saying yes after a long time.
18. Clarity in business policy – When there is clarity and transparency in business policy; it reduces the unexpected expectation level.

4. DISCUSSION

This study attempted to examine the influence of Supremacy and Politics on channel sales. Harrel- Cook and Dulebohn (2000) found that supremacy and politics in the channel sales are very important in any competitive business and the pharma products trade falls in the similar category. The main finding of the research is that for an effective trade business it is very important to create an environment where politics does not harm the business. The findings strongly support the work of Baum (1989) that systems and policies should be strong enough with clarity to all so to avoid the impact of undue supremacy and politics.Butcher and Clarke(2001,2008) found that role of effective communication and timely decisions are very important to counter the impact of this into the trade. Breaux and Ferris (2009) reported that while creating the network utmost care is required to assess the mutual requirements and expectations. Davidson and Perrewe (2005) pointed that long term as well as short term goals must be kept in mind while dealing with channels. Emerson (1962) asserts that periodic development and training is an essential component.

Role of senior management is very crucial and the real delegation and emsupremacyment of front line executives and different layers in hierarchy would help in reducing the political impact on the business. Nobody should be allowed to take the undue advantage of the position and situation and clarity and transparency must be maintained at all levels. Information flow should also follow the systematic route and without bypassing any relevant link. Decision making process needs to be speedy and in line with the business policy.

Focus should always be there on quality of product at reasonable cost with timely delivery with all applicable services. If these components are better than the competition, negative impact of politics would be minimal. Also if the channel earn reasonable margin in the product and company takes care of the smooth pull among the customers, politics cannot easily impact the business.

Research work of Russ and Fandt (1989) further contributed in understanding that in those businesses where product is monopolistic in nature or the competition is not intense different approach may take place or alternatively the supremacy of channels would be too low. Mayes and Allen (1977) quoted however in competitive products all aspects need to be taken care off. Gandz and Murray (1980) included all the aspects and factors of the study may be studied further individually and deeper study

may be done to analyze as why such behavior is visible or what all factors contributes to a particular behavior. This research leaves scope of research where the similar study may be done in different zones. Also a comparison may also be done between different geographies with in the country or with global scenario.

5. CONCLUSION

Supremacy and politics play important role in both the success and failure of organizations. It is important to judge the right equilibrium for supremacy and politics to make it functional. The weak links in channel partners occur because of these imbalances. The right approach for having smoother trade systems would be having positivism in roles of supremacy and politics among channel partners. As the strength and success of such businesses depends on the quality network, it is very important for the organizations to take care of mutual interests. It must have a close watch on routine developments and must take timely actions and decisions, including expansion, before the supremacy of channel partners go beyond their control. Also organizations should discourage the growth of politics and suppress it for the larger interest of all.

REFERENCES

1. Aizawa, T. Kawano (2002) T. Optimization systems in production and distribution of the pharma products industry. Industry Applications, IEEE Transactions, 695-703
2. Allen, R., Madison, D., Porter, L., Renwick, P.& Mayes, B. (1979). Organizational politics: Tactics and characters of its actors. California Management Review, 22, 77-83.
3. Baum, H. (1989). Organizational politics against organizational culture: A psychoanalytic perspective. Human Resource Management, 28, 191-206.
4. Brass, D. J.&Burkhardt, M. E. (1993). Potential supremacy and supremacy use: An investigation of structure and behavior. Academy of Management Journal, 36, 441-470.
5. Breaux, D. M., Munyon, T. P., Hochwarter, W. A.& Ferris, G. R. (2009). Politics as a moderator of the accountability–job satisfaction relationship: Evidence across three studies. Journal of Management, 35, 307-326.
6. Butcher D and Clarke M (2001, 2008) Smart Management: Using Politics in Organizations. Basingstoke, UK: Palgrave.
7. Coopey J and Burgoyne J (2000) Politics and organisational learning. Journal of Management Studies, 37,869–885.
8. Cropanzano, R.& Li, A. (2006). Organizational politics and workplace stress. In E. Vigoda-Gadot& A. Drory (Eds.), Handbook of Organizational Politics,39-160. Cheltenham, UK: Edward Elgar.
9. Cropanzano, R. Howes, J. C., Grandey, A. A.&Toth, P. (1997). The relationship of organizational politics and support to work behaviors, attitudes, and stress. Journal of Organizational Behavior, 18, 159-180.
10. Emerson, R. (1962). Supremacy–dependence relations. American Sociological Review, 27, 31-41.
11. Fedor, D., Maslyn, J., Farmer, S.&Bettenhausen, K. (2008). The contribution of positive politics to the prediction of employee reactions. Journal of Applied Social Psychology, 38, 76-96.
12. Ferris, G. R., Davidson, S. L.&Perrewe, P. L. (2005). Political skill at work: Impact on work effectiveness. Mountain View, CA: Davies-Black.
13. Ferris, G. R., Harrell-Cook, G.&Dulebohn, J. H. (2000). Organizational politics: The nature of the relationship between politics perceptions and political behavior. In S. B. Bacharach & E. J. Lawler (Eds.), Research in the sociology of organizations, 17, 89-130. Stamford, CT: JAI Press.
14. Ferris, G. R., Russ, G. S.&Fandt, P. M. (1989). Politics in organizations. In R. A. Giacalone& P. Rosenfield (Eds.), Impression management in the organization,143-170. Hillsdale, NJ: Lawrence Erlbaum.
15. Gandz, J.& Murray, V. (1980). The experience of workplace politics. Academy of Management Journal, 23, 237-251.

A CONNECTIONIST NETWORK APPROACH TO FIND NUMERICAL SOLUTIONS OF DIOPHANTINE EQUATIONS

Siby Abraham*
Dept of Mathematics & Statistics, G.N.Khalsa College, University of Mumbai, India. Email: sibyam@gmail.com
Corresponding author

Sugata Sanyal
Corporate Technology Office, Tata Consultancy Services, Gateway Park, Andheri (E), Mumbai, India. Email: sugata.sanyal@tcs.com.

Mukund Sanglikar
Dept of Mathematics, Mithibai College, University of Mumbai

ABSTRACT

The paper introduces a connectionist network approach to find numerical solutions of Diophantine equations as an attempt to address the famous Hilbert's tenth problem. The proposed methodology uses a three layer feed forward neural network with back propagation as sequential learning procedure to find numerical solutions of a class of Diophantine equations. It uses a dynamically constructed network architecture where number of nodes in the input layer is chosen based on the number of variables in the equation. The powers of the given Diophantine equation are taken as input to the input layer. The training of the network starts with initial random integral weights. The weights are updated based on the back propagation of the error values at the output layer. The optimization of weights is augmented by adding a momentum factor into the network. The optimized weights of the connection between the input layer and the hidden layer are taken as numerical solution of the given Diophantine equation. The procedure is validated using different Diophantine Equations of different number of variables and different powers.

Keywords: *Back propagation, Connectionist network, Diophantine equations, Feed forward, Neural network*

1.INTRODUCTION

A Diophantine equation [1] [2] is a polynomial equation,This paper is an attempt to find numerical solutions of Diophantine equations using Artificial Neural Networks or Connectionist Networks [7] [8] [9]. The paper introduces a given by

$$f(a_1,a_2,\ldots..,a_n, x_1, x_2, \ldots\ldots, x_n) = N \qquad (1)$$

where $a_i$and N are integers. Diophantine equations (DE) have been named after the third century BC Alexandrian Mathematician Diophantus. In 'Arithmetic', he inquired about 150 algebraic problems and its solutions [3]. Such problems are now collectively referred as Diophantine equations. Diophantine equations and its particular types gave rise to some important results in Mathematics. Fermat's last theorem, Pythagorean triplets, Elliptic curves, Pell's equation and Waring Conjecture are few of them [4]. David Hilbert has been credited with giving a new direction to the interest shown on Diophantine equations by Mathematicians for centuries. In 1900 at the second International Congress on Mathematicians, he presented twenty three unsolved problems that he believed were important. The tenth problem he presented was: "Given a Diophantine equation with any number of unknowns and with rational integer coefficients: devise a process, which could determine by a finite number of operations whether the equation is solvable in rational integers." Since then, the problem is known as Hilbert's tenth problem [5] [6] and has been proved later that there exist no general method to solve this problem.

This paper is an attempt to find numerical solutions of Diophantine equations using Artificial Neural Networks or

Connectionist Networks [7] [8] [9]. The paper introduces a feed forward three layer neural network with back propagation learning [10] [11]. It experimentally validates its effectiveness by finding numerical solutions of a class of Diophantine equations given by equation (2).

$$x_{1p1} + x_2 p^2 + \ldots.. + x_{npn} = N \qquad (2)$$

The paper is structured in six sections. Section 2 gives an overview of Connectionist Networks. Section 3 describes the related works done in the field of Diophantine equations and back propagation networks. Section 4 explains the procedure proposed to find numerical solutions of the given class of Diophantine equations. Section 5 deals with implementation and experimental results. Section 6 discusses final conclusion.

Connectionist network, which are also called Artificial Neural Networks (ANN), is a computational model based on the working

of biological neural network of brain. ANN resembles brain in two respects [12]: Knowledge is acquired by the network through a learning process and inter-neuron connection strengths known as synaptic weights are used to store the knowledge. Connectionist networks are comprised of densely interconnected adaptive processing units, known as neurons [13], which help to replace the usual 'programming' in solving problems by the concept of 'learning by example'. This is made possible using many neural network models and learning algorithms.

There are different neural network models. They can be broadly classified as Feed forward Network, Radial basis Function Network, Kohonen Self Organizing Network,Recurrent Network, Stochastic Network and Modular network [14]. These network models use different learning algorithms for training the network.These algorithms come under three different learning paradigms. They are supervised learning,un-supervised learning and reinforcement learning.

Back Propagation (BP) learning algorithm, which is also called generalized delta rule, is a supervised learning algorithm for a feed forward multi layer neural network and is one of the most widely used learning processes in ANN. The basic architecture of the Back Propagation Network [15] [16] [17] consists of an input layer, one output layer and one or more intermediate layers known as hidden layers.The training algorithm of back propagation involves four stages. They are: initialization of weights, feed forward, back propagation of errors and updating of the weights. The name 'back propagation' originates from the fact that the errors of hidden units are derived from propagating backward the error obtained from the output unit. After a sufficient number of times, the error values will be minimized to the expected level and the output generated will be almost matching with the expected result. This process is repeated for different input-output pairs and the same helps to obtain the optimized weights finally. Now, the system is said to have been trained or learnt and hence is expected to classify similar input values and give predictable output values in real time.

2. RELATED WORKS

There have been many attempts to unravel the mysteries around Hilbert's tenth problem. Davis et al. [18] proved that an algorithm to determine the solvability of all exponential Diophantine equations is impossible. Matiyasevich [19] extended this work by showing that there is no algorithm for determining whether an arbitrary Diophantine equation has integral solutions, ending attempts of centuries for finding a general method.

Though Hilbert's famous tenth problem was settled unilaterally and conclusively, Diophantine Equations, which has more open problems than results [20], is an area which is engaging and challenging. This has become all the more important as the significance of Diophantine equations has not just been restricted to the abstract and theoretical realm of Mathematics as it has found newer application areas in the fields like Publickey Cryptosystems [21] [22], Computable economics [23], Elliptic curves [24] [25], Data dependency in super computers [26] [27] and Theoretical Computer Science [28 [29].

In this context, attempt to find numerical solutions of DE is inspiring and interesting. However, this turned out to be a hard problem as the search space [30] [31] of (1) consists of Nn elements. Since following an exhaustive, gradual and incremental method involved high degree of computational complexity, soft computing approach of Artificial Intelligence [32] [33] were looked at. There have been some attempts to find numerical solutions of Diophantine Equations in this direction. Abraham and Sanglikar [34] applied Genetic Algorithm (GA) with mutation and crossover as genetic operators to find numerical solutions of a class of DE. They [35] explained the process of avoiding premature converging points using 'Host Parasite Co-evolution' in a typical GA. Abraham and Sanglikar [36] also explained a method involving evolutionary and co-evolutionary computing techniques to find numerical solution of DE. Their paper [37] described a simulated annealing based computational approach to find numerical solution of a DE. Abraham et al [38] introduced particle swarm optimization for finding numerical solutions of such equations.

Though there are some attempts to find numerical solutions of Diophantine equations using various soft computing paradigms [39], to where the Connectionist networks belongs, the authors are yet to find literature on Diophantine equations using connectionist networks except the work by Joya et al [40]. They have showed that higher order Hopfield networks can be used to find numerical solutions of DE. It is quite surprising that there is only one work of connectionist networks in the field of Diophantine equations as connectionist networks with learning mechanisms like back propagation are tried and tested mechanisms on a wide range of problems belonging to diverse backgrounds, few of which are mentioned in the following paragraph. It is all the more relevant as the back propagation is the often used learning mechanism of all others in the connectionist networks. This paper is an honest and sincere attempt to fill that void.

Cun et al [41] described an application of back propagation networks to recognize handwritten digits of low level presentation of data with minimal preprocessing. Kamruzzaman et al [42] introduced a double back propagation assisted neural network for character recognition which first preprocesses input pattern to produce a translation, rotation and scale invariant representation and then classifies characters using a neural net classifier. Temdee et al [43] explained back propagation based face recognition where fractal codes from the edge pattern of the face region are fed as inputs to a back propagation neural network for training the network and hence identifying a person. Durai and Anna Saro [44] described how back propagation network can be used for image compression wherein the gray levels of the pixels in an image and their neighbors are mapped such a way that the difference in the gray levels of the neighbors with the pixel is minimum so that the compression ratio as well as the convergence of the network is improved. R Chang et al [45] dealt with a learning methodology using back propagation neural networks with sample-query and attribute-query in developing an intrusion detection system (IDS). Hossam Osman et al [46] proposed a back propagation neural network for the classification of ship targets in airborne synthetic aperture radar (SAR) imagery. K Shihab [47] talked about a symmetric encryption mechanism based on artificial neural networks where a multi-layer neural network, which is trained by back propagation learning algorithm, is used for the decryption scheme and the public key creation. Pokorny and Smizansky [48] proposed a method called Page Content Rank (PCR) based on the page content exploration in Web Content Mining.

3. PROPOSED SYSTEM

The system developed to find numerical solutions of Diophantine equations, which we call Neural Network based Diophantine Equation Solver (NEURO-DOES) introduces a dynamically constructed architecture for the feed forward neural network with back propagation learning.

3.1 Network Architecture NEURO-DOES uses network architecture of three layers of one each of input, hidden and output layers. The number of neurons in the hidden layer and output layer is fixed to be one.The number of neurons in the input layer changes corresponding to the type of the equation. If the given Diophantine equation has n variables then input layer also will have that many numbers of neurons. The powers of the given Diophantine equation are given as input to the neurons in the input layer. The values of the variables are taken as weights of the connection between the input layer and the hidden layer. The learning process starts by assigning small random integral values as initial weights. The solution of the given Diophantine equation is the resultant weights of the connections between the input layer and the output layer obtained once the system is fully trained.

3.2 Initial Weights All connection weights, which are initialized as small random integral values, are taken to be positive integers as we are interested in only positive integral solutions of the equation. Initial weights for the connection between the input layer and the hidden layer are chosen randomly, as is the usual practice, from a small range between 1 and 10. The rare chance of the procedure not converging to the optimum weights and hence not getting the solution for the given Diophantine equation is resolved by having the option to restart the whole process with initial random distribution of weights from another range. The weight of the connection between the hidden layer and the output layer is assigned to be one and is kept fixed.

3.3 Feed Forward Each neuron in the input layer receives the powers pi of the variables as input signal and transmits them into the next layer i.e. hidden layer. The weights wi connecting the neurons in the input layer and the hidden layer correspond to the prospective values of the variables, which satisfies the equation. The units in the hidden layer receive signals in the form of wi pi, which differs from wipi as is the usual practice in Back propagation networks, to accommodate the constraints unique to the Mathematical problem under study. The neuron in the hidden layer calculates the exponentially weighted sum of the signals. Thus, we have

$$\mathbf{Q = \Sigma\, wi^{pi}} \qquad \mathbf{(3)}$$

as the output from the hidden unit. The unit in the hidden layer is connected to the unit in the output layer. The weight of this connection is fixed to be 1. Here, we have only one connection to the output layer: Q with weight 1, which is a pseudo weight, as the value of this weight does not have any bearing on the final result and is fixed. The unit in the output layer is taken as the weighted sum of this signal and output as a linear function. This is the output of the output unit and is denoted by OP. If OP is equal to N, the network is said to have been trained to give optimized weight values for the given input and these optimized values are taken as the solution of the given equation. Any other value of OP shows an error and requires further training of the network.

3.4 Back Propagation of Errors The value of OP other than N shows that there is an error in the output and the system needs to be trained. The value of this error is calculated as

$$\mathbf{E = Error = OP - N.} \qquad \mathbf{(4)}$$

E can either be positive or be negative. We define

$$\mathbf{\delta = Sgn\,(E) = 1 \text{ if } E > 0}$$

$$\mathbf{= -1 \text{ if } E < 0}$$

$$\mathbf{= 0 \text{ if } E = 0.} \qquad \mathbf{(5)}$$

This value of 'δ' is propagated back to the unit in the hidden layer. We call 'δ' as the error factor. Since there is only one connection connecting hidden layer and output layer, the error factor of the previous layer is also taken as 'δ'. In practice, the value of the error factor as +1 means that the network needs to increment the weights of the connections between input layer and hidden layer .Similarly the -1 value directs the Network to decrement the weights between the input layer and hidden layer. When 'δ' takes value 0, then the system is said to have been learnt and the optimized weights give the solution. This back propagation of +1 or -1 error message helps the network to optimize the weight vector of the connection between the input layer and hidden layer.

3.5 Update of Weights The amount by which the network weights between the input layer and the hidden layer are to be incremented or decremented is decided by the extent of the error. This quantity is taken to be dependent on |Error| 1/ (Max * n),where 'Max' is the maximum of the powers of the variables and 'n' is the number of variables of the given equation. The weights of the connection between the input layer and the hidden layer are updated by Δwi based on the following three different cases:

Case 1. $\delta > 0$: If $\delta > 0$ the weight updating is done in the straight forward fashion using formula:

$$\mathbf{\Delta wi = \delta\, |Error| 1/(Max * n), for\ i = 1, 2, \ldots, n} \qquad \mathbf{(6)}$$

Equation (6) helps weight updating faster. This happens usually at the beginning of the procedure when the weights are small random values and the error is quite high. The quick pace of the weight updating facilitates the convergence of the weights to the vicinity of the optimized weights.

Case 2. $\delta < 0$ and w i $\neq$ 1: If $\delta < 0$ and if w i $\neq$ 1 for all i=1, 2… n then the weights are adjusted using the formula given by

$\Delta w1 = \delta.\min \{1, |Error|\ 1/ (Max * n)\}$ **(7)**

and Δ w i = 0 for I = 2, …. N. **(8)**

Equation (7) helps to adjust the weight of the first connection by keeping other connection weights constant. The selection of nominal adjustment of only one connection is deliberate as otherwise weights might oscillate between the optimized weights in the weight space. This way the convergence of the weight is directed by focusing on one weight at a time when the error value crosses the positive boundary.

Case 3. $\delta < 0$ and wj = 1: If $\delta < 0$ and if wj = 1 for some j = i where i= 1, 2…n, then weight adjustment is done using the following formulae:

Δ w j = count * min {1, |Error| 1/ (Max * n)} **(9)**

Δ w j+1 =δ. Min {1, |Error| 1/ (Max * n)} **(10)**

and Δ w i = 0 for i $\neq$ j, j+1 **(11)**

Here 'count' is the number of previous consecutive iterations with $\delta < 0$. This case arises because the reduction of weights cannot be applied when the weight of any connection hits 1, the smallest positive integer, as we are interested only in the positive integral solution of the given equation. This necessitates a modification of Equation (7) corresponding to the case 2. This is achieved by incorporating Equations (9), (10) and (11) in the process. The case is handled in three folds. Firstly, the weight, whose value is 1, is adjusted using a momentum as shown in Eq. (9). Momentum is added to a neural network to speed up the convergence in the positive direction. Here the quantity 'count' is taken as the momentum factor for speedier convergence. Secondly, the weight of the connection, next to the connection with weight 1, is reduced nominally as provided by Eq. (10). Thirdly, all other connection weights are kept constant as shown by Eq. (11). In this way the procedure is directed towards the optimal weights.

4. EXPERIMENTAL RESULTS

The procedure discussed in the work is implemented in C-language. The data structures like arrays, pointers and structures are used to implement the program constructs. Experimental results of running the program for different cases show encouraging results.

4.1 Results on equations with different variables Table 1 shows the results obtained when the system was run on Diophantine equations with varying number of variables. It discusses solutions of nine different Diophantine equations with nine different number of variables, changing from two to ten. The system provides solutions even when the number of variables is competitively high. The last column of the table 1 shows that if the number of variables is comparatively less, then the system gives the solutions in much lesser iterations as the convergence of the optimized weights takes place very fast.

Table 1 Results on equations with varying number of variables

Sr. No	Diophantine Equation	No. of variables	Solution Found	Iterations required
1	$x_1^2+x_2^2 = 149$	2	10, 7	10
2	$x_1^2+x_2^2+x_3^2 = 244$	3	12, 6, 8	6
3	$x_1^2+x_2^2+\ldots +x_4^2= 295$	4	1, 2, 13, 11	51
4	$x_1^2+x_2^2+\ldots. +x_5^2= 325$	5	1, 5, 9, 7, 13	33
5	$x_1^2+x_2^2+\ldots. +x_6^2= 420$	6	1, 1, 2, 7, 13, 14	97
6	$x_1^2+x_2^2+\ldots. +x_7^2= 450$	7	1, 1, 2, 2, 10, 14, 12	457
7	$x_1^2+x_2^2+\ldots. +x_8^2= 590$	8	1, 1, 1, 1, 5, 13, 14, 14	1669
8	$x_1^2+x_2^2+\ldots. +x_9^2= 720$	9	1, 1, 1, 2, 2, 14, 12, 12, 15	1373
9	$x_1^2+x_2^2+\ldots. +x_{10}^2=956$	10	1, 1, 1, 1, 1, 1, 1, 15, 20, 18	9068

4.2 Results on Equations with Varying Degrees Table 2 demonstrates the effectiveness of the system by showing the results obtained for different values of powers. It also has nine different Diophantine equations but the powers of the equations are varied this time. Different powers from two to ten are used with different equations. It shows that the system gives the numerical solutions even when powers are large.

On comparing the last columns of table 1 and table 2, it is observed that the number of iterations required to find the solutions is much lesser in the case of powers than in the case of different variables. This is because the search space is not very complex in the case of large powers, which is not the case for equations with large number of variables.

Table 2 Results on equations with varying degrees

Sr. No	Diophantine Equation	Degree	Solution	Iterations required
1	$x_1^2 + x_2^2 = 625$	2	20, 15	7
2	$x_1^3 + x_2^3 = 1008$	3	2, 10	23
3	$x_1^4 + x_2^4 = 1921$	4	6, 5	10
4	$x_1^5 + x_2^5 = 19932$	5	7, 5	9
5	$x_1^6 + x_2^6 = 47385$	6	6, 3	6
6	$x_1^7 + x_2^7 = 4799353$	7	9,4	5
7	$x_1^8 + x_2^8 = 16777472$	8	8, 2	2
8	$x_1^9 + x_2^9 = 1000019683$	9	3, 10	12
9	$x_1^{10} + x_2^{10} = 1356217073$	10	7, 8	4

4.3 Results on Equations with Varying Degrees

Figure 1 shows convergence of weights in the weight space for an elementary equation given by

$$x_1^2 + x_2^2 = 4000 \qquad (12)$$

Initially, the convergence is very rapid and the process follows an almost linear pace. This is because of the higher learning rates at

the initial stage of the convergence. As the weights reaches in the vicinity of optimized weights, the procedure slows down as the error becomes comparatively small. Now on, the learning rates are reduced and the process gradually moves towards the optimum weight values.

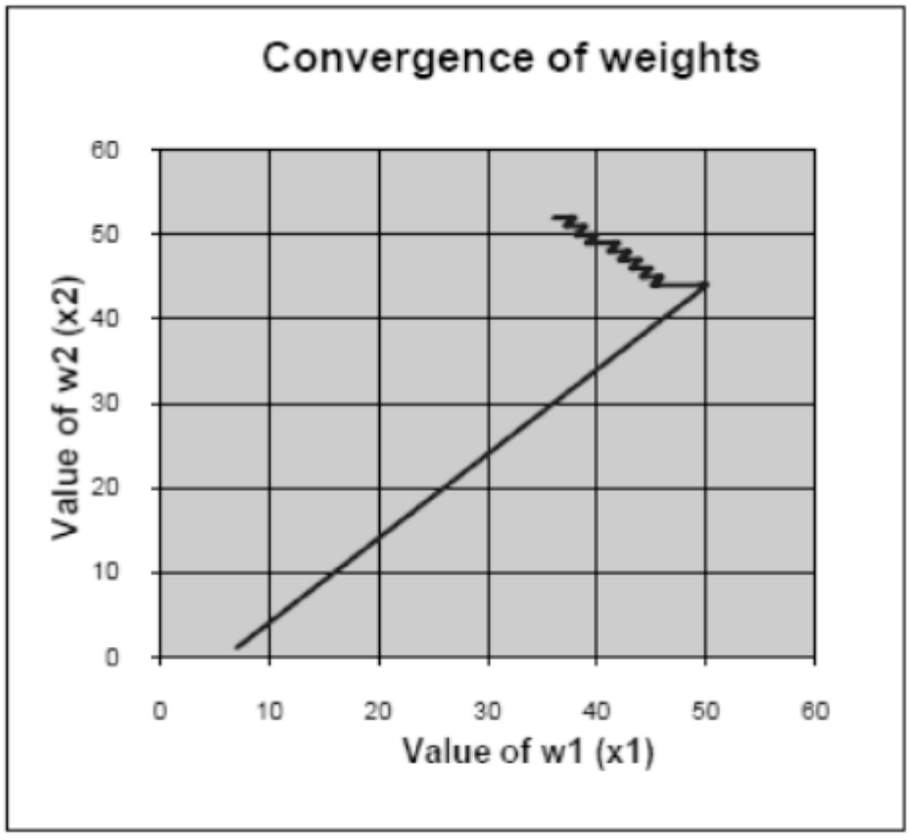

Figure 1 Convergence of weights

4.4 Reduction of Error Figure 2 shows the reduction of errors corresponding to the equation (12) on the process of optimizing the weights. It shows that there are large error values at the initial stage of the weight optimization process. Gradually, they are brought to small values as the process becomes matured. Toward the optimum weights, the error values fluctuate between positive and negative values within a smaller range and are brought to the optimum value by the momentum factor incorporated in the procedure. The contribution of momentum factors to fasten the optimization process is evident from the figure.

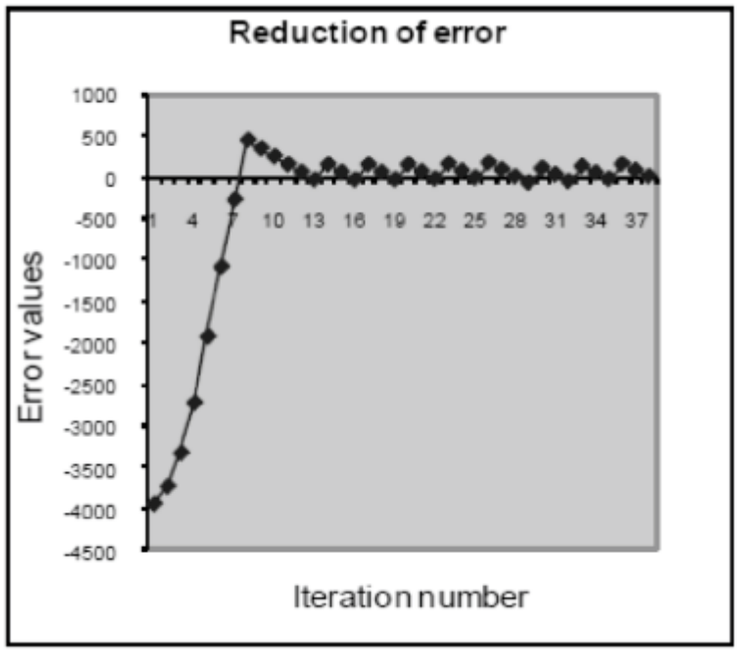

Figure 2 Reduction of error

4.5 Learning Rates Figure 3 shows the learning rates attained by the procedure during the process of optimizing weights for the same equation (12). Initially, there is a comparatively large learning rate. But as the process becomes stabilized, the learning reduces and the changes in two consecutive iterations become negligible. The gradual convergence to the optimized weights is represented by the almost steady learning rates at those stages. The figure also shows the iteration number where the learning rate becomes zero, which shows that the solution has been encountered by the system

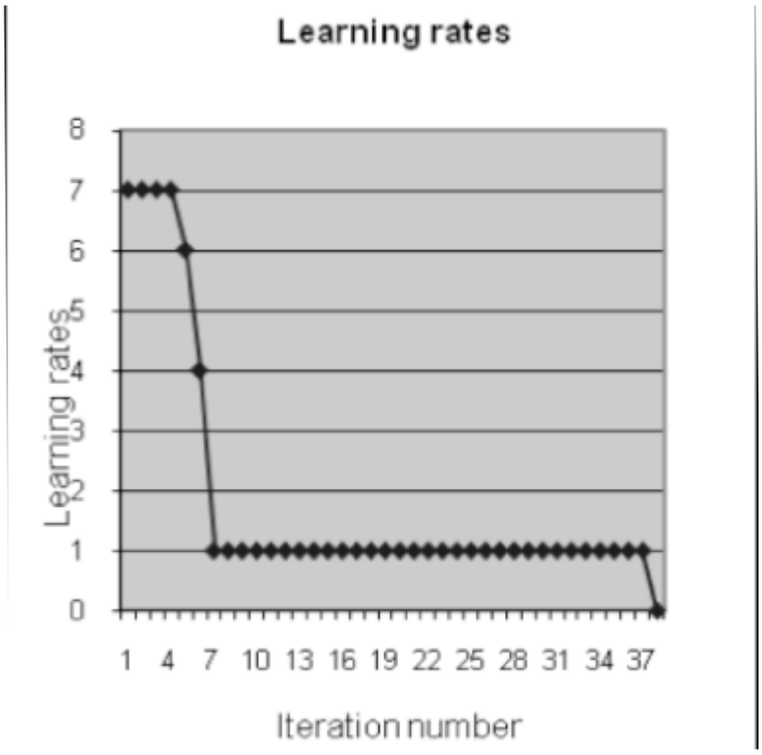

Figure 3 the learning rates attained by the procedure

5. CONCLUSION AND FUTURE WORK

The paper introduces a connectionist network based approach to find numerical solutions of Diophantine equations. It uses a three layer feed forward network with back propagations as the sequential learning strategy. The judicious selection of network architecture to take care of the domain specificity of Diophantine equations resulted in the convergence of optimum weights giving numerical solutions of the equations.

Though the system could offer solutions of Diophantine equations with different number of variables and different powers, the procedure has the tendency to find solutions of which coordinates are more close to one another. The further works involve obtaining solutions with distinct coordinates as a Diophantine equation can have many solutions. This is expected to be achieved by a better learning strategy.

REFERENCES

1. Cohen, H: 'Number Theory, Vol. I: Tools and Diophantine Equations and Vol. II: Analytic and Modern
2. Rosen, Kenneth: 'Elementary Number theory and its applications', Addison-Wesley Publication.
3. O'Connor, J J and Robertson, E F: 'Diophantus of Alexandria', Available at http://www-history.mcs.stand.ac.uk/biographies/diophantus.html.
4. Niven, I., Zuckerman, H. S. and Montgomery, H.L.: 'An introduction to the Theory of Numbers', 5th edition, January, 1991.
5. Borowski, E. J. and Borwein, J. M. (Eds.). 'Hilbert Problems', Appendix 3 in the Harper Collins Dictionary of Mathematics: New York: Harper-Collins, 1991.
6. Hilbert, D: 'Mathematical problems', Bull. Amer. Math. Soc. (N. S.) 37 (2000), No. 4, 407–436 (electronic). MR 1 779 412. Reprinted from Bull. Amer. Math. Soc. 8 (1902), 437–479.
7. Kostanic, I. and Ham F. M: 'Principles of Neuro computing for science & Engineering', Tata McGraw Hill, India, 2002.
8. Hausson M: 'Fundamentals of Artificial Neural Networks', Prentice Hall India, 2005.
9. Rajasekharan, S. and Pai, G. A. Vijaylakshmi: 'Neural Networks, Fuzzy Logic and genetic Algorithm', Prentice Hall India, 2007.
10. Satish Kumar: 'Neural Networks- A Classroom Approach', Tata McGraw Hill, India, 2006.
11. Sivanandam, S; Sumathi, S and Deepa S N: 'Introduction to Artificial Neural Networks using Matlab' Tata McGraw

Hill, India, 2006.

12. Haykin S: Neural Networks A Comprehensive Foundation, Second Edition, Prentice Hall India, 2006.
13. Fu, Limin: Neural Networks in computer intelligence, Tata McGraw Hill, 2003
14. Yegnanarayan, B: 'Artificial Neural Networks', Prentice Hall India, 2006
15. Werbose, PJ: 'Back propagation through time - How it does and how to do it', Proceedings of IEEE, vol.78,1990, pp. 1550- 1560
16. Rumelhart, D; Hinton, G and Williams, R L: 'Learning Representations by Back-Propagating Errors', Nature, vol. 323, 1986, pp. 533-536.
17. Freeman, James and Skapura, David: 'Neural Networks: Algorithms, Applications and Programming Techniques', Pearson Education, India, 2007.
18. Davis, M: 'Hilbert's Tenth Problem is Unsolvable', Appendix 2 in HTU Computability and Unsolvability.UTH New York: Dover, 1999-235, 1982.
19. Matiyasevich, Y.V: 'Hilbert's Tenth Problem', MIT press, 1993.
20. Waldschmidt, M: 'Open Diophantine problems', Moscow Mathematical Journal, Vol 4, Number 1, January– March 2004, Pp 245–305.
21. Lin, CH; Chang, CC and Lee, R C: 'A new public-key cipher system based upon Diophantine equations', IEEE Transactions on Computers, Vol 44, Jan 1995.
22. Laih, CS and Gau, MJ: 'Cryptanalysis of Diophantine equation oriented public key cryptosystem', IEEE Transactions on Computers, Issue 4, April 1997, pp 511-512.
23. Velupillai, K: 'Computable Economics: The Arne Memorial Lecture Series', Oxford University Press, 2000.
24. Brown, E and Myers, B: 'Elliptic Curves from Mordell to Diophantus and Back', the Mathematical Association of America Monthly 109, August–September 2002, pp 639-649.
25. Stroeker, R J and Tzanakis, N: 'Solving elliptic Diophantine equations by estimating linear forms in elliptic logarithms' ACTA Arithemetica LXVII.2 (1994), 174-196.
26. Jacobson, Tim and Stubbendieck, Gregg: 'Dependency analysis of For-Loop structures for automatic parallelization of C code', MICS 2003 Proceedings of the 36th Annual Midwest Instruction and Computing Symposium.
27. Temam, O; Wijshoff, H; Eisenbeis, C and Ternarel, O: 'On efficiently characterizing solutions of linear Diophantine equations and its application to data dependence analysis', Proceedings of Seventh International Symposium on Computer and Information Sciences, Antalya, Turquie, 1992.
28. Ibarra, O H and Zhe, Dang: 'On Two ways FA with monotone counters and quadratic Diophantine equations', Theoretical Computer Science, Vol 312(2-3), 2004.
29. Guarari, EM and Ibarra, OH: 'Two way counter machines and Diophantine equations', Journal of ACM, 29(3) 1982.
30. Rich, Elaine and Knight, Kevin: 'Artificial Intelligence', Tata McGraw Hill Publication, 1991.
31. Russell, Stuart and Norwig, Peter: 'Artificial Intelligence –A modern approach' Second Edition, Pearson Publication, 2003.
32. Luger, G: 'Artificial Intelligence-Structures and Strategies for Complex Problem Solving', Pearson education, India, 2006.
33. Padhy, N:'Artificail Intelligence and Intelligent Systems', Oxford University Press, India, 2005.
34. Abraham, S and Sanglikar, M: 'A Diophantine Equation Solver- A Genetic Algorithm Application', Mathematical Colloquium journal, Vol 15, Sept 2001.
35. Abraham, S and Sanglikar, M: 'Nature's way of Avoiding Premature Convergence: A case study of Diophantine Equations', Proceedings of the International Conference on Advances in Mathematics: Historical Developments and Engineering Applications, Pantnagar, Uttarakhand, India, Dec 19-22 2007,
36. Abraham, S and Sanglikar, M: 'Finding Solution to a Hard Problem: An Evolutionary and Co-evolutionary Approach', Proceedings of the International Conference on Soft Computing and Intelligent Systems, Jabalpur, India, Dec 27-29, 2007.
37. Abraham, S and Sanglikar, M: 'Finding Numerical Solution to Diophantine Equation: Simulated Annealing as a Viable Search Strategy', Proceedings of the International Conference on Mathematical Sciences, University of UAE, Al Ain, UAE, 3rd-6th March 2008.
38. Abraham, S; Sanyal, Sugata and Sanglikar, M: 'Particle Swarm Optimization based Diophantine Equation Solver, International Journal of Bio-inspired Computation, Vol 2, No 2, 2010
39. Eberhart, Russ and Shi, Yuhui: 'Computational Intelligence – Concepts to implementation', Morgan Kaufmann Publishers, 2007.
40. Joya, G; Atencla, M.A and Sandoval, F: 'Application of Higher order Hopfield neural networks to the Solution of Diophantine equation', Lecture Notes in Computer Science, Vol. 540, Springer Berlin/Heidelberg, 1991.
41. Cun, Y Le; Boser, B; Denkar, J S; Howard, E; Habbard, W; Jackal, L D and Henderson, D: 'Handwritten Digit Recognition with a Back-Propagation Network', Proceedings of Advances in Neural Information Processing Systems II (Denver 1989).

42. Kamruzzaman, J and Aziz, S M: 'Character recognition by double back propagation neural network', Proceedings of IEEE Region 10 Annual Conference on Speech and Image Technologies for Computing and Telecommunications. Volume 1, Issue 4, 4th Dec.1997 Pp.:411-414.

43. Temdee, P; Khawparisuth and Chamnonglhai, K.: 'Face Recognition by Using Fractal Encoding and Back propagation Neural Network' 5th International Symposium on Signal Processing and its Applications, ISSPA 99, Brisbane, Australia, 22- 25 August, 1999 Brisbane, Australia

44. Durai, Anna and Annasaro, E: 'Image Compression with Back-Propagation Neural Network using Cumulative Distribution Function', Proceedings of world academy of Science, engineering and Technology Vol. 17, Dec 2006.

45. Chang, R I; Lai, Liang-Bin; Su, Wen-De; Wang, Jen-Chieh and Kouh, Jen-Shiang: 'Intrusion Detection by Back propagation Neural Networks with Sample- Query and Attribute-Query', International Journal of Computational Intelligence Research. Vol.3, No. 1 (2007), pp. 6-10.

46. Osman, Hossam; Pan, Li; Blostein, S D and Gagnon, Langiset: 'Classification of Ships in Airborne SAR Imagery Using Back propagation Neural Networks', Proceedings of SPIE Conference on Radar Processing, Technology and Applications II, p. 126-136 (1997).

47. Shihab, K: 'A Back propagation Neural Network for Computer Network Security', Journal of Computer Science 2 (9): 710-715, 2006.

48. Pokorny, J and Smizansky, J, 'Page content rank: an approach to the web content mining', Proceedings of IADIS International Conf. On Applied Computing, Volume 1, February 22-25, 2005, Algarve, Portugal, IADIS Press, pp. 289-296.

A COMPARATIVE ASSESSMENT OF AEROSOL OPTICAL PROPERTIES OVER GUWAHATI THROUGH LIDAR AND SATELLITE OBSERVATION

Bandita Choudhury*
Department of Physics, Gauhati University, Guwahati-781014, India, Tel: 03612676607
Corresponding author

Manoj Saikia
Department of Physics, Gauhati University, Guwahati-781014, India, Tel: 03612676607

Minakshi Devi
Department of Physics, Gauhati University, Guwahati-781014, India, Tel: 03612676607

Ananda Kumar Barbara
Department of Physics, Gauhati University, Guwahati-781014, India, Tel: 03612676607
Email:bandita.choudhury8@gmail.com

ABSTRACT

The paper presents analysis of backscatter counts obtained from Micro Pulse Lidar (MPL) to extract the extinction coefficient and aerosol optical depth (AOD) over Guwahati (26^0 N, 92^0 E). The study shows a seasonal pattern in variation of aerosol extinction coefficient reaching a peak at vernal equinox and trough at autumnal equinox. Data from Moderate Resolution Imaging Spectro-radiometer (MODIS) are analyzed to obtain the AOD, which follows the same seasonal pattern as by MPL observations. A comparison between AODs received from the MODIS and MPL shows a good correspondence in the autumnal period with a correlation factor 0.853; while in vernal months correlation factor of 0.743 is slightly different. To eliminate this discrepancy, statistical approach is adopted for the best fit of AOD values obtained from both of the systems.

Keywords: *Aerosol, Lidar, extinction coefficient, MODIS, AOD*

1. INTRODUCTION

Atmospheric aerosol is one of the major climatic forcing agents. During recent years, there has been emphasis on understanding the role of aerosol in shaping the climatic character of a region1,2. To understand such aspects of aerosol, it is essential to examine two fundamental properties of aerosol; extinction coefficient (σ/km) and Aerosol Optical Depth (AOD). For this investigation, a numbers of ground based, in-situ or satellite measurements are in operation throughout the globe. Amongst many the techniques, Lidar remote sensing of atmosphere is proved to be very effective both from research and application points of view. This system has advantage over spatio-temporal resolution and flexibility of probing wavelengths that may vary from UV to IR regions. Monitoring of atmospheric aerosol through satellite based sensors is also very effective because of their revisit cycle and huge area coverage3,4,5,6,7. These measurements though have the demerit of poor resolution, they provide spatial and temporal distribution of aerosol on a global scale. Therefore serious efforts need to be given when satellite observations are to be compared with Lidar observations. The attempts made by researchers in this direction focus on complexity of such exercises [8,9,10,11].

In this paper, we have studied two optical properties of aerosol: Aerosol σ/km and AOD. We have compared AOD derived from extinction coefficient observed through Lidar system operated at Gauhati University with those obtained from MODIS. The paper also describes the statistical approaches to form a semi empirical correction formula for obtaining high resolution AOD from MODIS in absence of Lidar. The adopted approach will be utilized in future to identify the source of aerosol over semi urban area over Gauhati University by using MODIS data.

2. METHODOLOGY AND DATA

In this paper two optical properties of aerosol namely aerosol extinction coefficient and optical depth will be the basic inputs of analysis. To understand these two optical properties of aerosol, let us consider the propagation of radiation of wavelength λ through a layer of thickness dr perpendicular to a beam of intensity I (λ). The extinction of radiation on traversing an infinitesimal path length dr is linearly proportional to the amount of matter along the path

$$I(r + dr) - I(r, \lambda) = -\sigma(r, \lambda) I(r, \lambda) dr \quad (1)$$

Where, $\sigma(r, \lambda)$ (units of inverse length) called extinction coefficient gives the attenuation of the radiation per unit wavelength

of propagation. Again, the AOD is defined as the amount of signal attenuated for a given path length and it can be calculated by integrating the extinction profile from the ground up to a certain height r_{max}.

Therefore, for a path length of r_{max}, AOD is expressed as:

$$AOD = \int_0^{r_{max}} \sigma(r)dr \quad (2)$$

AOD, over Gauhati University a suburban station is obtained from extinction coefficient from GU Lidar and also from MODIS. Before presenting this comparative analysis brief description of GU Lidar system developed by this group in collaboration with Chiba University is given below.

The block diagram (Figure 1) shows the component modules of the instrument. The Lidar system consists of a trans-receiver unit, a beam expander for eye safety, a scalar unit for controlling trans-receiving signal, a data acquisition system and a data storage and computing unit. The GU Lidar system transmits 532 nm signal in a co-axial mode and therefore the shadow zone is narrowed down to 120m. The Lidar system is capable of receiving backscatter counts from aerosol and cloud upto 5 and 15km respectively with a vertical resolution of 15-30m. These backscatter counts are received by a telescope of diameter 20 cm fitted with a PMT at the focus of a pinhole size (iris) of 0.2mm diameter. The input received in photon counting mode, is filtered by a 2.28 nm optical filter for reducing background illumination. The amplified signal from the PMT after conversion to TTL level is passed to the scalar for averaging and processing.

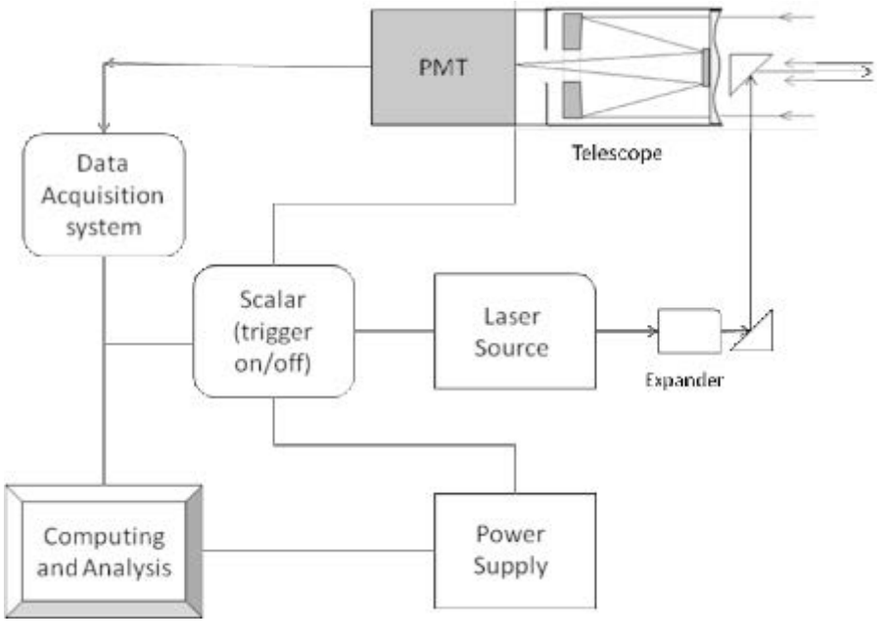

Fig. 1: The basic building blocks of the GU Lidar

To convert the counts into the optical characteristics like extinction coefficient (σ/km) and backscatter extinction coefficient (β/km) we use the basic Lidar equation expressed as

$$P(r) = P_0 \left(\frac{A}{r^2}\right)\left(\frac{ct}{2}\right)\beta(r)\exp\left(-2\int_0^r \sigma(r)dr\right) \quad (3)$$

Where,

P_0 Transmitter power, P(r) Receiving power from a range r, A aperture of the telescope, c velocity of light, t profiling time.

The equation (3) can be written as

$P(r)\ P_0\ C\ \beta(r)T^2(r)/r^2$ (4)

Where, C, the system constant is expressed as

$C = P(r)\ r^2/P_0[\beta(r)T^2(r)]$ (5)

Here,

$$T^2 = \exp\left[-2\int \sigma(r)dr\right] \quad (6)$$

To obtain the extinction coefficient, it is necessary to determine the system constant C and β(r) at a constant height. The system constant C and Lidar ratio $S=[\sigma(r)/\beta(r)]$ had been calculated by this research group by adopting different approaches12 described elsewhere. Again, the Lidar equation needs correction for errors due to overlap, dead-time and after-pulse factor, for eliciting error-free information and also for realizing system sensitivity in temporal and spatial scales. The detail processes of correction of such errors and calibration of the system are presented elsewhere13,14,15. After obtaining errorless Lidar equation, extinction

coefficient can be calculated by utilizing the Eq. (5) and (6).

The PMT output is processed in LabView environment for obtaining aerosol and cloud features. The output is available as intensity- time profile for a single sounding from where, the height-time-intensity plot is obtained in diurnal basis. A representative height-time profile of Lidar backscatter counts and extinction profile are shown in Fig. 2.

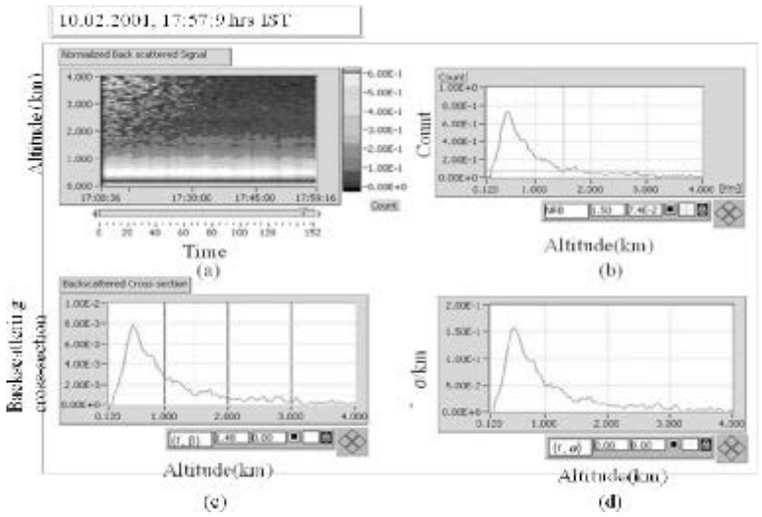

Fig. 2: A typical Lidar echogram showing (a) backscatter counts for probing period of 17.08.36 to 17.59.16 hrs, IST, on 10-02-2001; (b) counts for the time indicated by the arrowhead in Fig. 2 (a); (c) backscatter cross-section and (d) extinction coefficient for the corresponding counts of Fig. 2(b).

Figure 2 (a) shows a typical backscatter counts echogram of aerosol for the month of February, 2001. Here the probing period is from 17:8:36 hrs to 17:59:16 hrs IST and maximum altitude is kept at 4 km. In this echogram a layer of high backscatter counts is seen at a height of 0.5km. Fig. 2 (b) shows the count profile for the time indicated by the arrowhead in Fig. 2(a) and significant count of aerosol is obtained upto 2km. Variation of aerosol backscatter coefficient as well as extinction coefficient σ/km with altitude is shown in Fig. 2(c). The maximum σ/km (0.15/km) attains at an altitude of 0.5km and reaches its minima at a height of 4 km. The variation of aerosol backscatter counts and extinction profiles depends on the number of particulates present in the environment and loading of aerosol which vary with time of a day and season. Therefore, to characterize the seasonal pattern of aerosol extinction coefficient, a large number of Lidar output is processed in LabView environment. The monthly average of peak aerosol σ from these diurnal extinction profiles for the year 2001-2003 over Guwahati is characterized.

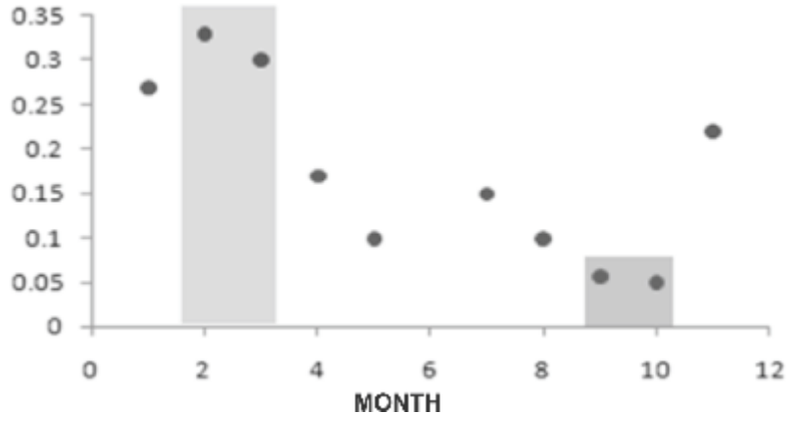

Fig. 3: Seasonal pattern of aerosol σ over Guwahati

The above figure shows that the aerosol σ becomes high (0.35-0.3) during Feb-April and it goes to the minimum (0.05) during the month of September-October. Aerosol σ in Feb-April is 30% higher compared to that in the autumnal month. In this connection it is interesting to note the difference in aerosol loading pattern in the two equinoxial months.

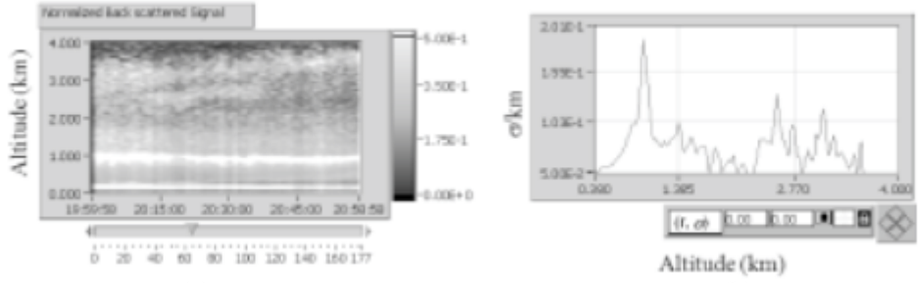

(a) (b)

Fig. 4: (a) normalized backscatter counts for a vernal equinoxial month (20th March, 2001); (b) Aerosol Extinction Coefficient profile with altitude, for the same period marked by arrowhead in Fig. (a)

The Lidar echogram of Fig. 4(a) shows normalized backscatter counts of aerosol for vernal equinoxial month of March, 2001during 19:59:58 hrs to 20:58:58 hrs IST. Fig. 4(b) shows variation of aerosol σ with altitude for the time marked by the arrowhead in Fig. 4(a). Here, the maximum aerosol σ is 0.2/km. In Fig. 4(a) two distinct layers at different altitude are observed: (1) a white thick structure seen at an altitude of 1 km with aerosol σ 0.18/km (2) free tropospheric aerosol beyond the layer (1) are seen at least two more aerosol layers of weaker extinction at about 2.5 and 3.0 km. But we see a significant difference in aerosol distribution during autumnal season. During this period, the environment remains very clear and well-mixed upto about the tropopause height. For example, a representative plot of Lidar echogram for autumnal equinoxial month of October, 2001 is shown below.

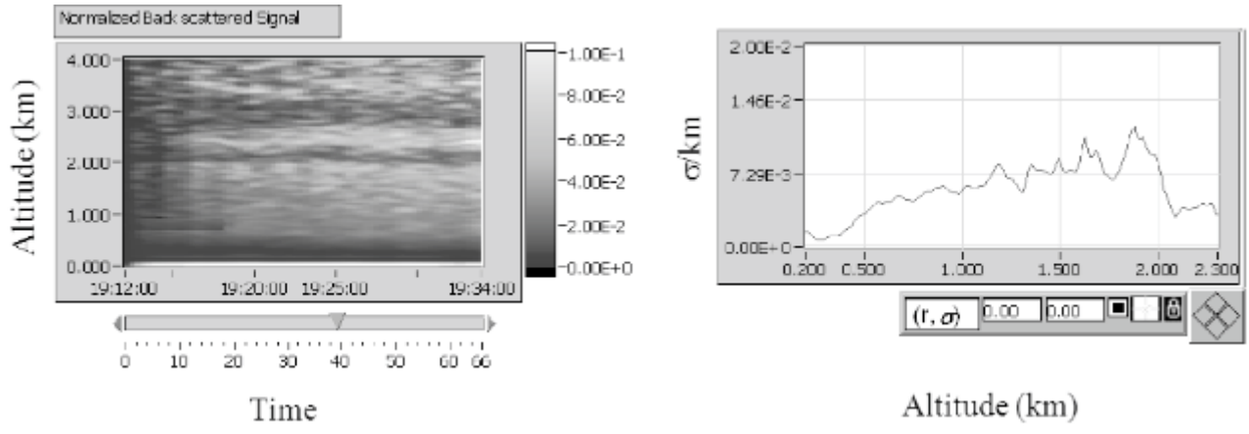

(a) (b)

Fig. 5: (a) A representative normalized backscatter counts for an autumnal equinoxial month (10th October, 2001); (b) Aerosol Extinction Coefficient Profile with altitude, for the same period marked by arrowhead in Fig. 5(a).

Here the maximum aerosol σ reaches 0.01/km at an altitude of 1.8km. The absence of peak aerosol count near to the surface as detected in the vernal equinoxial month suggests a uniform distribution of similar aerosol particles up to the height of 4 km in autumnal season. Now, we take MODIS Level-3 gridded daily AOD product16 for the period of 2001-2003 to compare these data with the Lidar derived AOD. A few imagery of AOD for vernal and autumnal seasons are shown in Fig. 6.

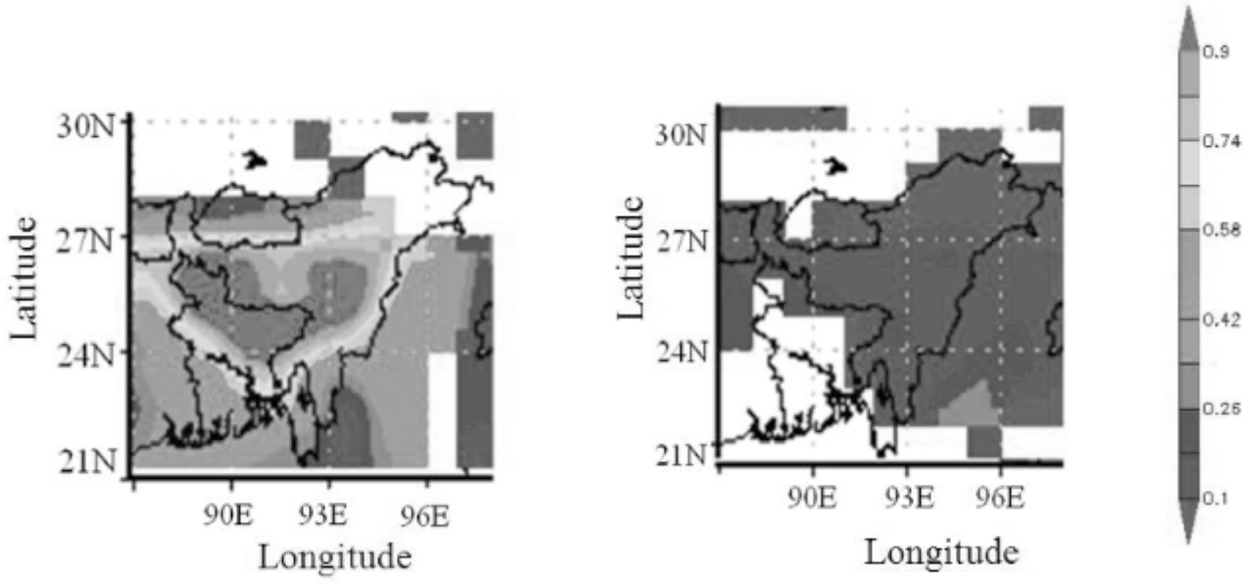

(a) (b)

Fig. 6: AOD imagery from MODIS for (a) vernal equinoxial month (b) autumnal equinoxial month

Figures 6(a) and 6(b) represent the AOD imagery over NE India for the two equinoxial seasons in the year 2001. In this figure, AOD is high (>0.82) in vernal equinox over Guwahati whereas in autumnal equinox a clear environment with AOD less than 0.18 is observed. We have examined MODIS AOD data for the year 2001 to 2003 and plotted the seasonal variation of AOD as shown in Fig. 7 which is similar to that we have obtained from Lidar observation.

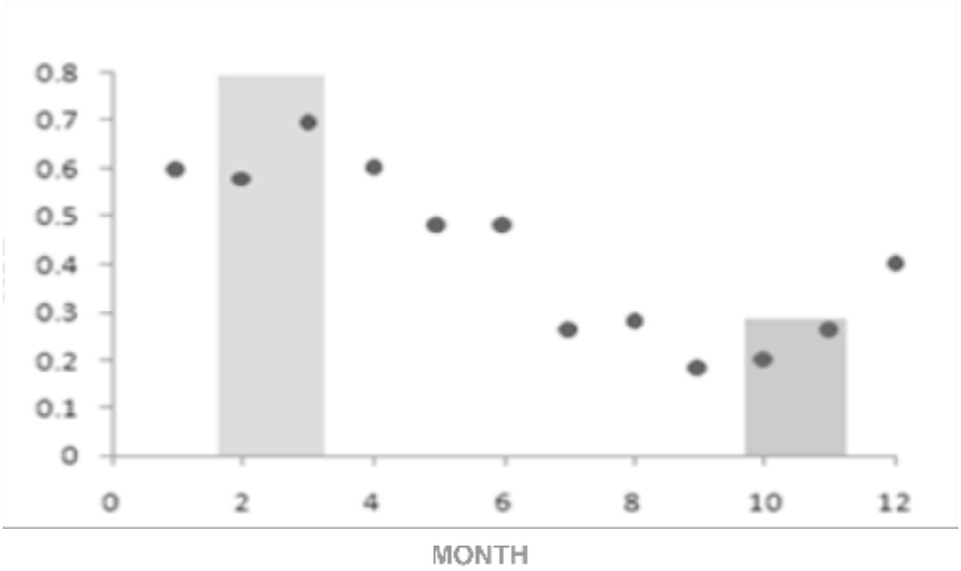

Fig. 7: seasonal variation of AOD obtained from MODIS

Here, AOD at vernal equinoxial months is obtained to be 40% high compared to that of autumnal equinoxial months. It is now necessary to convert Lidar extinction coefficient value to its respective AOD for comparing Lidar obtained AOD with those obtained from MODIS.

3. COMPARISON BETWEEN MODIS AND LIDAR AOD FOR TWO DIFFERENT SEASONS: DETERMINATION OF AN EMPIRICAL RELATION BETWEEN THEM

The Eq. (2) is used here for converting Lidar peak σ to its respective AOD values at least 10 days of each month of the two equinoxial seasons. The average Lidar derived AOD is plotted in Fig. (8) along with the MODIS AOD.

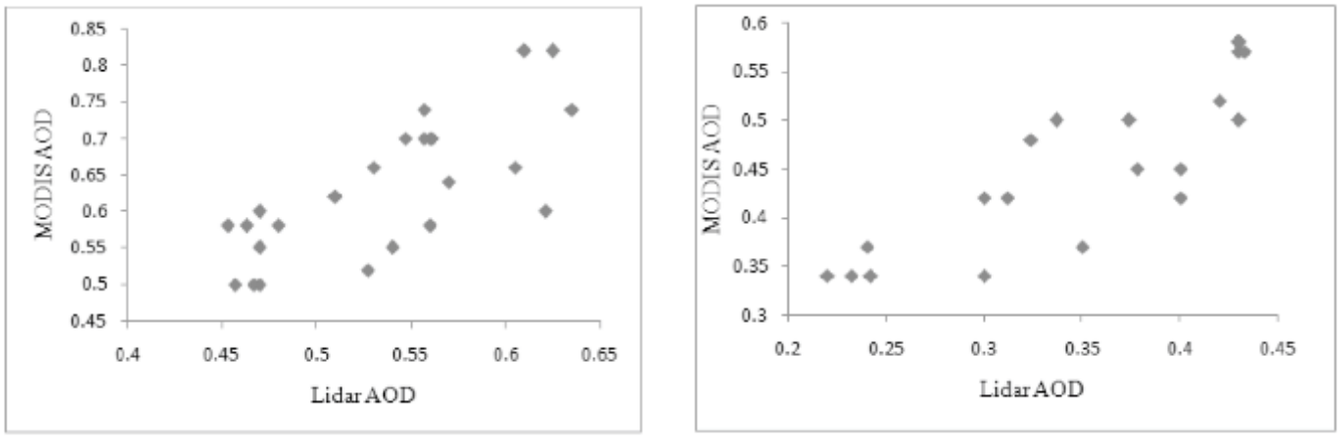

(a) (b)

Fig. 8: scatter plot of Lidar AOD against MODIS AOD for (a) vernal equinoxial month (b) autumnal equinoxial month

The scatter plot of AOD derived from Lidar and obtained from MODIS shows that the reliability of utilizing Lidar extinction coefficient in terms of AOD is more in autumnal months than that of the vernal months. The Lidar derived AOD shows a good correlation with MODIS one for autumnal season with a correlation coefficient of 0.853whereas in vernal equinoxial season Lidar shows a less correlation with correlation coefficient of 0.743. The analysis suggests that it is necessary to apply statistical approach for the best fit of above mentioned relation if MODIS data could be utilized for obtaining vertical AOD profile in absence of Lidar data. Therefore, it is necessary to derived statistical relation between Lidar AOD and MODIS AOD. Starting with the fundamental equation for linearity with linear variables Xi and Yi given by Yi=A+BXi, we have to estimate the values of A and B using least-square method for best fit adopting equation (6) and (7).

$$\sum Y_i = nA + B\sum X_i \quad (6)$$

$$\sum X_i Y_i = A\sum X_i + B\sum X_i^2 \quad (7)$$

Where, n no. of observation and i varies from 1 to n.

Using the experimentally obtained AOD from Lidar (Xi) and MODIS (Yi) observations, the unknown values of A and B are calculated and relevant relation between Yi and Xi are determined for two equinoxial seasons defined by equations (8) and (9) respectively.

$$Y_{ver}=1.12X_{ver}+0.034 \quad (8)$$

$$Y_{aut}=0.99X_{aut}+0.11 \quad (9)$$

The minimum value of X_i depends upon the season and in the chosen equinoxial month, it varies between 0.3 for vernal to 0.1 for autumnal. The relation (8) and (9) will be utilized for deriving AOD from one of the sources (say) Lidar to obtain MODIS AOD in absence of such data. A few output of calculated MODIS AOD (Y_i) from Lidar AOD (X_i) are shown in the Table 1 and 2 for two equinoxial seasons.

Table 1: A representative AOD values: MODIS observed, MODIS estimated and Lidar observed during vernal equinoxial season

MODIS observed AOD	MODIS calculated AOD value from empirical relation	Lidar observed AOD
0.82	0.73	0.61
0.7	0.66	0.56
0.7	0.65	0.55
0.64	0.67	0.57
0.6	0.56	0.47
0.58	0.55	0.46
0.57	0.52	0.43

Table 2: A representative AOD values: MODIS observed, MODIS estimated and Lidar observed during autumnal equinoxial season

MODIS observed AOD	MODIS calculated AOD value from empirical relation	Lidar observed AOD
0.57	0.53	0.43
0.5	0.48	0.37
0.48	0.43	0.32
0.42	0.4	0.3
0.37	0.34	0.24
0.34	0.33	0.23
0.42	0.4	0.3

4. DISCUSSION AND CONCLUSION

The exercise of measuring AOD is an evolved one as AOD is not directly measurable and is retrieved from observation of atmospheric spectral transmission and through path integrated extinction co-efficient parameters. Therefore AOD value derived is sensitive to small calibration error and also to the chosen method. In this paper, we address these aspects while comparing AOD obtained from MODIS with those derived from Lidar. Starting with graphical analysis to examine the relation between the AOD values obtained from two sources an empirical equation derived between them for deriving AOD values from one of the available sources. The correlation coefficient of 0.743 and 0.853 obtained between derived AOD from Lidar source and the observed one from MODIS, at two different atmospheric conditions over this suburban study area points to the necessity of establishing such empirical relation at different seasons as AOD has a strong seasonal components. Similar work done by Chan [2009] at different spatial resolution of MODIS AOD obtained that the 1-km resolution AOD product from MODIS have better correlation with the Lidar AOD in comparison to the 10-km resolution product. The correlation coefficient of 0.78 obtained by him at 1-km resolution is lower than what we have obtained for autumnal equinoxial season. Lewis et al. [2010] shows that comparisons with MODIS AOD at 10 km × 10 km and 5 km × 5 km resolutions show good agreement with that of aircraft Lidar observations having correlation values of 0.82 and 0.88, respectively over Hampton, Virginia, the values approaching to the result obtained by us in autumnal equinox. Young et al. also compares MODIS AOD at 5 km × 5 km resolutions with that obtained from ground based and airborne Lidar measurement. They have shown that below an altitude of 1 km, the Lidar aerosol and MODIS AOD exhibit good agreement over Norfolk-Virginia Beach area and the California Central Valley, US.

Therefore, we can conclude that the adopted approach will be utilized in future to identify the source of aerosol over semi urban area over Gauhati University by using MODIS data.

REFERENCES

1. Andreae, M.O. Ocean–atmosphere interactions in the global biogeochemical sulfur cycle, Mar. Chem. 30, 1990, p.1.
2. Charlson R. J.; Schwartz S. E.; Hales J. M.; Cess R. D.; Coakley J. A.; Hansen J. E. & Hofmann D. J., Climate forcing by anthropogenic aerosols, Science, 255, 1992, p.423.
3. Chu X. Z. Characteristics of Fe ablation trails observed during the 1998 Leonid Meteor Shower, Geophys. Res. Lett. 27, 2000, p.1807.
4. Kaufman, Y. J.; Tanre´, D.; Remer, L. A.; Vermote, E. F.; Chu, A. & Holben, B. N. Remote sensing of Tropospheric Aerosol from EOS-MODIS over the land, J. Geophys. Res., 102 (D14), 1997a, p.17051.
5. Kaufman, Y. J.; Tanre´, D. & Boucher O. A satellite view of aerosols in the climate system, Nature, 419, 2002, p.215.
6. King, M. D. Cloud and aerosol properties, precipitable water, and profiles of temperature and water vapor from MODIS, IEEE Trans. Geosci. Remote Sens., 41, 2003, p. 442.
7. Penner J. E.; Andreae M.; Annegarn H.; Barrie L.; Feichter J.; Hegg D.; Jayaraman A.; Leaitch R.; Murphy D.; Nganga J. & Pitari G. Aerosols, their Direct and Indirect Effects, in: Climate Change 2001: The Scientific Basis, edited by: Houghton J. T.; Ding Y.; Griggs D. J.; Noguer M.; Van der Linden P. J.; Dai X; Maskell K. & Johnson C. A. Report to Intergovernmental Panel on Climate Change from the Scientific Assessment Working Group (WGI), Cambridge university Press, 2001,289–416.
8. Chan, P.W. Comparison of Aerosol Optical Depth (AOD) Derived from Ground-Based LIDAR and MODIS, The Open Atmospheric Science Journal, 3, 2009, p.131.
9. Tripathi, S. N.; Dey, S.; Chandel, A.; Srivastava, S.; Singh R.P. & Holben, B. N. Comparison of MODIS and AERONET derived aerosol optical depth over the Ganga Basin, India, Annales Geophysicae, 23, 2005, p.1093.
10. Lewis; Jasper; Young R. D. & Chu D. A. A Study of Air Quality in the Southeastern Hampton–Norfolk–Virginia Beach Region with Airborne Lidar Measurements and MODIS Aerosol Optical Depth Retrievals, J. Appl. Meteor. Climatol., 49, 2010,p.3.
11. Young R. D.; Szykmanb, J.; Severancec, K.; Chud, D. A.; Rosene, R. & Al-Saadia, J. Aerosol Lidar and MODIS Satellite Comparisons for Future Aerosol Loading Forecast, Remote Sensing of Aerosol and Chemical Gases, Model Simulation/Assimilation, and Applications to Air Quality, edited by Allen Chu, James Szykman, Shobha Kondragunta, Proc. of SPIE Vol. 6299, 2006.
12. Baishya, R.; Devi; M. & Barbara, A. K. Software for lidar data analysis: development and application on MPL setup, Ind Jr. Radio and Space Phys., 32, 2003, p.114.
13. Devi, M.; Barbara, A. K.; Saikia, M. & Chen, W. Vertical distribution of optical parameter of aerosol by using portable atmospheric lidar system of Gauhati University, Ind. Jr. Radio & Space Phys., 37(5), 2008, p.333.
14. Devi, M.; Barbara, A. K.; Saikia, M.; Choudhury, B. & Sarmah, H. Micro Pulse Lidar: A tool for analyzing interactive relation between Aerosol and Cloud formation, Int. J. Engg. Sc. & Mgmt. 2 (1), 2012, p.82.
15. Saikia Manoj. Measurement of Optical Properties of Aerosols and Methane Concentration through Lidar and DIAL Set up of Gauhati University, 2010, Ch. 3.
16. King, M. D.; Kaufman, Y. J.; Menzel, W. P. & Tanré, D. Remote-sensing of cloud, aerosol, and water-vapor properties from the Moderate Resolution Imaging Spectrometern (MODIS),IEEE Trans. Geosci. Remote Sens., 30, 1992, p.2.

BIANCHI TYPE III AND KANTOWSKI- SACHS MODELS WITH BULK VISCOSITY, COSMOLOGICAL AND GRAVITATIONAL "CONSTANTS"

S. Kotambkar*
Department of Mathematics, Laxminarayan Institute of Technology, Nagpur, India
Corresponding author
Email: shubha.kotambkar@rediffmail.com

G. P. Singh
Department of Mathematics, Visvesvaraya National Institute of Technology, Nagpur, India
Email: gpsingh@vnitnagpurac.in

ABSTRACT

In this paper we have studied anisotropic Bianchi type III and Kantowski-Sachs bulk viscous cosmological Models with cosmological and gravitational "constants". Exact solutions of the field equation have been obtained. The physical and Dynamical behaviours of the model have also been discussed.

1. INTRODUCTION

The observational evidences suggest that the anisotropy is negligible in the large scale picture of the universe. However, it is not so if we consider small scale picture of the universe. In the early stages universe did not have the property of isotropy as we find today. Misner [1] has suggested that the initial highly irregular universe approaches to the FRW model stage in the process of cosmological evolution. According to the group theoretic criterion the spatially homogeneous space-times are of two types (1) Bianchi type (I to IX) and (2) Kantowski-Sachs space-times [2]. A number of authors [3-5] have studied Bianchi-type solutions. Bianchi Type I cosmological models with variable G and have been discussed by several authors in different context [6-9]. Harko and Mak [10] have investigated Bianchi Type I cosmological models with irreversible matter creation, while Bali and Jain[11] have studied Bianchi Type I Inflationary universe in general relativity. Tachyonic potential in Bianchi Type I universe has been discussed by Suresh[12]. Bianchi Type I cosmological models with viscous fluid has been studied by Saha [13]. Singh and Singh [14] have studied Bianchi-type III and Kantowski-Sachs cosmological models in Lyra geometry. Anisotropic cosmological models have been extensively studied in the literature by a number of authors [15-17].

Eckart [18] was the first one who described the cosmic viscous fluid. It has been widely discussed in the literature that bulk viscosity may arise during evolution of the universe such as decoupling of neutrinos during the radiation era, the decoupling of matter from radiation era, particle creation processes during the formation of galaxies[19] . Eckart's theory suffers from serious shortcomings namely causality and stability. The problem arises from the first order nature of the theory i.e. it considers only the first order deviations from equilibrium. In fact, to prevent non- causal and unstable behaviour it is necessary to consider second order terms. These terms transform the equations governing dissipative quantities from the algebraic first order type to differential evolution equations. To overcome the shortcomings of Eckart theory, Israel and Stewart [20], Pavon et al [21], developed a fully relativistic formulation of the theory by considering higher order theories i.e. extended irreversible thermodynamics (EIT). Grøn [22] and Maartens [23] have presented exhaustive review of the research on cosmological models with non-causal and causal thermodynamics respectively. The possibility of bulk viscosity driven inflationary solutions of the full Isreal-Stewart theory in different cases are discussed in [24] and [25]. The role of bulk viscosity during early stages of evolution has been discussed by several authors (refer[26] and references therein).

A cosmological constant was originally introduced by Einstein in 1917 in his field equations in order to satisfy Mach's Principal. In the last more than one decade the remarkable progress made in various types of astrophysical and cosmological observations has profoundly changed the cosmology by predicting an accelerated expansion of the universe. The existence of a positive cosmological constant is strongly favoured by Supernovae Ia observations [27-30]and anisotropy measurements of cosmic microwave background (CMB)made by WMAP experiment[31-32]. It is widely believed that cosmological constant was very large at the early stage of the universe, strongly influenced acceleration of the universe and now relaxed to its present small value[33-40].

In order to achieve a possible unification of gravitation and elementary particle physics many authors [41-42] have proposed extensions of Einstein theory, with time dependent G. Dersarkissian [43] has studied the possibility of variable G and in Einstein theory. Bertolami [44] has considered cosmological models with time dependent G and and suggested. A R^{-2} t^{-2} number

of authors [45-48] have proposed linking the variation of G with that of in the framework of general relativity. This approach is appealing because it leaves Einstein's equations formally unchanged since a variation in is accompanied by a variation in G. Generalized field equations with time-dependent G and have been extensively studied in the literature [49-51]. Beesham [52] studied a universe consisting of cosmological "constant" and bulk viscosity. Abdel-Rahman [53] considered a model in which the gravitational constant G varies with time but the energy is conserved. Recently Arbab [54] has studied viscous cosmological models with variable and G. Golda et al [55] have shown that the bulk viscous fluid with FRW symmetries can structurally approximate to the dynamics of the classical FRW model. Both the truncated and full version of the causal thermodynamic theory are used by Romano and Pavon [56] Considering above studies it is worthwhile to study anisotropic Bianchi type III and Kantowski-Sachs models with bulk viscosity, cosmological and gravitational "constants".

The Field Equations

For perfect fluid distribution Einstein's field equations with gravitational and cosmological "constants" may be written as

$$R_{ij} \quad \frac{1}{2} R g_{ij} \qquad 8\ GT_{ij} \qquad g_{ij} \tag{1}$$

where Tij is the energy momentum tensor of the cosmic fluid which in the presence of bulk viscosity takes the form

$$T_{ij} \quad (\qquad p \qquad)u_i u_j \quad (p \qquad)g_{ij} \tag{2}$$

Here p represent equilibrium pressure, is the bulk viscosity coefficient, and is the expansion scalar defined as

$$\frac{3\dot{V}}{V} \quad \mathrm{V}^3 = (-g_{11}g_{22}g_{33})^{1/2} \tag{3}$$

During this investigation it has been assumed that an observer has a comoving velocity u_i $\overset{i}{4}$ and the space-time metric be of the form

$$ds^2 \quad dt^2 \quad R_1^2 dx^2 \quad R_2^2[d^{\ 2} \quad f^2(\ )d^{\ 2}] \tag{4}$$

where R1 and R2 are functions of time t only. The field equations (1)-(2) for the metric (4) reduce to

$$\frac{2\dot{R}_1}{R_1} \quad \frac{\dot{R}_2}{R_2} \quad \frac{\dot{R}_2}{R_2} \quad \frac{1}{fR_2^2}\frac{d^2 f}{d^{\ 2}} \quad 8 \quad G \tag{5}$$

$$\frac{\ddot{R}_1}{R_1} \quad \frac{\ddot{R}_2}{R_2} \quad \frac{\dot{R}_1}{R_1}\frac{\dot{R}_2}{R_2} \qquad 8\ G(p \qquad) \tag{6}$$

$$2\frac{\ddot{R}_2}{R_2} \quad \frac{\dot{R}_2}{R_2}^{\ 2} \quad \frac{1}{fR_2^2}\frac{d^2 f}{d^{\ 2}} \qquad 8 \quad G(p \qquad) \tag{7}$$

For f( ) = sinh metric (4) reduces to Bianchi type III space-time metric and for f( ) = sin metric (4) produces geometry of Kantowski-Sachs space-time. In the next section Bianchi type III and Kantowski-Sachs models have been considered separately.

Bianchi type III Cosmological Model

Taking f( ) = sinh the space-time metric (4) reduces to Bianchi type III space-time metric

$$ds^2 \quad dt^2 \quad R_1^2 dx^2 \quad R_2^2[d^{\ 2} \quad \sinh^2 \quad d^{\ 2}], \tag{8}$$

and the set of field equations (5)-(7), may be written as

$$\frac{2\dot{R}_1}{R_1} \quad \frac{\dot{R}_2}{R_2} \quad \frac{\dot{R}_2}{R_2} \quad \frac{1}{R_2^2} \quad 8 \quad G \tag{9}$$

$$\frac{\ddot{R}_1}{R_1} \quad \frac{\ddot{R}_2}{R_2} \quad \frac{\dot{R}_1}{R_1}\frac{\dot{R}_2}{R_2} \quad 8 \quad G(p \qquad) \tag{10}$$

$$2\frac{\ddot{R}_2}{R_2} \quad \frac{\dot{R}_2}{R_2}^{2} \quad \frac{1}{R_2^2} \quad 8 \quad G(p \qquad) \tag{11}$$

Equations (9)-(11) produces the continuity equation

$$\cdot \quad (p \qquad) \frac{\dot{R}_1}{R_1} \quad \frac{2\dot{R}_2}{R_2} \qquad \frac{\dot{G}}{G} \qquad \frac{\cdot}{8 \quad G} \tag{12}$$

The conservation of energy-momentum ($T^{i\,j}_{;\,j}$ 0) suggest the continuity equation

$$\cdot \quad (p \qquad) \frac{\dot{R}_1}{R_1} \quad \frac{2\dot{R}_2}{R_2} \quad 0 \tag{13}$$

Equations (12) and (13), suggests

$$\cdot \quad 8 \quad \dot{G} \tag{14}$$

Since there are only three basic equations viz. (9)-(11) and seven unknowns viz. R_1, R_2, $_p$, , G, and therefore four more physically plausible relation will be considered for solving the set of equations. The four conditions are: The equation of state for p as

$$p = (\ -1) \quad , \tag{15}$$

The cosmological constant varies as inverse square of t

$$\frac{A}{t^2} \tag{16}$$

The power-law relations

$$R_1 = a_0 \, t^a, \tag{17}$$

$$R_{2\,=} b_0 \, t^b \ . \tag{18}$$

They have been taken into the consideration for further investigations. Here a, a_0, b and b_0 are constants. On differentiating equation (16), and using equation (14), one can get

$$8 \quad \dot{G} \quad \frac{2A}{t^3} \tag{19}$$

With help of equations (16)-(18), equation (9) yields

$$8 \quad G \quad \frac{(2a \quad b)bb_0^2 \quad Ab_0^2 \quad t^{2b} \quad t^2}{b_0^2 t^{2b} \quad 2} \tag{20}$$

Further, dividing equation (19) by equation (20), one can find

$$\frac{\dot{G}}{G} \quad \frac{2A}{2a \quad b \; b \quad A \; b_0^2 \quad t^{2(1 \quad b)} \quad t} \tag{21}$$

For b =1, equation (21), gives the solution

$$G \quad G_0 t^{\frac{2Ab_0^2}{Mb_0^2 \ 1}}, \tag{22}$$

where M = 2a + 1 - A.

By use of equation (22), equation (20) suggests

$$\frac{Mb_0^2 \ 1}{8 \quad b_0^2 \ G_0} \frac{1}{t^{2(2ab_0^2 \quad b_0^2 \ 1)/(Mb_0^2 \ 1)}} \tag{23}$$

The condition $Mb_0^2 \quad 1$ ensures the positivity of energy density. Using the definition (3) for expansion scalar and equations (17)-(18), the expansion scalar may be expressed as the function of time co-ordinate

$$\frac{a \quad 2}{t} \tag{24}$$

By making use of set of equations (15)-(18), and (22)-(24), equation (10) yields

$$\frac{(a^2 \quad 1 \quad A)(\quad 1)\, b_0^2 \quad Mb_0^2 \quad 1}{8 \quad (a \quad 2)(\quad 1)b_0^2 G_0} \frac{1}{t^{(4ab_0^2 \quad 2b_0^2 \ 1)/(Mb_0^2 \ 1)}} \tag{25}$$

The shear scalar may be defined as [57],

$$^2 \quad \frac{1}{12} \quad \left(\frac{\dot{g}_{11}}{g_{11}} \quad \frac{\dot{g}_{22}}{g_{22}}\right)^2 \quad \left(\frac{\dot{g}_{22}}{g_{22}} \quad \frac{\dot{g}_{33}}{g_{33}}\right)^2 \quad \left(\frac{\dot{g}_{33}}{g_{33}} \quad \frac{\dot{g}_{11}}{g_{11}}\right)^2 \tag{26}$$

equations (17)-(18) and (26), suggest

$$^2 \quad \frac{2(a \quad 1)^2}{3t^2} \tag{27}$$

The deceleration parameter is related to the expansion scalar as

$$q \quad \frac{3 \quad ^2}{^2}$$

Further, with help of equation (24), the expression for deceleration parameter q may be obtained as

$$q \quad \frac{1 \quad a}{2 \quad a} \tag{28}$$

Kantowski-Sachs Cosmological Model

Considering f( ) = sin , the space-time line element (4) reduces Kantowski-Sachs space-time metric

$$ds^2 \quad dt^2 \quad R_1^2 dx^2 \quad R_2^2[d \ ^2 \quad \sin^2(\ )d \ ^2] \tag{29}$$

In this case the set of field equations (5)-(7) take the form

$$\frac{2\dot{R}_1}{R_1} \quad \frac{\dot{R}_2}{R_2}\frac{\dot{R}_2}{R_2} \quad \frac{1}{R_2^2} \quad 8 \quad G \tag{30}$$

$$\frac{\ddot{R}_1}{R_1} \quad \frac{\ddot{R}_2}{R_2} \quad \frac{\dot{R}_1}{R_1}\frac{\dot{R}_2}{R_2} \quad 8 \quad G(p \qquad) \tag{31}$$

$$2\frac{\ddot{R}_2}{R_2} \quad \left(\frac{\dot{R}_2}{R_2}\right)^2 \quad \frac{1}{R_2^2} \quad 8 \quad G(p \qquad) \tag{32}$$

With equations (16)-(18), equation (30) yields

$$8 \quad G \qquad \frac{(2a \quad b)bb_0^2 \quad Ab_0^2 \quad t^{2b} \quad t^2}{b_0^2 t^{2b \quad 2}} \tag{33}$$

Equation (19) and (33), yields

$$\frac{\dot{G}}{G} \quad \frac{2A}{2a \quad b\,b \quad A\,b_0^2 \quad t^{2(1 \quad b)} \quad t} \tag{34}$$

Substituting b = 1, equation (34), on integration yields

$$G \quad G_0 t^{\frac{2Ab_0^2}{Mb_0^2 \quad 1}} \tag{35}$$

From equations (33) and (35), the expression for energy density may be found as

$$\frac{Mb_0^2 \quad 1}{8 \quad b_0^2 \, G_0} \frac{1}{t^{2(2a\,b_0^2 \quad b_0^2 \quad 1)/(Mb_0^2 \quad 1)}} \tag{36}$$

Again by making use of set of equations (15)-(18), (24), (35)-(36), one can easily obtain the expression for bulk viscosity coefficient in terms of t as

$$\frac{(a^2 \quad 1 \quad A)(\quad 1)\,b_0^2 \quad Mb_0^2 \quad 1}{8 \quad (a \quad 2)(\quad 1)b_0^2 G_0} \frac{1}{t^{(4ab_0^2 \quad 2b_0^2 \quad 1)/(Mb_0^2 \quad 1)}} \tag{37}$$

2. CONCLUSION

In this work Bianchi type III and Kantowski-Sachs cosmological models with bulk viscosity, cosmological and gravitational "constants" have been studied. These models suggest the relation $G(t) \quad (t) \quad t^{-2}$. This type of result has been reported in the references [49,58]. Further for Machian Cosmological solution the condition $G(t) \quad (t) \quad H^2$ is also satisfied. In the both Bianchi type III and Kantowski-Sachs models power law increasing behaviour of G in an expanding universe have been obtained. The possibility of an increasing G has been discussed by several authors (refer [58] and references therein). In present model the deceleration parameter is constant. When t expansion stops and shear dies out.

Acknowledgment Authors will like to thank UGC New Delhi for providing financial support to carry out our research work under the scheme of Major research project.

REFERENCES

1. Misner, C. W. (1968). Astrophys. J., 151, 431; Ellis, G. F. R. in Relativistic Cosmology, ed. Sachs, R. K. (Academic New York, 1971); Borrow, J. D. and Matzner, (1977). Mon. Not. R. Astr. Soc., 181, 719; Hu, B. L. (1983) in Advances in Astrophysics, eds. Fang, L. Z. and Ruffini, R. (World Scientific, Singapore)
2. Kantowski, R. and Sachs, R. K.(1966). J. Math. Phys.,7,443.
3. Siklos, S. T. C. (1984); in Relativistic Astrophysics and Cosmology, Eds. Fustero, X. and Verdauger, World Sci. Pub., Singapore, 201-248.
4. Lorenz, D. (1984); In Solutions of Einstein's Equations: Technique and Results, Eds. Hoenselaers, C. and Dietz, W. Springer-Verlag, Berlin, 1984, 403-435.
5. Maartens, R. and Maharaj, S. D. (1990). Gen. Rel. Grav., 20.
6. Beesham, A. (1994). Gen. Rel. Grav, 26, 159.
7. Kalligas, D., Wesson, P. S., Everitt, C. W. F. (1995). Gen. Rel. Grav., 27, 645.
8. Arbab, I. Arbab. (1998). Gen. Rel. Grav., 30, 1401.
9. Vishwakarma, R. G. (2005). Gen Rel. Grav., 37, 1305.
10. Harko, T. and Mak, M. K. 92000). gen. Rel. Grav. 32, 865.
11. Bali, R., Jain, U. C. (2002). Pramana, 59, 1.
12. Suresh, P. K. (2003) [gr.qc/0309043].
13. Saha, B. (2005). Chin. J. Phys. 43, 1035; Int. J. Thor. Phys., 45,952; (2006)Astrophys Space Sci.,302,83.
14. Singh, T. and Singh, G. P. (1991). Astrophys. Space. Sc., 181, 89.
15. Reddy and Rao(1998). Asrophysics Space Sc. 257, 293.
16. Pradhan, A. and Singh, S. K., (2004a), Int. J. Mod. Phys. D.13,503;, Pradhan, A.and Pandey, P., Singh, G. P.,,

Deshpande, R. V., (2005), Spacetime subset, 6, 116.
17. Singh, SureshKumar and Singh, C. P.(2007)., Astrophys. Space. Sc., 312, 57.
18. Eckart, C. (1940). Phys. Rev. D, 58, 919.
19. Ellis, G.F.R. (1971); Sachs,R.K.,General Relativity and Cosmology,Enrico Fermi course, Academic New York; Hu, B.L. (1983),I L. J. Fang and R. Ruffini, Advance in Astrophysics, world Scientific, Singapore.
20. Israel, W. and Stewart, J. M. (1976). Phys.Lett. A, 58, 213.
21. Pavon, D., Jou, D. and Casas Vazquez, (1982). Ann. Inst. Henri Poincare A, 36, 79.
22. Grn, . (1990). Astrophys. Space Sc., 173, 191.
23. Maartens, R. (1995). Class. Quant. Grav., 12, 1455.
24. Zimdahl, W. (1996). Phys. Rev. D, 53, 5483.
25 Mak, M. K. and Harko, T (1998). Gen. Rel. Grav., 30, 1171.
26 Singh, G. P.,, Deshpande, R. V.,Singh T, (2002), Astrophys. Space. Sci.282,489.
27. Bennet, C.L., (2003), Asrophys, J., 583,1.
28. Spergel, D. N.,et,al (2003)., ApJS, 148, 175.
29. Hinshaw, G, et al.(2007)., ApJS, 170, 288.
30. . Spergel, D. N.,et,al (2007)., ApJS, 170, 377.
31. Perlmutter, S. J. et al (1998). Nature (London) 391 51; (1999). Astrophys. J., 517, 565.
32. Riess, A. G. et al (1998). Astron: J. 116, 1009.
33. Weinberg, S. (1989)., Rev. Mod. Phys. 611.
34. Chen, W. and Wu, V. S.(1990)., Phys. Rev., D41, 695.
35. Abdel Rahman A-M., M.(1992))., Phys. Rev., D,45, 3492.
36. Berman, M.S.,(1991)., Gen. Rel. Grav.23, 465.
37. Ozer , M. and Taha M. O., (1998)., Phys. Lett.A13, 571.
38 Sahni, V and Starobisky,A.,(2000), Int. J. Mod. Phys. D9, 373.
39. Vishwakarma, R. G.(2000), 19. Spergel, D. N.,et,al (2003)., ApJS, 148, 175. 17, 3833; (2001) Class. Quant. Grav, 18, 159;(2001)Gen. Rel. Grav.33, 1973; (2002), Class. Quant. Grav.19.776.
40. Debnath, P.S. and Paul, B. C.,(2007) Physical Review D 76, 123505.
41. Dirac, P. A. M. (1975). The General theory of relativity. (Wiley: New York).
42. Brans, C. and Dicke, R. M. (1961). Phys. Rev., 124, 925.
43. Dersakissian, M. (1985). Nuovo Cimento B, 88, 29.
44. Bertolami, O. (1986). Nuovo Cimento B, 93, 36; (1986). Fortschr. Phys., 34, 829.
45. Sistero, R. F. (1991). Gen. Rel. Grav., 23, 1265.
46. Kalligas, D., Wesson, P., and Everitt, C. W. F. (1992). Gen. Rel. Grav., 24, 351.
47. Beesham, A. (1994). Gen. Rel. Grav., 26, 159.
48. Abdusattar and Vishwakarma, R. G. (1997). Class. Quant. Grav., 14, 945.
49. Singh, T., Beesham, A. and Mbokazi, Ws. (1998). Gen. Rel. Grav., 30, 537.
50. Harko, T. and Mak, M. K. (1999). Gen. Rel. Grav., 31, 849.
51. Singh, G. P. and Kotambkar, S. (2001). Gen. Rel. Grav., 33, No. 4.
52. Beesham, A. (1993). Phys. Rev. D, 48, 3539.
53. Abdel-Rahaman, A-M. M. (1990). Gen. Rel. Grav., 22, 655; (1992). Phys. Rev. D, 45, 3497.
54. Arbab I Arbab (1997). Gen. Rel. Grav. , 29, 61.
55. Golda, Z. , Heller, M. and Szydlowski, M. (1983). Astrophys. Space. Sci., 90, 313.
56. Romano, V. and Pavon, D. (1994). Phys. Rev. D, 50, 2572.
57. Raychaudhuri, A. K. (1955). Phys. Rev., 98, 1123.
58. Singh, G. P. and Kotambkar, S. (2003). Gravitation and cosmology, 9,1

INTERNATIONAL JOURNAL OF ENGINEERING SCIENCES AND MANAGEMENT (ISSN: 2231-3273)

International Journal of Engineering Sciences and Management is a bi-annual journal of Dronacharya Group of Institutions, Greater Noida, UP, India.

1. SCOPE OF THE JOURNAL

To publish full-length research papers in any one or more of the following disciplines: Computer Science & Engineering, Information Technology, Electrical, Electronics & Communication Engineering, Mechanical Engineering, Civil Engineering, Physics, Mathematics, Economics, and Management

2. PURPOSE OF THE JOURNAL

To keep the academic community abreast of the research and technical scenario in the stated disciplines in the world.

3. CHERISHED AIM OF THE JOURNAL

To excite and ignite the young minds and to motivate them for involving themselves in research and development activities. This will empower our manpower in the context of fast changing technologies across the globe.

4. GUIDELINES FOR AUTHORS

Submission of Manuscripts: Soft copy of the manuscript for consideration of publication should be sent (as MS Word Windows 2007 attachment) by Email to the Executive Editor at advisor.r&d@gnindia.dronacharya.info

All papers, received for consideration of publication and complying with the below-mentioned format will be sent for review to at least two referees. In accepting the paper for publication, the Editors and reviewers will give special weight to readability and interest value for a wide readership besides the originality and the high-standard of its contents. The Executive Editor's decision is final in case of non-unanimity of opinion of referees. Under normal circumstances, the authors will be informed about the status of their papers by the Executive Editor within eight weeks of their submission.

Preparation of Manuscripts:

- **Manuscript:** Manuscript should be in English, the preferred spelling being that of the Concise Oxford Dictionary. It should be in 'Times New Roman', single-spaced, and typed on 8.5" x 11" or A4-size paper with margins of 1" (25 mm) on each side. Manuscript should be typed in single column only (and not in double or triple columns).
- **Title of Paper:** Font size 16, ALL CAPITALS, bold, centered, and not underlined. The title must be 12.5 mm below the top of the page (in addition to the standard 25 mm margin). The Title should adequately describe the contents of the paper
- **Full names of all Authors,** with * as superscript with corresponding author's name and his/her Email ID (Font size 12, centered) and also the contact number. A blank line should be left between the title and the author's name(s).
- **Full postal address** along with affiliations (Font size 10, centered).
- **Abstract** (Font size 10, centered) All papers must have a non-mathematical abstract of not more than 200 words. The abstract should indicate the general scope of the paper, the important findings and the conclusions drawn. The abstract should include only text. It should be specific about the methodologies used and the conclusion drawn of the work reported. Please avoid the use of abbreviations and references. (Text of the Abstract: Font size 9, single-space, justified).
- **Keywords:** Include up to six keywords that describe your paper for indexing and for web searches. The more discriminating your keywords are, the greater is the likelihood that your article will be found and cited. (Font size 9, italics, left-justified).
- **Text:** (Font size 10, Justified). The paper must be divided into sections starting preferably with "Introduction" and ending with "Conclusion". The main sections should be numbered 1, 2, 3 etc and subsections as 2.1, 2.2 etc. Main headings should be typed in capitals, subheadings in lower case. Both types of heading should be underlined and left-justified. Footnotes should be avoided. Equations should be typewritten and with the equation number placed in parentheses at the right margin. Reference to the equation should use the form 'Eq. (3)'. Use extra line spacing between equations, illustrations, figures and tables. The use of SI units is strongly recommended
- **Tables and Figures:** Tables and Figures should be integrated with the text (and not sent separately at the end of the manuscript) and numbered consecutively in the order in which reference is made to them in the text of the paper. All captions must be centrally located above a Table and below a Figure (Font size 10). All tables and figures must be numbered consecutively in Arabic numerals (not Roman) (e.g., Table 3 or Fig. 3) in the order of appearance in the text. Tables & Figures should be reproduced in the exact format and at the exact place as desired to appear in the journal.
- **Conclusion:** A conclusion section must be included and should indicate clearly the advantages, limitations and possible

applications of the paper. Authors may also discuss about the scope of future work.

- **Acknowledgements:** An acknowledgement section may be included after the 'Conclusion'.
- **References:** References should be placed at the end of the text, should be numbered consecutively in order of their citation in the text and be indicated by superscripts in the text of the manuscript. Examples of different citations as References are given below:

(i) In case of referring to an Article in a Journal

Kuebel, D.; Lahiri, M. & Wolf, E. An Inverse Problem in the Theory of Stochastic Electromagnetic Beams, Opt. Commn., 282, 2009, p.141.

(ii) In case of referring to a Book/Monograph

Rao, C.N.R. & Raveau, B. (Eds.). Transition Metal Oxides, Wiley-VCH, 2nd Edition, 1998, Ch. 2.

(iii) In case of referring to a Conference Paper

Ctvrtnickova, T.; Mateo, M; Yanez, A. & Nicolas, G. Characterization of Coal Fly Ash Components by Laser-Induced Breakdown Spectroscopy. Presented at the Fifth International Conf. on Laser-Induced Breakdown Spectroscopy, Berlin, Adlershof, Germany. Sep 22-26, 2008, CP-15, p. 67-68.

(iv) In case of referring to a Report

Marine, R.E. & Iliff, K.W. Application of Parameter Estimation to Aircraft Stability and Control. NASA, USA, 1986, Report No. NASA-RP-1168.

Papers quoting the LATEST references from the referred journals will be preferred for publication unless the original contribution from the author/s is of a very high standard.

UNDERTAKING

Authors must include, in the covering Email that their paper has not been published//accepted/submitted for publication/presentation to any other journal/ book/conference in any form and the work submitted by them is their own and original. The same 'Undertaking' should also be attached, on a separate page, along with the manuscript. This ethical policy of the Journal will be strictly adhered to.

Note: Manuscripts not in conformity with these 'Guidelines' will not be forwarded to the experts for review.

Notes

Notes

Notes

DRONACHARYA
GROUP OF INSTITUTIONS

Targeted in pursuit of your career

B.TECH | MCA | MBA

www.dronacharya.info






Courses Offered

COMPUTER SCIENCE AND ENGINEERING

INFORMATION TECHNOLOGY

ELECTRONICS & COMMUNICATION ENGINEERING

MECHANICAL ENGINEERING

CIVIL ENGINEERING

ELECTRICAL & ELECTRONICS ENGINEERING

MASTERS IN COMPUTER APPLICATIONS

MASTERS IN BUSINESS ADMINISTRATION

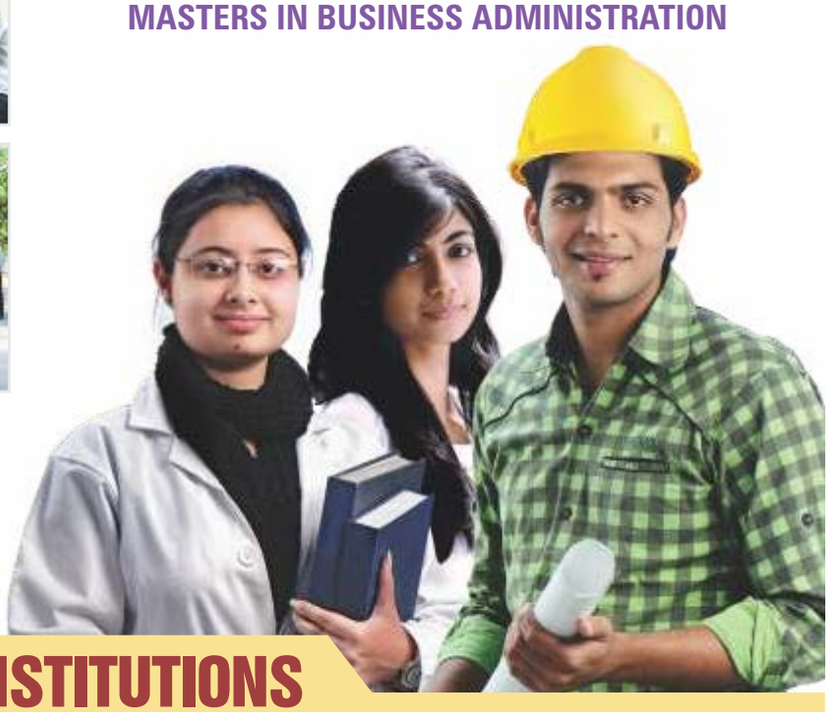

Approved by:
All India Council for Technical Education, New Delhi

Affiliated to:
Mahamaya Technical University, Noida

DRONACHARYA GROUP OF INSTITUTIONS

Campus: #27, Knowledge Park- III, Greater Noida (UP) Phone: 0120-2323851-58 Email: info@dronacharya.info

Approved by
All India Council for Technical Education, New Delhi

Affiliated To:
Mahamaya Technical University, Noida

Corporate Office:
76P, Part-III, Sector-5, Gurgaon, 122001, Haryana (India)
Phone: 0124-2251602, 2253144, Email: info@dronacharya.info

www.dronacharya.info

design: www.studio1-india.com